Micro-Raman spectroscopy of nanomaterials: applications in archaeology

A thesis submitted by

Linda C Prinsloo

in partial fulfilment of the requirements for the degree of

PHILOSOPHIAE DOCTOR

Physics

in the Faculty of Natural and Agricultural Sciences of the University of Pretoria

Promoter: Prof. DJ Brink

April 2008

Micro-Raman spectroscopy of nanomaterials: applications in archaeology.

Candidate: Linda C Prinsloo
Supervisor: Prof. DJ Brink
Degree: Philosophiae Doctor

SUMMARY

"Nanomaterials" is a generic term used to describe nano-sized crystals and bulk homogenous materials with a structural disorder at the nanoscale. Ancient (and modern) ceramics and glasses derive some of their properties (eg. pliability and low sintering temperature) from the fact that their raw material namely natural clay is nanosized. Furthermore the pigments used to colour ceramics and glasses need to have particle sizes <500 nm for the object to appear homogenously coloured to the human eye. Raman spectroscopy intrinsically probes chemical bonds and is therefore one of the few techniques that has been proven useful to provide information at the nanoscale. It is an excellent tool to study ceramics and glasses as a Raman spectrum can be used to identify phases, analyse amorphous domains in the silicate network and identify pigments on a nano-scale. The characteristics of a glass, ceramic or ceramic glaze derived through its Raman spectrum can then be linked to the technology used to produce an artefact and in this way provide information about its relative age and provenance. Likewise, the identification of pigments and binders in San rock art might provide information about production techniques and assist in the developement of conservation procedures.

In this thesis micro-Raman spectroscopy (with X-ray fluorescence, X-ray powder diffraction, electronmicroscopy and photoluminescence as supportive techniques) was utilised to study archaeological artefacts from the Mapungubwe Collection and San rock art. It was possible to re-date celadon shards excavated on Mapungubwe hill in 1934 to the Yuan or even later Ming dynasty in stead of its original classification as Song. A profile of the glass technology used to produce the Mapungubwe oblates, small trade beads from the "royal burials" on Mapungubwe hill was determined and quite a few unique characteristics of the beads may eventually help to establish their provenance. The possible influence of the presence of *rock hyraces* at rock art sites on the deterioration of rock art were investigated and during the study very rare polymorphs of $CaCO_3$ (vaterite and monohydrocalcite) were discovered in rock hyrax urine. This study was extended to analyse a San rock art fragment and another first was the identification of animal fat on the fragment, but the exact origin of the fat has to be verified by similar experiments.

ACKNOWLEDGEMENTS

I wish to express my sincere appreciation to the following people, who in one way or other, have contributed towards the completion of this study:

- Prof. Wolfgang Kiefer, editor of the Journal of Raman Spectroscopy, who in his capacity as chairman of the Steering Committee of the International Conference of Raman Spectroscopy, chose South Africa to host the XVI International Conference on Raman Spectroscopy in 1998, which served as inspiration for this thesis. The confidence he expressed in me by regularly asking me to referee articles for the journal has served as tremendous encouragement.

- Dr. Philippe Colomban, Head of the *Laboratoire de Dynamique Interaction et Réactivité*, Paris, whose work on ceramic glazes and glass provided the theoretical backbone for a large part of the thesis. His willingness to collaborate with me has provided me with a valuable mentor.

- Prof. Johan Brink, Department of Physics, University of Pretoria for his guidance and assistance throughout this study.

- The Physics Department of the University of Pretoria for funding several conferences and supporting me in the study.

- Me Sian Tiley, curator of the Mapungubwe Museum for her sustained cooperation and help with permits.

- All my co-authors for their collaboration, encouragement and time.

- The staff of the XRF and XRD Laboratory and the Electronmicroscope unit of the University of Pretoria for their help.

- My husband Gerhard, two sons and many friends for their continuous support.

CONTENTS

LIST OF FIGURES

Chapter 4

Chapter 5

INTRODUCTION CHAPTER 1

In 1998 the XVI International Conference on Raman Spectroscopy, held in Cape Town, South Africa highlighted the application of Raman spectroscopy in the study of Art and Archaeology, which at that time was a very novel research field. The papers presented at this conference dealt with fascinating study objects such as ivories, oriental manuscripts, gemmology, lichen from the antartic, Egyptian papyri, artefacts from the wreck of the *Pandora* and cave paintings in France, to mention but a few. Since then the applications in this field have grown dramatically, as illustrated in the figure below where the number of research papers published in this field from 1998 to 2007 is plotted against the publication year.

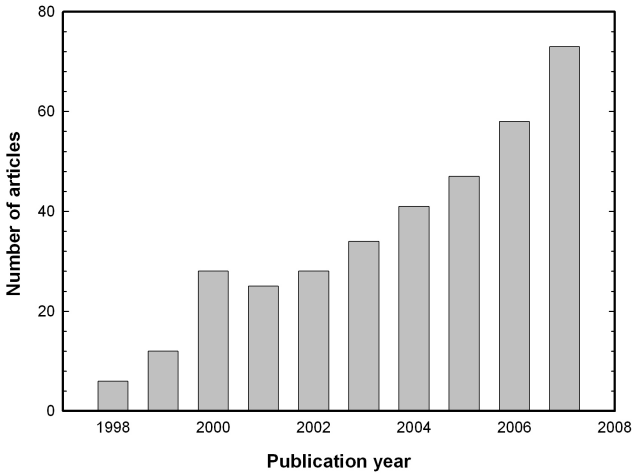

Figure 1: Growth of the number of research papers on Raman spectroscopy in art and archaeology (1998-2007), according to a survey on the Web of Science.

This thesis is based on the results of four studies in this research field, which was inspired by the conference; two on artefacts from the Mapungubwe collection and two on rock art. It is presented as four original articles published in the Journal of Raman Spectroscopy (Impact factor = 2.133) during the time span 2001-2008, together with a preceding chapter explaining the theoretical background used in the research.

Two of the studies were performed in collaboration with Ms Sian Tiley, the curator of the Mapungubwe Museum, which opened its doors in January 2000. In both studies imported artefacts excavated on Mapungubwe hill, namely celadon shards and glass trade beads, are investigated.

Imported glass beads, together with ceramics are the earliest and most abundant artefacts in the archaeological record, which clearly indicate international trade. Furthermore exotic

imports, when found in an archaeological context, have always provided a basic archaeological dating method if securely dated at their point of origin. In East Africa this is of cardinal importance since the only written records of the pre-Portuguese era consist of the Greek *Periplus Maris Erythraei (*2 AD), a few travel documents from Arab travellers and hearsay knowledge documented in Chinese sources. Two fragments of Chinese porcellaneous ware were excavated in 1934 during the first archaeological expedition to Mapungubwe and in 1991 another shard from the same vessel was found at the main entrance to Mapungubwe Hill. These shards and thousands of imported glass beads, mostly found in graves, connect Mapungubwe to the extensive maritime trade network, already established in the 1st century AD, which linked East Africa with the monsoon-based commercial systems of the Indian Ocean. Furthermore, the central position of Mapungubwe Hill, situated at the confluence of the Limpopo and Shashe rivers, also made it from the earliest times accessible via old camel caravan routes to Egypt and the Mediterranean trade. Likewise, trade along the African west coast was accessible via the interior, through Botswana and Angola, where Portuguese mariners had traded in beads imported from Europe 150 years before they rounded the Cape of Storms and also dominated the African east coast trade.

Therefore, research on the imported goods in the Mapungubwe Collection is of the utmost importance, as the discovery of the provenance of the artefacts would help to unravel the old trade routes through and around Africa. Indirectly it can also assist in refining the dating of the Mapungubwe archaeological site.

The other two studies followed after a field trip to the Mapungubwe Heritage site, where it became clear that Raman spectroscopy could also play a role in rock art research. San rock art sites are found throughout southern Africa; unfortunately this unique heritage is rapidly being lost through natural weathering processes as the paintings are mostly found in rocky shelters and underneath overhangs, which are exposed to the elements. This has led to various projects during which factors influencing natural weathering processes such as micro-climate, rock moisture and rock temperature have been studied. It is essential to know the chemical composition of the pigments and binders used by the San artists for the interpretation of rock weathering studies and it is also of primary importance for conservation purposes. Raman spectroscopy has been used successfully to analyse pigments and substrata in prehistoric rock art and it has been shown that it could also be useful in the study of San rock art deterioration.

In the concluding chapter the work is put in context and possible future research is discussed.

In this chapter the fundamentals of vibrational spectroscopy are described as it forms the theoretical basis of the analytical techniques used in all four studies. The focus of the discussion is micro-Raman spectroscopy as it was the main investigative technique. Infrared spectroscopy, inelastic neutron scattering and hyper Raman spectroscopy are briefly discussed as far as it is complementary to Raman spectroscopy. Resonance Raman spectroscopy is highlighted as it made it possible to detect nano-sized phases in rock art and glass. Raman spectroscopy of nanomaterials is illustrated through its application to the study of glasses and ceramic glazes; both materials with structural disorder at the nano-scale.

2.1 Fundamentals of vibrational spectroscopy

2.1.1 Vibrations in Crystalline Solids

All collective vibrations that occur in crystals can be viewed as the superposition of plane waves that virtually propagate to infinity. These plane waves, known as normal modes of vibration, are commonly modelled by quasi-particles called *phonons*. A normal coordinate of the form $Q=Q_0\cos(2\pi\nu_{vib}t)$, a linear combination of bond lengths and bond angles, is associated with each normal mode (ν_{vib}= vibration frequency, t = time).[1] For structures containing isolated covalently bonded entities, the "molecular description" (see § 2.2.3) applies and in this case, depending on the dominant term in the normal coordinate, modes can be classified as stretching (**ν**), bending (**δ**), torsional (**τ**), librational (**R'/T'** pseudo-rotations/translations) or lattice modes (the latter includes the relative displacement of the unit cells).

For a three-dimensional (3D) solid containing N unit cells with p atoms each, (3pN-6) different phonons can propagate[1] and their wavevectors ($\vec{k}$) all lie in a volume of reciprocal space called the Brillouin Zone (BZ)[2]. A phonon is characterised by its wave vector $\vec{k}$, with the length of the wave vector $\left|\vec{k}\right| = \frac{2\pi}{\lambda}$, where λ is the wavelength.[2] The direction of $\vec{k}$ can be either parallel or perpendicular to the particle motions, giving rise to longitudinal phonons (L), which

[1] There are 3pN degrees of freedom but the 6 rotations and translations of the whole solid are not considered to be proper vibrations.
[2] The BZ describes the geometrical distribution of the wavevectors in reciprocal space in the same way the unit cell describes the geometry and periodicity of the crystalline arrangement in direct space.

are vibrations in the propagation direction and transverse phonons (T) with vibrations perpendicular to the direction of $\vec{k}$. Phonons can further be classified into acoustic (A) and optical (O) branches. The former represents modes with in-phase oscillations with the electron cloud and the latter modes with out of phase oscillations.[3] The out-of-phase optical mode vibrations are associated with an electronic dipole moment, but the acoustic modes not. Consequently optical Raman modes are substantially stronger than acoustic ones. Fig. 1 is an illustration of the concept of phonons in crystals showing the transverse vibrations in a one-dimensional lattice where p=2.[1]

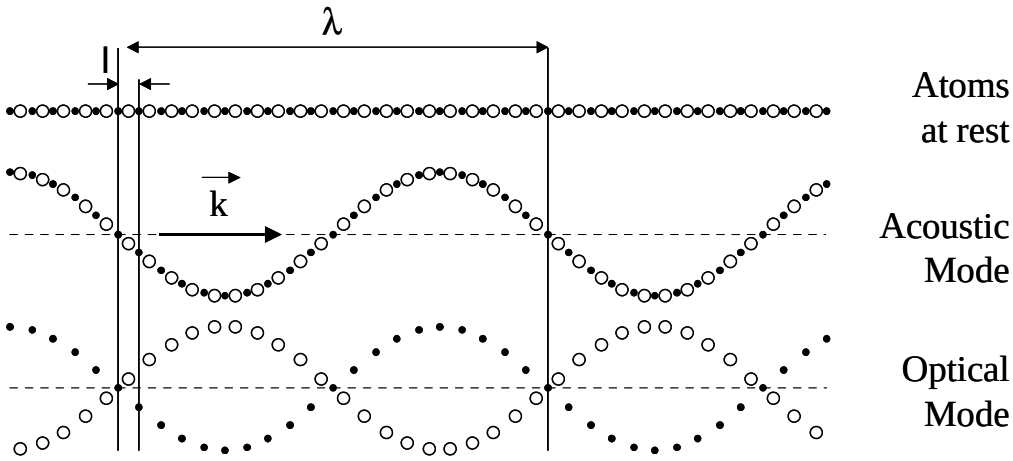

[3]**Figure 1: The transverse phonons ($|\vec{k}| = \frac{2\pi}{\lambda}$) in a 1D-solid with unit cell parameter l.**

The energy of a phonon ($E = \nu \cdot h$, where ν is the frequency of the phonon and h is Planck's constant) is dependent on the length and direction of the wavevector and dispersion curves relating the frequency to the wavevector $\vec{k}$ can be can be established with the use of neutron scattering experiments. The exact relationship between ν and $\vec{k}$ depends on the masses of the atoms and elastic constant of the crystal.[2] If there is only one atom per unit cell, the phonon dispersion curves are represented only by acoustic branches. In the case of more than one atom per unit cell a greater number of vibrational modes are available and both acoustic and optical branches appear. Generally for a crystal with N atoms per primitive unit cell there will be 3 acoustic branches (1 longitudinal and 2 transverse) and 3N-3 optical branches (N-1 longitudinal and 2N-2 transverse).[4] In Fig. 2 typical dispersion curves for a three-dimensional lattice, with partly ionic binding and cell length ***a*** are shown. Only the first Brillouin zone, $-\pi/a \leq \vec{k} \leq \pi/a$,

[3] Figure 1 from reference 1.

needs to be considered as values from outside only reproduce motions of atoms already described for $\vec{k}$ within these limits.[4]

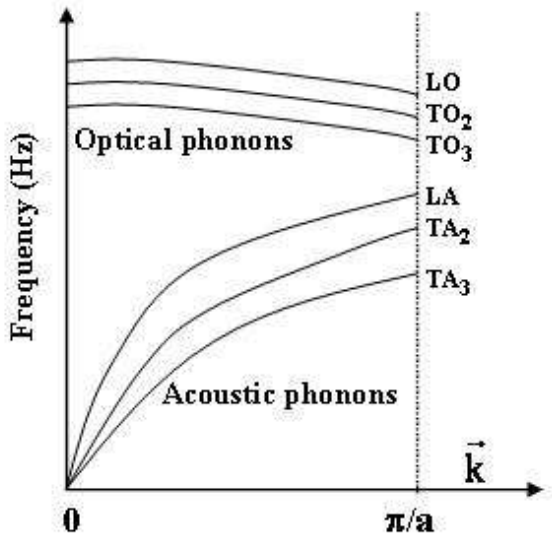

Figure 2: Typical phonon dispersion curves for the lattice vibrations, along a given crystallographic direction, of a three-dimensional anisotropic lattice with partial ionic binding.

Raman and infrared spectroscopy are the customary experimental methods to measure vibrational modes of materials. Neutron scattering is the only experimental method, which can be used to determine the dispersion curves, but is not commonly available.

2.1.2 The Raman Effect

The polarization of the dipoles excited in solids when a laser beam (amplitude E_0; frequency ν_{las}) interacts with phonons of frequency ν_{vib} depends on the polarisability tensor $\bar{\bar{\alpha}}$:

$$\vec{P} = \bar{\bar{\alpha}} \times \vec{E}_0 \cos(2\pi\nu_{las}t) \qquad \textbf{(1)}$$

$\bar{\bar{\alpha}}$ terms can be individually described as functions of the normal vibration coordinates Q using a Taylor approximation:[5]

$$\alpha_{ij} = \alpha_{ij}^0 + \left(\frac{\partial\alpha_{ij}}{\partial Q}\right)_{Q=Q_0} \times Q \qquad (i, j = x, y \text{ or } z) \qquad \textbf{(2)}$$

$$P_i = \sum_j \alpha_{ij} \times E_j = \sum_j \left[\alpha_{ij}^0 E_{0_j} \cos(2\pi\nu_{las}t) + \frac{E_{0_j}Q_0}{2}\left(\frac{\partial\alpha_{ij}}{\partial Q}\right)_{Q=Q_0} \times \left[\cos(2\pi(\nu_{las} - \nu_{vib})t) + \cos(2\pi(\nu_{las} + \nu_{vib})t)\right] + \ldots \right. \qquad \textbf{(3)}$$

With the scattered electric field proportional to $\vec{P}$, Eq. **(3)** predicts both quasi-elastic ($\nu \sim \nu_{las}$) and inelastic ($\nu = \nu_{las} \pm \nu_{vib}$) light scattering. The former is known as Rayleigh scattering and the latter, which occurs only if vibrations change polarisability ($\partial\alpha_{ij}/\partial Q \neq 0$), is Raman scattering.[5,6] The Raman scattered light consists of a Stokes ($\nu = \nu_{las} - \nu_{vib}$), as well as an anti-Stokes branch ($\nu = \nu_{las} + \nu_{vib}$), which is illustrated in Fig. 3. Stokes scattering occurs when the initial vibrational state is the ground state, excitation takes place to a virtual state and decays to a real vibronic state with higher energy than the initial state, therefore the scattered photon has a lower energy than the incident photon. In anti-Stokes scattering the initial state is the excited state and the scattered photon has higher energy that the incident one. At room temperature the population of vibrational excited states is low according to the Boltzman population of states, hence although the Stokes and anti-Stokes spectra contain the same frequency information, the Stokes spectrum is always more intense than the anti-Stokes spectrum and consequently generally used in Raman spectroscopy.

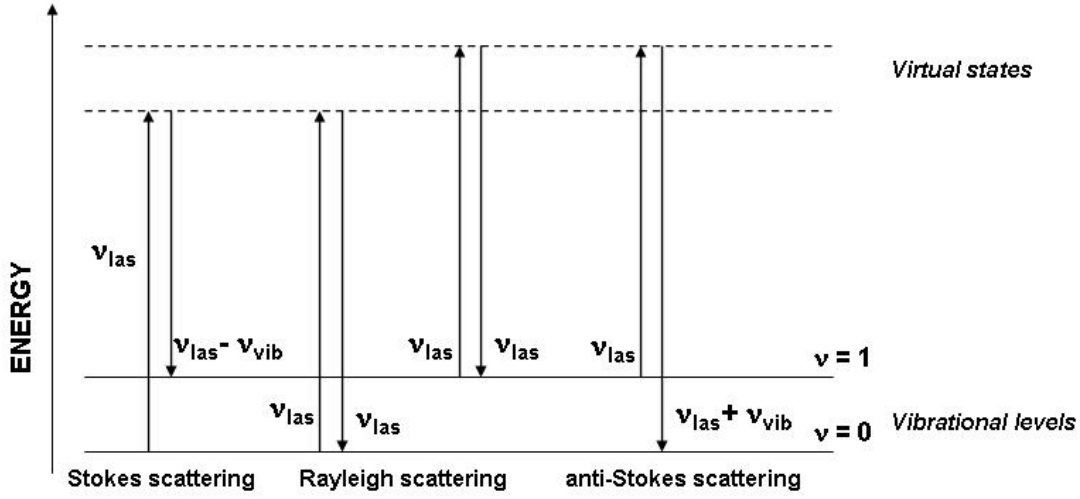

Figure 3: Illustration of linear Raman scattering processes

Raman spectroscopists normally refer to vibrational modes by their wavenumber $\bar{\nu} = \nu_{vib}/c$ (c the light speed, $\bar{\nu}$ in cm^{-1} unit) and the classical electromagnetic theory of radiations from an oscillating dipole demonstrates that Raman peaks have a Lorentzian shape.

$$I(\bar{\nu}) = I_0 \times \int_{(BZ)} \frac{d^3\vec{k}}{\left[\bar{\nu} - \bar{\nu}(\vec{k})\right]^2 + \left(\frac{\Gamma_0}{2}\right)^2} \qquad \textbf{(4)}$$

In Eq. **(4)**, $\bar{\nu}(\vec{k})$ represents the dispersion branch to which the mode belongs and Γ_0 is the half-width for the ordered reference structure.

The scattering of one photon ($\vec{k} \sim \vec{0}$) by n phonons (wavevectors $\vec{k}_i$) is governed by the momentum conservation rule:

$$\sum_{i=1}^{i=n} \vec{k}_i = \vec{k}_{scattered} - \vec{k}_{incident} \approx \vec{0} \qquad \textbf{(5)}$$

Therefore, only vibrations from the centre of the Brillouin zone, *i.e.* long wavelength phonons can be active in any one-phonon process (first order spectrum). However, not all of the phonons are active in Raman spectroscopy. According to Eq. **(3)**, $\partial\alpha_{ij}/\partial Q$ terms must be different from zero and this condition is governed by the symmetry of the crystals.[7]

An interesting feature of Eq. **(3)** is to reveal the dual sensitivity of Raman spectroscopy to the electrical (α_{ij}) and mechanical (ν_{vib}) properties of the investigated materials.[1] Two kinds of parameters will therefore influence the spectra:

(i) parameters acting on mechanical properties like atomic mass, bond strength or the system geometry (interatomic distances, atomic substitutions) will determine peaks positions (the eigenfrequencies of matter vibrations).

(ii) parameters acting on the "charge transfer" (iono-covalency, band structure, electronic insertion) will determine intensity, on the basis of vibration-induced charge variations at atomic bond scale.[1]

As polarisability changes for different kinds of bonds, Raman intensity is difficult to use for the quantitative determination of different phases. Covalent materials in general are good Raman scatterers, whereas ionic structures are more difficult to analyse with Raman spectroscopy. As for metals, their surface plasmons limit the penetration of light resulting in a very weak Raman signal.

The intensity of Raman scattering is given by the following equation:

$$I_R = I_o K \nu_{las}^4 \left| e_0 \bar{\bar{\alpha}} e_s \right|^2 d\Omega \qquad \textbf{(6)}$$

where $\bar{\bar{\alpha}}$ is the polarisability tensor, K a constant, e_o and e_s the unit vectors defining the directions of the electric field of the exciting and scattered light respectively, $\bar{\nu}_0$ the energy of

the excitation laser and dΩ the collection solid angle.[1] From equation 6 it is clear that high energy lasers (blue or violet lines) and backscattering measurements (i.e. the use of a high magnification objective with large aperture) will enhance the intensity. The Raman cross-section could vary many orders of magnitude as a function of the nature of the bond and the exciting wavelength used.

2.1.3 Resonance Raman Spectroscopy

If the energy of the laser excitation (usually in the UV-nIR range) approximately matches the energy of an electric dipole allowed transition of the material under investigation (usually coloured material), a strong enhancement of some vibrational modes (near-resonance/resonance Raman scattering) can be expected. In other words, the virtual state energies of the Raman effect approaches that of the electronic excited states. Resonance can increase the intensity as much as a factor of 10^6 and concerns mainly the symmetric vibrational modes and their overtones and combinations.[7]

In chapter 6 this effect made it possible to identify nano sized quantities of two different carotenoids in San rock art paint as carotenoid pigments experience a strong resonance enhancement due to electron-phonon coupling of the π-electrons of the polyacetylenic backbone.[7] In chapter 4 the presence of the Fe-S chromophore in black glass beads is also detected through a resonance effect.

2.1.4 Infrared spectroscopy

In infrared spectroscopy the nature of the light-matter interaction is not the same as in Raman spectroscopy and the fundamental differences between the two processes determine the selection rules, which control the Raman or infrared activity of a normal mode of vibration. Interaction of infrared radiation with a normal mode of vibration only occurs when the electric vector of the radiation field oscillates with the same frequency as instant dipoles caused by atomic vibrations. A normal vibration is therefore infrared active only if a change in the dipole moment of the vibration occurs and is a one-photon process, as only the photon absorbed is involved.[7] Therefore infrared spectra offer additional information to that obtained from Raman spectra, where a change in polarisability is necessary for a normal mode to be active. Several authors have outlined group theoretical methods, by which the symmetries of the normal modes

of vibration of molecules and crystal lattices can be determined.[8-11] In general infrared spectroscopy probes polar modes (vibrations that modify existing dielectric dipole moments) and Raman spectroscopy non-polar modes.

2.1.5 Inelastic neutron scattering

Inelastic neutron scattering is the process by which neutrons collide with atomic nuclei and either gain or lose kinetic energy. In this it is conceptually very similar to Raman scattering, but there are significant differences. The major difference is that photons (electromagnetic radiation) interact primarily with the electrons of a sample, while neutrons interact with the nuclei. The strength of the interaction is very dependent on the particular nuclide involved, isotopes and spin states. Another difference is that the wavelength of the electromagnetic radiation used for Raman experiments in the visible or near UV region has wavelengths of hundreds of nanometers, while neutrons have wavelengths slightly less than 0.2 nm (room temperature).[12] This means that the size of the neutron is comparable to the spacing between atoms, therefore there are no "selection rules" as is the case for optical spectroscopy and all vibrational modes are active but modified by the atomic diffusion length. Except for localised modes of protonic species (H cross section is ~x80 that of other atoms), identification of modes is difficult and the spectrum consists of a vibrational density of states (VDOS).

2.1.6 The hyper Raman effect

Generally the induced electric dipole moment $\vec{P}$ of a system is related to the electric field $\vec{E}$ of the radiation by a power series (see also Eq. **3**)

$$\vec{P} = \alpha\vec{E} + \tfrac{1}{2}\beta\vec{E}\,\vec{E} + \tfrac{1}{6}\gamma\vec{E}\,\vec{E}\,\vec{E}\ldots\ldots \qquad \textbf{(7)}$$

where α is the polarizability, β the hyperpolarizability and γ the second hyperpolarizability. α, β and γ are tensors of rank 2, 3, 4, etc. respectively, $\vec{E}$ is the electric field and $\vec{E}\,\vec{E}$ is the dyadic product of two electric fields etc.[7] The non-linear terms in Eq. **(7)** are usually negligibly small, but when the electric field is sufficiently large as in the case of giant-pulse lasers (Q-switched), contributions from the second term in Eq. **(7)** are sufficiently intense to be detected and is called hyper Rayleigh ($2\nu_{las}$) and hyper Raman scattering ($2\nu_{las} \pm \nu_{vib}$).[7] The hyper Raman effect is a three-photon process involving two virtual states of the scattering system (Fig. 4).[7] Two laser

photons of frequency ($2\nu_{las}$) are simultaneously scattered to give photons with frequencies $2\nu_{las}$ (hyper Rayleigh) or $2\nu_{las} \pm\nu_{vib}$ (hyper Raman) when a vibration is excited or destroyed respectively. Thus, hyper Raman lines are found in the spectral neighbourhood of the second harmonic ($2\nu_{las}$) of the incident laser radiation. It should be mentioned that Rayleigh scattering always occurs, but hyper Rayleigh scattering only occurs if the scattering material does not have a centre of symmetry.[7] Hyper-Raman spectroscopy is a very useful technique to study glass.

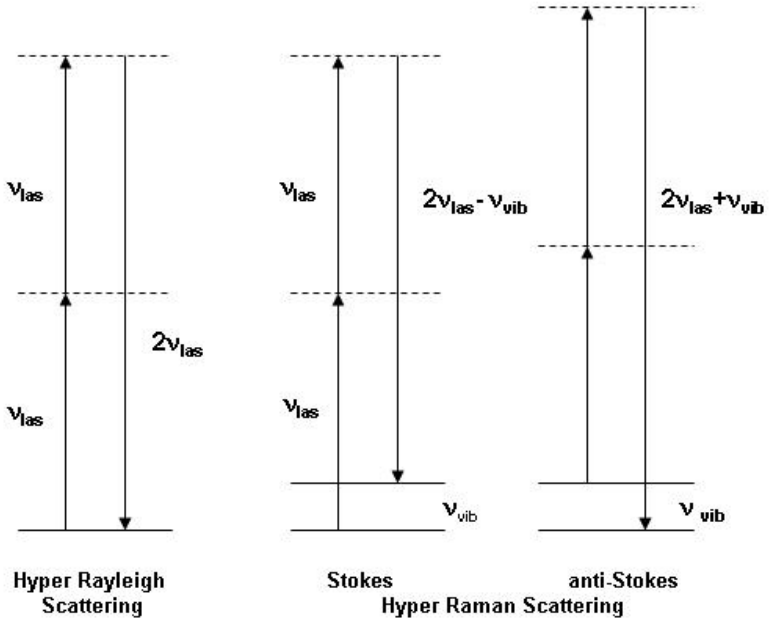

Figure 4: Schematic level diagram for hyper Rayleigh and hyper Raman scattering

2.2 Nanomaterials

Reducing the dimension of matter domains down to the nanometer scale confines the electronic and vibrational wavefunctions and vastly increases the ratio of surface area to volume, which results in unique properties of materials. It opens a wide range of potential applications in fields as different as optics, mechanics, electrical devices, magnetic devices, reactivity and biomedicine.[1]

The challenge for nanotechnologists is to achieve perfect control of nanoscale-related properties. This obviously requires correlating the parameters of the synthesis process (self-assembly, microlithography, sol-gel, polymer curing, electrochemical deposition, laser ablation…) with the resulting nanostructure. Not every conventional characterization technique

is suitable for that purpose but the use of Raman spectroscopy has already been proven to be successful.[1]

2.2.1 Raman spectroscopy of nanomaterials

The translational symmetry of crystalline materials is broken at grain boundaries, which results in the appearance of specific surface and interface vibrational contributions. These two factors are often neglected in Raman spectroscopy but become very significant in nano-crystals, where the concentration of grain boundaries is very high.[1]

However, in many nanomaterials the Raman spectrum remains sufficiently similar to that of the corresponding single crystal to make direct identification of phases possible.[13] Both crystallographers and Raman spectroscopists characterize disorder through peak broadening. Yet, while a loss of long distance translational periodicity is always associated with broadening for diffraction patterns, only lattice and librational (R', T') modes are sensitive to the same "long distance" disorder in Raman spectroscopy.[13] The width of the other Raman modes is mainly sensitive to the "local" crystal field and if the "molecular" description of vibrations applies (see §2.9), then Raman bending modes are specifically sensitive to local geometric disorientation and Raman stretching modes to the neighbouring disorder (particularly atoms from other sublattices or electric defects resulting from substitutions/vacancies). Therefore the modifications of the vibrational signature is very small for stretching modes (bond lengths are very similar in crystals and amorphous materials), detectable for bending modes (sensitive to orientational disorder) and significant for librational and lattice modes (the lower energy motions) as only lattice modes reflect the long-range symmetry which determines the X-ray unit cell.[1]

There are two ways of truly isolating the Raman signal coming from nano-particles. One is by having a nanoparticle to be the only one of its kind in the laser beam's path as is possible with Surface Enhanced Raman Spectroscopy (SERS), while the other involves a breaking of the $\lambda/2$ diffraction limit (Abbe criterion) of optical microscopes (nano-Raman). SERS is not always practical and the development of nano-Raman techniques is still in its infancy. However, although conventional Raman micro-spectrometers cannot provide laser spots smaller than ~ $1\mu m^2$ the spectra stem from vibrations of chemical bonds.[1] This intrinsic "nanoprobing" makes Raman spectroscopy very sensitive to the short-range structure and qualifies it as a nano-analytical technique.[13]

2.2.2 Raman Microscopy

Up-to-date Raman equipment would include holographic gratings for improved excitation light rejection, a set of monochromators and a liquid nitrogen- or Peltier effect-cooled CCD detector (Fig 5a).[6] The size of the sample analysed (laser spot) can be reduced to ~1 µm diameter by using high-magnification microscope objectives. Owing to the diffraction of light, the intensity coming from a point observed through a microscope is distributed over an "Airy disk". The lateral resolution R, which is the smallest distance between two points to still appear distinctively on the microscope image, is half the width of the Airy disks. According to the Rayleigh criterion:

$$R = \frac{0.61 \times \lambda}{NA} \qquad \textbf{(8)}$$

In Eq. **(8)**, λ is wavelength of the light and NA represents the numerical aperture (Fig. 5b).

As for the axial resolution (Δz) of µRS, an estimate is given by the depth of field, which is defined as half the width of the axial intensity profile (modern instruments usually have a confocal hole which rejects the shadowed light and facilitates a more accurate in-depth analysis ($\Delta z_{conf} < \Delta z$)), which is approximated by the following equation:

$$\Delta z = \frac{\lambda}{n \sin^2\theta} \Rightarrow \Delta z_{\text{through air (n=1)}} = \frac{\lambda}{(NA)^2} \qquad \textbf{(9)}$$

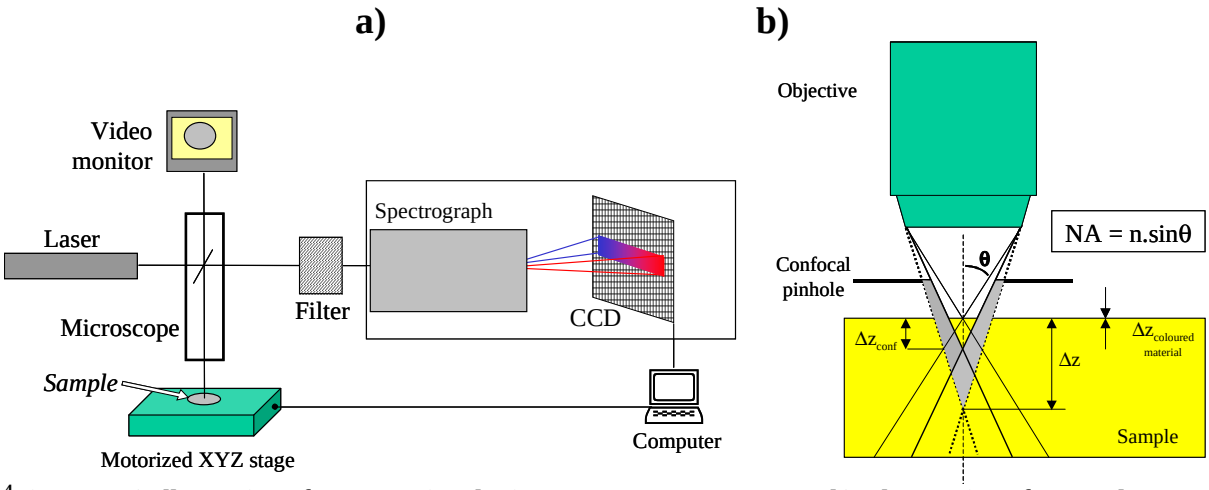

[4]Figure 5: a) Illustration of a conventional micro-Raman spectrometer – b) Observation of a sample through a microscope (NA: Numerical Aperture; n is the refractive index of the medium separating the objective from the sample). A confocal hole rejects the shadowed light and facilitates a more accurate in-depth analysis ($\Delta z_{conf} < \Delta z$).

Under "standard" conditions (n=1, λ=500nm, NA=0.5), the typical lateral and in-depth resolutions of µRS are about 1 - 2 µm. Even with the smallest visible wavelength (~ 400 nm) and

[4] Figure 5 is from reference 1

the highest numerical apertures (oil immersion objectives with n=1.515; NA~1.4), one should not expect a lateral resolution better than R=0.2 µm (the Abbe criterion states that the wave nature of light prevents the distinction of points closer than λ/2) and a field depth below Δz=0.4 µm. Therefore a large amount of "nano-sources" contribute to the Raman signal.[1]

2.2.3 Analysis of "isolated" vibrational units

Vibrational modes in crystals are extended plane waves. In contrast vibrational waves in disordered systems are never single plane waves and cannot be described in terms of a single ***k***-vector. Furthermore, for sufficiently large degrees of disorder, vibrational excitations may become spatially localised.[14] In this case clusters of strong covalently bonded atoms are isolated from one another by weaker ionic bonds and thus become the relevant vibrational units (localized vibrations).[15-17] All atoms from such a unit must exclusively belong to it for the normal coordinates of Eq. **(2)** & **(3)** to coincide with given bond lengths and bond angles. The spectra then consist of stretching and bending modes equivalent to the internal vibrations of polyhedral (mostly tetrahedral or octahedral) isolated molecules. The molecular scheme describes most organic polymers and also crystalline/amorphous inorganic polymers such as silicates, phosphates, carbonates, niobiates, titanates and all compounds with polyatomic cations such as NH_4^+, H_3O^+ or $N_2H_5^{2+}$.[18-20] A given vibration then always appears in the same region, its exact position giving information about the local environment of the corresponding bonds, both in the amorphous and crystalline state. Literature on silicate glass has to be read with caution as many authors simultaneously use several vibrational units. In a low polymerized silicate glass, i.e. in a depolymerised network where many Si-O bonds have been broken by silicon/sodium,

Table 1: Symmetry and main activity of a SiO_4 tetrahedron with T_d symmetry, C_{2v} site symmetry in a D_{6h} crystal structure.

Modes	Symbol	Symmetry T_d	Symmetry C_{2v} in D_{6h}	Main activity	Wavenumbers cm^{-1} SiO_4
Symmetric stretching	ν_1 or ν_s	A_1	$A_{1g}+E_{2g}+E_{1u}$	Raman	800-1000
Asymmetric stretching	ν_3 or ν_{as}	F_2	$E_{2g}+E_{1u}+E_{1g}+A_{2u}+A_{1g}$	IR	900-1200
Symmetric bending	ν_2 or δ_s	E	$A_{1g}+E_{2g}+E_{1u}$	Raman & IR	400-600
Asymmetric bending	ν_4 or δ_s	F_2	$E_{2g}+E_{1u}+E_{1g}+A_{2u}+A_{1g}$	IR	500-700
Rotational libration	R'			Raman & IR	300
Translational libration	T'			Raman & IR	100-200

potassium or lead substitution, the use of the SiO_4 tetrahedron as vibrational unit is a good choice. On the contrary in pure silica, where all oxygens belongs to 2 tetrahedra, the Si-O unit can be used.[21-23] Some authors prefer to use Si-O-Si units.[24] For instance the bending mode of SiO_4 tetrahedra can also be described as the scissoring mode of Si-O-Si units. An isolated SiO_4 tetrahedron has T_d symmetry and in an ordered structure with known site symmetry (eg. C_{2v}) and crystal structure (eg. D_{6h}) the main vibrational modes, Raman or infrared activity can be predicted by group theory (Table 1).

2.3 Application of Raman spectroscopy to ceramic glazes and glasses

2.3.1 The Raman spectrum of vitreous silica

In a classic paper Zachariesen proposed in 1932 that the interatomic distances (force constants) in glass and crystals must be similar as their mechanical properties are of comparable magnitude and that glass is also made up of a three-dimensional lattice, which is not symmetric or periodic (from the diffuse character of x-ray data).[25] Each atom in a glass network then has a unique position and the influence of the local environment on Si-O bonds is not dictated by the symmetry of the crystallographic site and space group as in a single crystal with a periodic structure. In fact as glass can be described as "liquid" from the physical point of view the influence of the surroundings on the Raman/IR spectrum can be compared to that of a solution on the spectra of solutes. This leads to a broadening of the vibrational modes as illustrated in Figure 6 (top: Raman, bottom: FTIR), where the spectrum of crystalline α-quartz is compared to that of α-quartz glass (the example is fulgerites form Witsand, Kalahari, South Africa). The broadness of the bands in the spectra of the glass is consistent with a statistical distribution of many different vibrations of varying strength. It is clear that the transformation from the crystalline to glassy phase is much more visible in the Raman spectrum than in the infrared. Due to the long-range interaction of electric dipoles, IR bands are much broader than their Raman counterparts, especially in a glassy material and only the small factor group splittings, observed in the crystalline spectrum (such as the characteristic 778/792 cm^{-1} doublet of α-quartz), disappear in the amorphous one.

The broad bands in the spectra can readily be understood in terms of a continuous "random" network, but the two sharp peaks in the Raman spectrum commonly known as D_1 (495 cm^{-1}) and D_2 (606 cm^{-1}) modes are reminiscent of crystalline phases (Fig. 6, top). They have been assigned

by various authors to breathing modes of small 3 and 4 membered silicon cycles, which have decoupled from the network vibrations,[26-30] but actually correspond to bending modes of nano-crystals, although protons also play a role.[31] The other sharp peak in the spectrum of the glass at 458 cm^{-1} belongs to nano sized crystallites of α-quartz (main peak at 462 cm^{-1}) imbedded in this natural glass, but its peak position has shifted to lower wavenumbers, indicating a lenghtening of the Si-O bonds due to tensile stress experienced in the silica glass matrix. This arises from the

Fulgerites are formed in sand (α-quartz) by lightning, which transforms the sand into natural glass

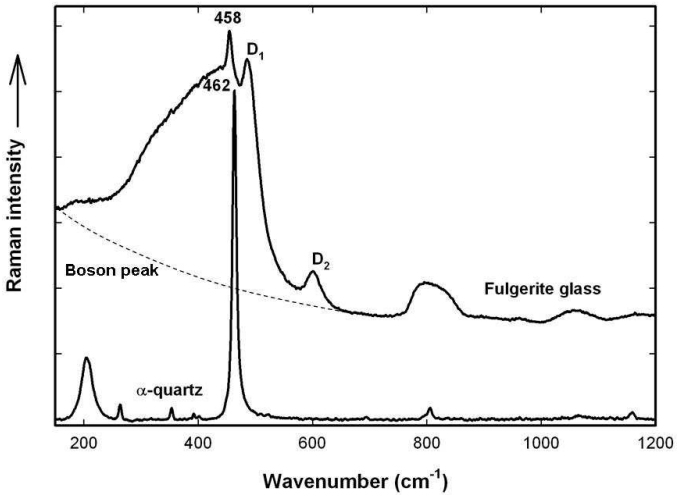

The inner side of an fulgerite is pure silica glass, on the outside small grains of crystalline α-quartz (sand) are imbedded in the glass

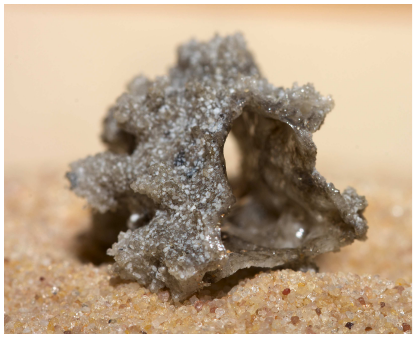

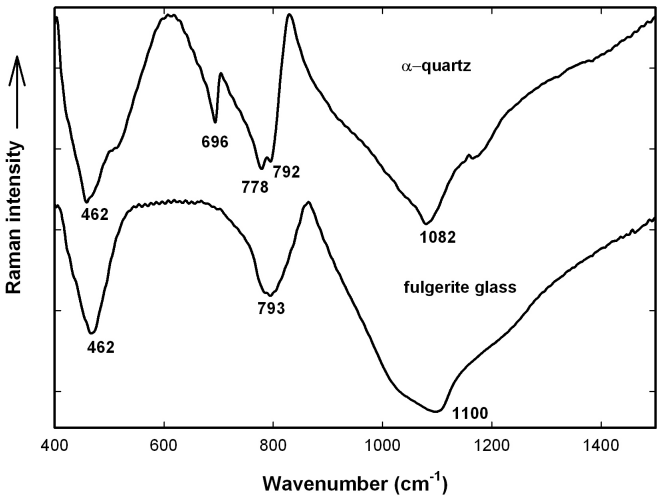

Figure 6: Comparison of the vibrational spectra of crystalline and glass quartz Raman (top) and FTIR (bottom)

thermal expansion mismatch between crystalline quartz, which for quartz is ~60x10^{-7}cm K^{-1} and for amorphous glass ~2x10^{-7}cm K^{-1}. At high temperatures there is equilibrium between the two phases, but on cooling when the viscosity and fusing increase, the silica matrix experience very little thermal contraction, which is imposed on the quartz grain, hindering its normal contraction process. This causes the lengthening of the Si-O bonds in the quartz, which induces the

downshift. This phenomenon is also observed at the interface between a ceramic body and its glaze (see chapter3).

Also indicated on the figure is part of the Boson peak, which occurs between 0-100 cm^{-1} in all glasses (the rest of the peak is out of the detection limits of the instrument) and is so called as its intensity obeys a Bose-Einstein distribution. The origin of this peak has been highly debated by physicists[32-36] but recent Hyper Raman measurements (see §2.1.6) confirm the assignment made by chemists, namely the Boson peak corresponds to the projection of lattice/external modes of the SiO_4 vibrational units similar to those in crystals.[37-38] Various theoretical models have been proposed to remove the Boson peak, but essentially the results of these methods are very close to that obtained by using a four-point straight-line background subtraction.[39-40]

2.3.2 The Raman spectra of historic glass

The melting temperature of pure α-quartz glass is 1700°C which is not easily attainable for practical applications in the science, art and technology of glass, glazes and enamels. By adding fluxing agents (sodium, potassium, calcium, lead) the nanostructure of the three dimensional Si-O network is modified by replacing Si^{4+} covalently bonded atoms by non-covalent bonded atoms, hence decreasing the number of Si-O bridges and the connectivity of the network. Consequently, the firing temperature decreases and many other physical/chemical properties related to the density and network connectivity are modified accordingly.[41]

The transition from a highly connected tetrahedral structure (such as α-quartz glass, Fig.6, top) to weakly connected tetrahedral units, as caused by the addition of fluxing agents is reflected in the Raman spectrum by the appearance of a broad band in the region of Si-O stretching vibrations (~1000 cm^{-1}). This is analogous to the appearance of stretching vibrations in crystalline forms of silicates, where the network connectivity decrease in comparison with a fully connected α-quartz structure. Fig. 7 compares Raman spectra of the different classes of silicates such as nesosilicates (isolated SiO_4 tetrahedra eg. forsterite), sorosilicates (Si_2O_7 entities), cyclosilicates, innosilicates (chains), phyllosilicates (slabs) and tectosilicates (3D connectivity). It is clear that when going from a highly connected tecto-silicate to a neso-silicate without network connectivity, the ratio of stretching vibrations to bending vibrations increases.

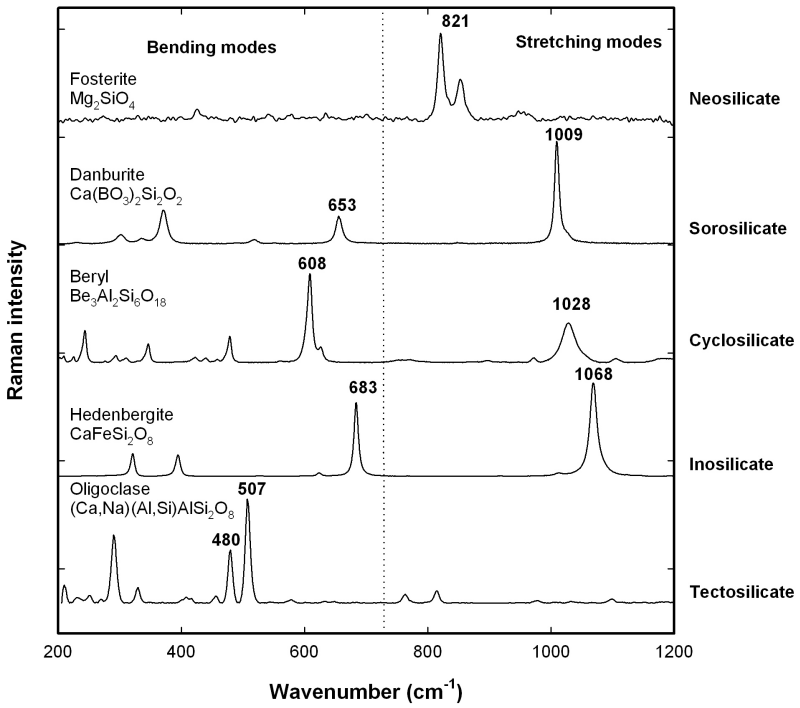

Figure 7: Raman spectra of various different crystalline silicates.

The Raman spectrum of a typical alumina/silica glass then consists of two broad bands around 500 and 1000 cm^{-1}. The band around 500 cm^{-1}, originates from the ν_2 bending vibration of SiO_4 tetrahedra and the one around 1000 cm^{-1} to coupled ν_1 and ν_3 Si-O stretching vibrations.[39,42] As the amount of fluxing agents increases the Raman intensity of the bending modes decreases, while the stretching modes become more intense; reflecting a loss in the degree of polymerisation in the network. This is demonstrated in Fig. 8a where Raman spectra of glasses with different compositions, from a refractory silica-rich porcelain glaze (bottom) to a lead-rich glaze composition with a low melting point (top) are plotted showing the development of the band originating from the stretching modes.[39] Except for the broadness of the bands it mirrors the trend in Fig. 7 of the crystalline counterparts.

The relationship between the Raman index of polymerisation ($I_p = A_{500}/A_{1000}$ with A being the area under the Raman band), the glass composition and the processing temperature is well documented and has been used to classify glasses into various groups.[39,42-44] In Fig. 8b it is shown how the Index of Polymerisation varies for different types of glass and in chapters 3&4 the use of this classification system is illustrated.

In many instances a comparison of the I_p of ancient glass/glaze samples with Fig. 8b (in reference 39) is sufficient to distinguish between two different glass technologies (see chapter 3), but to make a distinction between closely related technologies, it is necessary to analyse the

Raman spectrum further. In order to do this the broad bands of the glass spectrum has to be deconvoluted and the individual bands thus obtained assigned to different species or vibrational units according to a well-defined model.

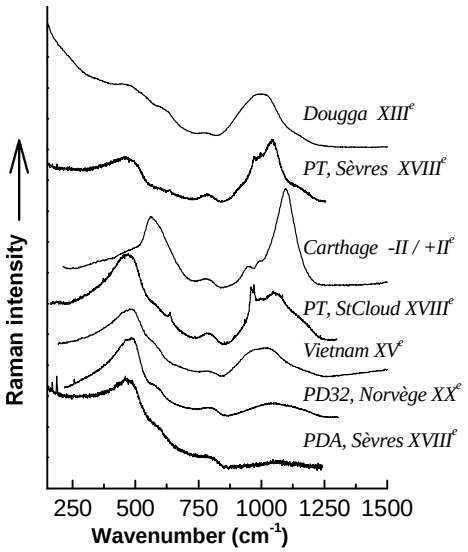

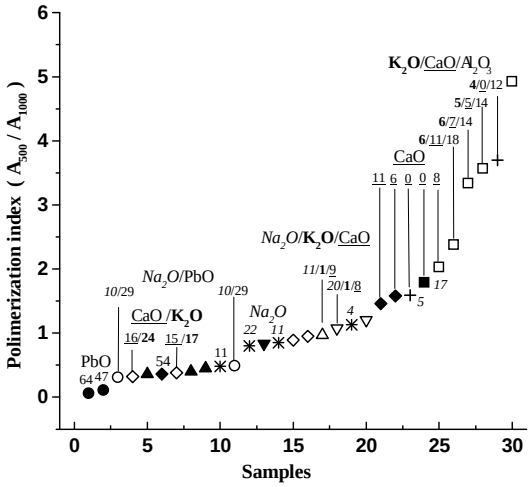

[5]**Figure 8a: Raman spectra of glasses having different compositions showing the development of the band originating from the stretching modes. (See details in ref 39)**

Figure 8b: Comparison of the Polymerisation index of different silicate glasses (See details in ref 39) Molar ratios of the fluxing oxides are indicated on the figure.

Historic glasses usually also have varying concentrations of aluminium (dependent on the composition of the sand used) as part of the network. On the basis of geometrical packing the ionic radius of Al is intermediate between the optimum radii for four-fold and six-fold coordination. Due to this factor and the amphoteric nature of aluminium, Al^{3+} can be either a network forming or network-modifying cation in aluminosilicate melts. As a tetrahedrally coordinated cation within a silicate network Al^{3+} is typically associated with a charge balancing cation such as an alkali or alkaline-earth cation.[45-48] Because of the more ionic character of Al-O bond in comparison to the covalent Si-O bonds, its contribution to the Raman spectrum of aluminosilicate is close to nil.[39] Aluminium ions are thus not a glass forming species from the vibrational point of view and influence the silicate network in a similar way as other cations used as fluxing agents.

2.3.3 Defining a vibrational unit for glass: the Q_n model

A common nomenclature system known as the Q_n notation, where n is the number of bridging oxygens per tetrahedron, has been in use since the 70's.[48-52] A tetrahedron fully linked into the network via four bridging oxygens is designated as a Q_4 unit, while an isolated

[5] Figure 8 a&b is from reference 39

tetrahedron with no bridging oxygens is designated as a Q_0 unit (Fig. 9). Based on the spectra of crystalline phases the positions of the various Q_n structures could be assigned to silica vibrations with zero (Q_0, 800-850 cm^{-1}, compare fosterite), one (Q_1, ~950 cm^{-1}), two (Q^2, ~1020-1040 cm^{-1}), three (Q_3, ~ 1100 cm^{-1}) and four (Q^4, ~1150-1250 cm^{-1}) bridging oxygens per tetrahedral group.

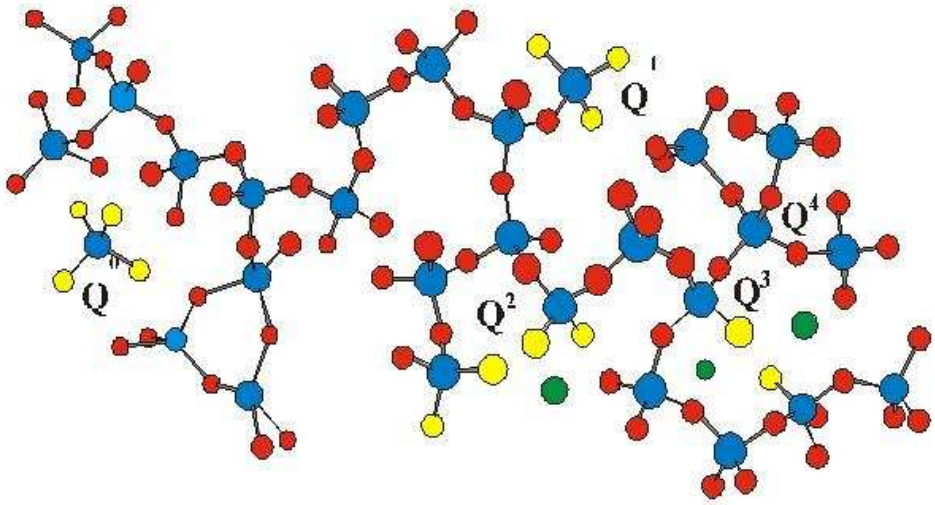

[6]Figure 9: Sketch of a silicate framework. SiO_4 tetrahedron (Si^{4+}, large circle, O^{2-} ion small circle) can be isolated or connected by 1, 2, 3 or 4 oxygen atoms. Fluxing cations (Na^+, K^+, Ca^{2+},…) are represented by isolated circles.

The main advantage of the Q_n model is that it is applicable to all silicate compositions and is therefore a very realistic model. However the following assumptions are made:

i) only one symmetric mode is expected for a given Q_n tetrahedron, thus splitting due to site symmetry is neglected. Asymmetric modes are ignored (see Table 1),

ii) it is assumed that the intensity of the above symmetric Q_n stretching mode does not vary with glass composition,

iii) it is also assumed that the bandwidth of each component have similar values.

Note that the model implies that there are only 5 bands and that extra bands do not belong to the signature of the glassy silicate network. If additional components with narrow bandwidths are present, they could correspond to nanocrystals. Based on this a workable model for the analysis of any glass sample based on a silicate network consists four basic steps, illustrated in Table 2.

[6] Figure 9 is from reference 1

Table 2: Procedures to determine the I_p and Q_n components from a glass spectrum

a. A four-point baseline subtraction to remove contributions from the Boson peak and other fluorescence that may be present in very old samples	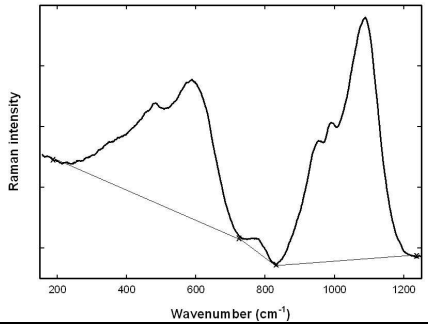
b. Integration of the areas under the two peaks (Lapspec software of Dilor works well) and calculation of I_p and comparison with the existing database.	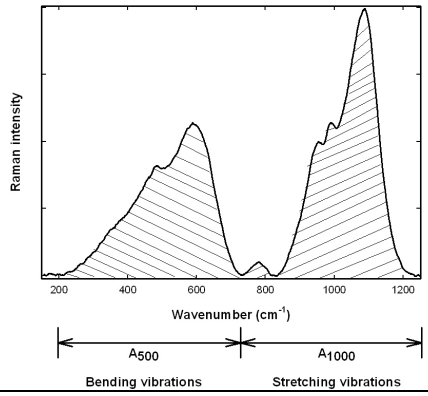
c. Peak fitting of the stretching vibrations envelope by choosing 5 Gaussian components, with a restriction that the FWHM < 100. Sharp peaks are attributed to crystalline phases, chosen as Lorentzian, with a restriction of FWHM = 20. (The Origin Peakplot program was used in this study)	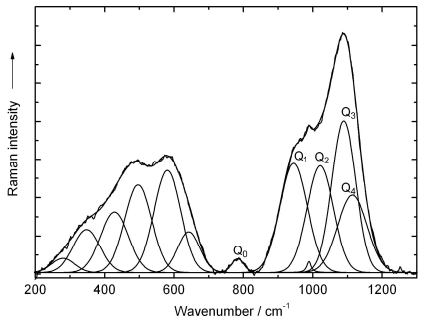

A combination of the I_p and various parameters determined through the deconvolution process, namely the wavenumber positions and areas Q_0-Q_4 makes it possible to correlate the parameters in 2D diagrams and with chemometrics methods as illustrated in reference 39. This is a powerful tool that has been successful in distinguishing between production technologies of closely related ceramic glazes.[39]

It is not only the modification of the silicon network (bond angles, force constants, etc.) that influences the Raman spectrum, but also the type of cation inserted within the matrix as fluxing agent. Both the size and oxidation state of the cation influence the bandwidth and position of the various peaks as illustrated by several authors.[52-54] The merit of a Raman spectrum is that all of these effects are encapsulated in one single spectrum and by utilizing the method above makes it possible to analyse any unknown archeological glass object. In chapter 4 it was not possible to match the glass beads analysed exactly to a glass in the existing database,

but all the necessary parameters have been determined and published. Hopefully this will lead to identification later on, as the database is continuously expanding

2.3.4 Glass weathering

In many instances ancient glass samples have undergone changes due to weathering processes, of which an in-depth understanding is very important for conservation studies of museum glass, stained glass windows and archaeological glass artefacts. Alteration of the glass is attributed to a reaction between the glass surface and aqueous solutions (such as rain or groundwater) in a two-stage process. In the first stage there is an ion-exchange between protonic species from the liquid and an alkali ion that is removed from the surface of the glass and the formation of an alkaline wet film on the surface. This film becomes increasingly alkaline and above pH 9 the second stage occurs, with decomposition of the silicate network. In the Raman spectra this is evidenced by the main Si-O stretching vibration shifting to lower wavenumbers and a decrease in intensity of the Si-O bending vibration at ~570 cm^{-1}, the narrow component and 950 cm^{-1} and the Boson peak. In addition Raman modes involving hydrogen occur in ranges where there is no overlapping with the modes involving other elements due to the low atomic mass of hydrogen (>1400 cm^{-1}, typically). Also the bond potential between a proton and other atoms is very anharmonic and thus combinations and harmonics have significant intensities and due and can be observed between 4000 and 8000 cm^{-1}, some times up to 20 000 cm^{-1}. Thus OH^- and $O\text{-}H^+$ groups, H_2O, H_2 can be observed both by Raman and IR spectroscopy. This is very useful in following glass deterioration processes.[55-58] In chapter 4 corrosion of glass beads could be identified through Raman spectra and water was detected in one bead with infrared spectroscopy, which differentiates it from other black beads with similar Raman spectra.

2.3.5 Pigments and (nano) crystalline inclusions

Glass colouring is obtained by doping the glass with 3*d*/4*f* ions or by the dispersion of coloured crystalline phases (pigments or metal nanoparticles) in the glass matrix. Colouring obtained by doping disperses ions (eg. Co) throughout the silicate matrix and in many instances no special Raman signal can be observed. Small crystallites is sometimes distinguishable under a microscope objective (especially in ancient glasses), which makes it possible to focus on the pigment directly and obtain a spectrum, which can be identified by comparing it with a spectra library of reference material. Since the first publication of a spectral library (56 inorganic

pigments used before 1850) various other libraries have been compiled and are readily available through the internet. A detailed account of useful databases can be found in reference 59. Other crystalline second phases, such as opacifiers (eg. SnO_2), crystallites formed during the production process (eg. wollastonite) or phases inherent in the starting material (eg. TiO_2-see chapter 3) can also be identified and may help in tracing the provenance of an artefact. In the rock art studies the identification of crystalline phases is richly illustrated.

References:

1. Gouadec G and Colomban Ph, *Prog Cryst Growth Ch.* 2007; **53**: 1-56.
2. Nissum M, Shabanova E and Nielson OF, *J. Chem. Ed*. 2000; **77**: 633.
3. Brink J, Honours Optics, Course Notes, University of Pretoria; 1998.
4. Cheetham AK and Day P, *Solid State Chemistry: Techniques*
5. D.A. Long, *Raman Spectroscopy*, McGraw-Hill International Book Company, London York 1977.
6. I.R. Lewis and H.G.M. Edwards (Eds.) *Handbook of Raman Spectroscopy - From the Research Laboratory to the Process Line*, Marcel Dekker Inc., NY, USA (2001).
7. Schrader B, *Infrared and Raman Spectroscopy*, John Wiley & Sons Ltd, London, 1995.
8. Ferraro JR and Ziomek JS, *Introductory Group Theory and its Applications to Molecular Structure*, Plenum Press, New York, 1969.
9. Adams DM and Newton DC, *Tables for Factor Group and Point group Analysis*, Beckman-RIIC Ltd, Croyden, England, 1970.
10. Rousseau DL, Bauman RP and Porto SPS, *J. Raman Spectrosc*. 1981; **10**: 253.
11. Fateley WG, Dollish FR, McDewitt NT and Bentley FF, *Infrared and Raman Selection Rules for Molecular and Lattice Vibrations, The Correlation Method*, John Wiley &Sons Ltd. London, 1995.
12. Dorner B, *Coherent Inelastic Neutron Scattering in Lattice Dynamics*, Springer-Verlag, 1982, Berlin.
13. Gouadec G and Colomban Ph, *J. Raman Spectrosc*. 2007; **38**: 598.
14. Taraskin SN and Elliott SR, *Physica B*, 2002; **316-317**: 81.
15. Condrate RA, *J. Non-Crystal. Solids* 1986; **84**: 26.
16. Colomban Ph, Glasses, *Glazes and Ceramics – Recognition of the Ancient Technology from the Raman Spectra*, in *RAMAN SPECTROSCOPY IN ARCHAEOLOGY AND ART HISTORY*, Ch13 pp 192-206, H.J. Edwards and J.M. Chalmers (Eds), 2004, Royal Society of Chemistry, UK
17. Faurel X, Vanderperre M, Colomban Ph, *J. Raman Spectrosc*. 2003; **34**: 290.
18. Griffith WP, *J. Chem. Soc. (A)* 1970; 286.
19. Griffith WP, *Nature* 1969; **224:** 264.
20. Griffith WP, *J. Chem. Soc.* (A) 1969: 1372.
21. Galeener FL, Lucovsky G, *Phys. Rev. Lett*. 1976; **37**: 1474.
22. Galeener FL, *J. Non- Crystal. Solids* 1990; 123: 182.
23. Galeener FL, Sen PN, *Phys. Rev.* B 1978; **17**: 1928.

24. Zachariasen WH, *J. Am. Chem. Soc.* 1932; **54**: 3841.
25. Handke M, Mozgawa W, *Vibr. Spectrosc*. 1993; **5**: 75.
26. Elliott R, *J. Non-Crystal. Solids* 1995; **182**: 1.
27. Galeener FL, *J. Non-Crystal. Solids* 1982; **49**: 53.
28. Galeener FL, Barrio RA, Martinez E and Elliot RJ, *Phys. Rev. Lett*. 1984; **53**: 2429.
29. Galeener FL and Thorpe MF, *Phys. Rev. B*, 1983; **28** (10): 5802.
30. Sitarz M, Mozgawa W and Handke M, *J. Mol. Struct*. 1999, **511-512**, 281-285.
31. Humbert B, Burneau A, Gallas JP, Lavalley JC, *J. Non-Crystal. Solids* 1992; **143**: 75.
32. Hassan AK, Börjesson L, Torell LM, *J. Non-Crystal. Solids* 1994; **172-174**: 154.
33. McInstosh C, Toulouse J and Tick P, *J. Non-Crystal*. Solids 1997; **222**: 335.
34. Taraskin SN, Loh YL, Natarajan G and Elliott SR, *Phys. Rev. B* 86 2001; **7**: 1255.
35. Inamura Y, Arai M, Yamamuro O, Inaba, Kitamura N, Otomo T, Matsuo T, Bennington SM, Hannon AC, *Physica B* 1999; **263-264**: 299.
36. Schroeder J, Wu W, Apkarian JL, Lee M, Hwa L-G, Moynihan CT, *J. Non-Crystal. Solids* 2004; **349**: 88.
37. Hehlen B, Courtens E, Yamanaka A and Inoue K, *J. Non-Crystal. Solids* 2002; **307-301**: 87.
38. Hehlen B, Courtens E, Vacher R, Yamanaka A, Kataoka M and Inoue K, *Phys. Rev. Lett*. 2000; **84**(23): 5355.
39. Ph. Colomban, A. Tournié, L. Bellot-Gurlet, *J. Raman Spectrosc*. 2006; **37**: 841.
40. B.O. Mysen, L.W. Finger, D. Virgo & F.A. Seifert, Curve-fitting of Raman spectra of silicate glasses, *Am. Mineral*. **67** 696-717 (1982).
41. Shelby JE, *Introduction to Glass Science and Technology*, 2nd Edition, The Royal Society of Chemistry, Cambridge, 2005.
42. Ph. Colomban, J. Non-Crystalline Solids 323 [1-3] (2003) 180-187.
43. Colomban, Ph, *Appl. Phys. A*, 2004; **79**: 167.
44. Colomban Ph and Paulsen O, *J. Am. Cer. Soc*. 2005; **88** (2): 390.
45. Rokita M, Handke, W and Mozgawa W, J. *Mol. Struct.* 1999; **511-512**: 277.
46. Mozgawa W, Handke Mand Jastrzębski, J. *Mol. Struct.* 2004; **704**: 247.
47. Tarte P, Rulmont A, Liégeois-Duyckaerts M, Cahay R and Winand JM, *Solid State Ionics*, 1990; **42**; 177.
48. Sharma, SK, Simons B and Yoder Jr. HS, *Am. Mineral*. 1983; **68**: 1113.
49. Mysen BO, Virgo D & Scarfe CM, *Am. Mineral*. 1980; **65:** 690.
50. Seifert F, Mysen BO & Virgo D, *Am. Mineral*. 1982; **67**: 696.

51. MacMillan PF, *Am. Mineral*. 1984; **69:** 622.
52. Brawer S, *Phys. Rev. B*, 1975; **11**: 3173.
53. Sitarz M, Handke M, Mozgawa W, Galuskin E and Galuskina I, J. *Mol. Struct.* 2000; **555**: 357.
54. Brawer S and White WB, *J. Non-Cryst. Solids*, 1977; **23**: 261.
55. Colomban Ph, Etcheverry M, Asquier M, Bounichou M and Tournié A, *J. Raman Spectrosc*. 2006; **37**: 841.
56. Tournié A, Ricciardi P and Colomban Ph, *Solid State Ionics*, 2008 submitted.
57. Robinet L, Coupry C, Eremin Kand Hall C, *J. Raman Spectrsc.* 2006; **37**: 789.
58. Robinet L, Coupry C, Eremin Kand Hall C, *J. Raman Spectrsc.* 2006: **37**: 1278.
59. Vandenabeele P, Edwards HGM and Moens L, *Chem. Rev.* 2007; **107** (3): 675.

CHINESE CELADON SHARDS CHAPTER 3

The unique Chinese ceramic shards, classified as Song celadon, excavated on Mapungubwe hill were the first objects to be studied. I applied the Raman spectroscopic methods described in the papers of Dr Philippe Colomban to analyse the ceramic glaze of the shards and found that it did not match spectra of glazes with high calcium content, which was the type of glaze used during the Song dynasty. This result motivated me to send a picture of the shard to Nigel Wood, world-renowned expert on Chinese ceramics for his opinion. His personal input in this research project, which utilized Raman spectroscopy, XRF (X-ray fluorescence) and XRD (X-ray powder diffraction) measurements together with the information published in his book on Chinese Glazes (1999), made it possible to re-date the celadon shards to the Yuan or even early Ming dynasty.

During the course of the study celadon shards excavated at Great Zimbabwe (in the collection of the Iziko Museums, Capetown) were also analysed with XRF for comparison purposes. Due to unfortunate circumstances it was not possible to analyse the shards with Raman spectroscopy at that time. Hopefully in the future this can be rectified and the project expanded to include all the celadon shards excavated at sites in the interior and African East Coast. Such a study would contribute significantly in reconstructing the prehistory of the African sub-continent.

The preliminary results of this paper were presented as a poster at *CSI XXXII (Colloquium Spectroscopicum Internationale)* held in Pretoria, South Africa, 9-13 July 2001.

LC Prinsloo and S Tiley, A Raman spectroscopic study of some artefacts from the Mapungubwe collection.

The poster won the award for the best poster in the Raman division of the conference, as well as the award for the best overall poster at the conference, awarded by Nobel Laureate Roald Hoffmann.

Further results were presented in an oral presentation at the Conference on Raman Spectroscopy in Budapest, Hungary 2002.

Linda C Prinsloo, Ian Meiklejohn, Andri Meyer and Adam Bumby, A Raman spectroscopic study of an Iron Age archaeological site in South Africa.

The full results were published in the Journal of Raman Spectroscopy and follows in full as chapter 3.

Linda C Prinsloo, Nigel Wood, Maggi Loubser, Sabine M C Verryn and Sian Tiley, Re-dating of Chinese celadon shards excavated on Mapungubwe Hill, a 13th century Iron Age site in South Africa, using Raman spectroscopy, XRF and XRD.

JOURNAL OF RAMAN SPECTROSCOPY
J. Raman Spectrosc. 2005; **36**: 806–816
Published online 16 June 2005 in Wiley InterScience (www.interscience.wiley.com). DOI: 10.1002/jrs.1367

JRS

Re-dating of Chinese celadon shards excavated on Mapungubwe Hill, a 13th century Iron Age site in South Africa, using Raman spectroscopy, XRF and XRD

Linda C. Prinsloo,[1]* Nigel Wood,[2] Maggi Loubser,[3] Sabine M. C. Verryn[3] and Sian Tiley[4]

[1] Department of Physics, University of Pretoria, Pretoria 0002, South Africa
[2] Research Laboratory for Archaeology and the History of Art, Oxford University, 6 Keble Road, Oxford OX1 3QJ, UK
[3] XRF and XRD Laboratory, University of Pretoria, Pretoria 0002, South Africa
[4] Mapungubwe Museum, University of Pretoria, Pretoria 0002, South Africa

Received 10 January 2005; Accepted 17 March 2005

Chinese celadon shards of the Longquan type, believed to date from the Southern Song dynasty (1127–1279 AD), were excavated in 1934 on Mapungubwe Hill, a 13th century Iron Age site in the Limpopo valley, South Africa. We studied the shards with Raman spectroscopy, x-ray fluorescence (XRF) spectroscopy and x-ray diffraction (XRD). The Raman polymerization index (I_p), calculated from the spectra of the glaze of the shards, indicated a higher firing temperature than expected for the relatively calcium-rich Longquan glazes of the Southern Song dynasty. XRF analysis of the glaze and XRD measurements of the bulk of the shards supported this view and date the shards to possibly the Yuan (1279–1368 AD) or even early Ming (1368–1644 AD) dynasties. These results have an impact on the chronology of the history of the region and therefore call for further research of a comparative nature of other Chinese celadon shards excavated on archaeological sites in Africa, in addition to additional carbon dates of Mapungubwe hill. Copyright © 2005 John Wiley & Sons, Ltd.

KEYWORDS: XRF; XRD; celadon; glaze

INTRODUCTION

The *Illustrated London News* reported on 8 April 1933, *'a remarkable discovery in the Transvaal: a grave of unknown origin, containing much gold-work, found on the summit of a natural rock stronghold in a wild region'*.[1]

This discovery turned the myths and legends surrounding the sacred hill Mapungubwe (TsiVenda for 'the hill of the jackal') into factual history. An ancient legend, suggesting certain death upon ascending the hill, helped to protect the last resting place of the rulers of a prehistoric African trade kingdom (ca 1000–1290 AD) for more than seven centuries. Furthermore, the occurrence of malaria and tsetse fly made the Limpopo valley the wildest and most desolate part of the Transvaal and helped to protect the site from looting, which occurred at most other Iron Age sites in southern Africa.[2] The discovery in 1933 of intact gold-bearing graves by prospectors was therefore a remarkable find of great archaeological and historical significance and marked the beginning of a 70-year archaeological project, which has recently resulted in the founding of the Mapungubwe Museum, University of Pretoria.

Two fragments of Chinese porcellaneous ware were excavated in 1934, during the first archaeological expedition to Mapungubwe, in the occupation layers on the hilltop, one at 4 ft and the other at 1 ft from the surface. They were classified in the same year by the British Museum as celadon from the late Southern Song dynasty (1127–1279 AD).[2] In 1991, another shard, belonging to the same vessel, was found at the main entrance to Mapungubwe hill.[3] The shards and thousands of imported glass beads, which were also excavated at the site, connect Mapungubwe to the extensive maritime trade network, established already in the 1st century AD, which linked East Africa with the monsoon-based commercial systems of the Indian Ocean (Fig. 1). African raw materials such as gold, rhinoceros horn, ivory, ambergris, frankincense and myrrh were exchanged for cotton, porcelain and glass trade beads.[4]

*Correspondence to: Linda C. Prinsloo, Department of Physics, University of Pretoria, Pretoria 0002, South Africa.
E-mail: linda.prinsloo@up.ac.za

Figure 1. Map depicting Mapungubwe and Great Zimbabwe in geographical context with the important ports and cities of the Islamic trade in the Indian Ocean.

Imported porcelain, stoneware and glass shards have been found at many excavated sites along the East African Swahili coast, such as the Islamic towns of Manda, Shanga and Gedi on the Kenyan coast and the ruins of the Islamic mosque Malindi on the trade island of Kilwa off the east coast of Tanzania. At all of these sites Chinese ceramic shards were found, together with Islamic wares imported from Iran, Persia and India.[4–11] Exotic imports, when found in a secondary archaeological context, have always provided a basic archaeological dating method if securely dated at their point of origin. In East Africa, it is of cardinal importance as the only written records of the pre-Portuguese era is the Greek *Periplus Maris Erythraei* (~2 AD), a few travel documents from famous Arab travellers such as Al-Masudi and Ibn Battuta (10th century) and hearsay knowledge documented in Chinese sources.[4] Numerous scholars have used particular varieties of Chinese pottery to refine chronology on the East African coast.[4–11]

Chinese ceramic shards have also been found at inland ancient Iron Age ruins, all of which are situated in a region spanning Zimbabwe, Zambia and the northern part of South Africa, where ancient pre-European gold, copper and tin mines occurred.[2] The known imported ceramics recovered from central African Iron Age sites amount to some 100 shards, of which over 90% come from Great Zimbabwe and are nearly exclusively celadon wares, which broadly dates the shards to pre-Portuguese times.[8] The porcelains traded by the Portuguese, who replaced the Islamic trade along the east coast after 1498, are largely Chinese blue-and-white porcelains and stonewares and were mostly excavated at established Portuguese trading posts.[8]

In 1934, R. L. Hobson of the British Museum ambiguously dated the shards excavated at Mapungubwe, the most southern ancient ruin where Chinese ceramic ware was found, as celadon from the 'late Southern Song dynasty, 13th to 14th century' (see Table 1).[2,8] He also dated the shards excavated at Great Zimbabwe as Southern Song, but other oriental scholars superseded his classification and agreed that most of the Zimbabwe celadons are Ming.[8] Classifications at this time were done on a subjective basis

Table 1. The time period of the dynasties of China mentioned in the text

Chinese dynasty	Period
Five Dynasties period	907–960 AD
Northern Song	960–1127 AD
Southern Song	1127–1279 AD
Yuan	1279–1368 AD
Ming	1368–1644 AD
Qing	1644–1911 AD

Plate 1. (a) Celadon potshards excavated on Mapungubwe hill. (b) Spouted vessel classified as Southern Song celadon. (c) Back side of a shard showing where two halves of the vessel have been joined. (d) Side view of shard. (e) Close up of shard glaze. Bar = 1 mm in (c)–(e).

and relied solely on slight colour variations, shapes and decorations.[12] It was generally assumed, though, that the origin of the shards is the famous Longquan (a district of southern Zhejiang) kilns, where the production of celadons reached their peak in the 13th and 14th centuries, when they were exported widely to Japan, East Africa, the Philippines and the Near East.

Renewed interest in Mapungubwe and the prehistory of South Africa instigated this study and we used Raman spectroscopy, x-ray fluorescence (XRF) spectroscopy and x-ray powder diffraction (XRD) to analyse the chemical composition of the shards in an attempt to determine their provenance and production date with greater accuracy and objectivity than before.

EXPERIMENTAL

Samples

The two shards (Acc. No. N/193) originally excavated on Mapungubwe hill in 1934 can be seen in Fig. 2a. There are three shards in the photograph as the smallest fragment has unfortunately broken off one of the shards through the years, but it can be seen that the shards originally belonged to one vessel (fourth shard found in 1991 not shown). The distinctive ribbed pattern, known as melon ridge, was popular in both northern and southern ancient China. It appears as if two 'bowls', originally moulded, were made and joined rim to rim (maybe off the wheel) and the inside of the shard clearly shows where the two pieces have been attached [Plate 1(c)]. The beautiful green glaze, typical of Chinese celadon ware, and the fine quality of the ceramic survived the harsh African weathering conditions remarkably well and is silent testimony to an ancient potter's craft.

The shards were ultrasonically cleaned to eliminate fluorescence from organic material, which could have adhered to the sample before excavation, by handling or contamination with naphthalene, which in the past was commonly used as a preservative in museum collections.

The original classification of the shards as Southern Song was supported by a study in which the fragments were visually compared with a Chinese celadon spouted vessel, from the Van Tilburg Collection, University of Pretoria (J. A. van Tilburg, a Dutch collector, emigrated in 1952 to South Africa and donated the collection to the University. The collection contains 3000 pieces of Chinese ceramic ware of high quality with representative pieces dating from the Chin to the Qing dynasty). The official museum description of the vessel is Longquan celadon from the Southern Song dynasty [Plate 1(b)]. The colour, texture of the ceramic, unique form and ribbed pattern were found to be so similar that it was positively stated that the potshard originated from a comparable object (referred to in the article as wine kettle).[13] However, Regina Krahl, independent scholar and a current expert on Chinese ceramics at Sotheby's, London, suggests that the shards may derive from a moulded jar or bowl of similar style, which tend to have deeper ribs than this type of ewer (R. Krahl, personal communication). We included the spouted vessel in our study for comparative reasons.

Techniques

Raman spectroscopy

Raman spectra were recorded with an XY Raman spectrometer from Dilor, using both 514.5 and 488 nm radiation from a Coherent Innova 90 argon ion-laser for excitation. The excitation powers at the samples were kept below 20 mW to avoid any thermal effects and the slit width was adjusted to obtain a resolution of at least 2 cm^{-1}. The 50× and 100× objectives were used in a backscattering configuration to collect spectra of the glaze and body of the samples.

The size of the confocal hole, magnification of the objectives and laser power were varied to obtain the optimum recording conditions at each sampling spot. At least 20 spectra were recorded from each phase to obtain statistically representative data. Spectra recorded on the spouted vessel were limited to specific spots owing to the bulkiness of the object, which could be placed in only a few positions underneath the microscope.

In the case of the shard, spectra of the glaze could also be recorded on the side of the fragment, as the glaze between indentations on the shard is fairly thick [Plate 1(c)].

Peak fitting and data processing

In the spectra used for curve fitting, the baseline was first subtracted with a polynomial fitting of x^3 or x^4 using Labspec (Dilor) software. The number of attach points was minimized and kept constant for attaching the baseline to the different spectra. A Gaussian shape was assumed and the same spectral window used for extraction of the components, using the Origin peak-fitting module. The methods applied by Colomban and co-workers in their extensive work on porcelain were followed as closely as possible in order to compare the results obtained in this study with the graphs generated by their group. The integral under each component envelope was also calculated with the Labspec software.

XRD

XRD data were collected from both the bulk and the glaze of the smallest shard on a Siemens D501 automated diffractometer equipped with a secondary graphite monochromator. The applied potential was 40 kV and the corresponding current was 40 mA. The primary x-ray beam was Cu Kα radiation. A pattern was recorded from 3 to 70° 2θ in steps of 0.04° 2θ. The measuring time was 1 s per step.

XRF

Two of the celadon shards were analysed using XRF spectroscopy. They were directly mounted in a 90° quadrant of a Perspex ring and introduced to an ARL 9400XP+ wavelength-dispersive (WD) XRF spectrometer. Analyses

Table 2. Analytical conditions used over the entire range for XRF measurements

Crystal	2*d* crystal / Å	Collimator divergence / °	Detector	X-ray tube anode	Tube setting kV	Tube setting mA	Primary beam filter
LiF220	2.8480	0.15	Scintillation	Rh	60	40	0.25Cu
LiF420	1.8000	0.15	Scintillation	Rh	60	40	
LiF220	2.8480	0.15	Flow proportional	Rh	40	60	
GE111	6.5320	0.15	Flow proportional	Rh	40	60	
AX06	55.400	0.60	Flow proportional	Rh	30	80	

were executed using the UniQuant 5 software program, specifying the weight and area of sample. The software analyses for all elements between F and U and only elements above the detection limits are reported. The spectrometer conditions used over the entire analytical range are displayed in Table 2.

Historically, energy-dispersive (ED) XRF spectroscopy was used for the analysis of porcelains because most WDXRF background and matrix correction software packages assume homogeneous, infinitely thick, flat specimens. The UniQuant 5 software program differs in this regard in that the author included in his algorithms factors to compensate for non-infinitely thick, irregularly shaped and small samples. This enables the analyst to use WDXRF in the same manner as EDXRF that historically had better matrix correction software, owing to the complexity of deconvoluting peaks in EDXRF.

RESULTS AND DISCUSSION

Raman spectroscopy

Raman spectroscopy has been used successfully to study the bulk material, glazes and pigments from a great variety of art objects such as porcelain, glass, jewellery, mosaics and pottery. It has proved to be extremely useful in determining the kind of pigments used, to distinguish between hard-paste and soft-paste porcelains, to differentiate between ancient and modern porcelain and to make deductions about the technology used in manufacturing processes.[14–27]

Raman spectra of the bulk material

The dense, pale-grey body of the shard is typical of Longquan celadon ware, which is considered in China as a type of porcelain. Indeed, it is far closer to white porcelain in its chemical composition than to any stoneware (including celadon) made in any other part of China.[28] Spectra of the bulk of the shard could be recorded through the glaze, in addition to directly on the bulk from the side, and in Fig. 2 representative spectra recorded on the bulk of the shard are presented.

In most spectra, the strong characteristic peak at 462 cm^{-1} of α-quartz was detected (not shown), which is expected of a silica-rich body. This is in accordance with the raw materials used in south Chinese high-fired ceramics, which

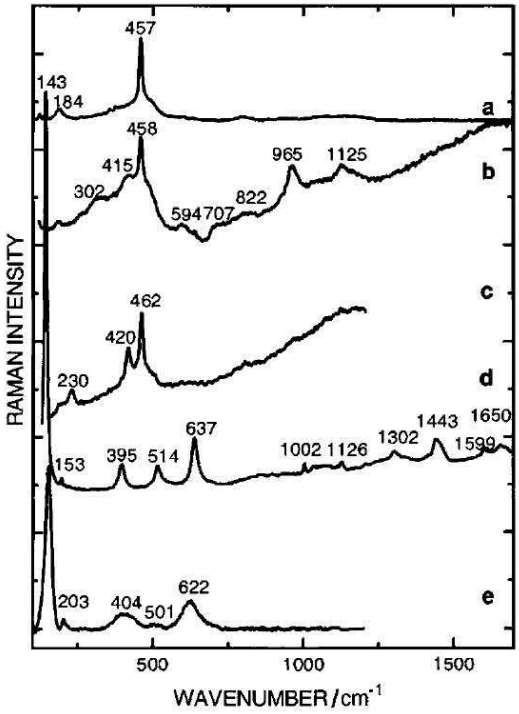

Figure 2. Spectra recorded on the bulk of the shard: (a) glassy silica and α-quartz; (b) glassy silica, α-quartz and mullite; (c) cristobalite; (d) anatase and organic phase; (e) anatase to rutile transition phase.

consisted of igneous rocky materials that were originally molten rock (magma). These materials were, in contrast to Northern Chinese raw materials, low in 'true clay' minerals such as kaolinite and consist instead largely of fine α-quartz and secondary potassium mica, which makes the ceramics rich in silicon and potassium oxides and relatively low in aluminium oxide.[29]

In spectra recorded of the body through the glaze or recorded in the interface region between body and glaze from the side, this peak occurs at 457 cm^{-1} [Fig 2(a)]. The shift of the peak from 464 cm^{-1} in pure SiO_2 to lower wavenumbers (457–460 cm^{-1}) has been attributed to tensile stress, which exists in small grains of quartz in the interface layer.[19] It should be noted, however, that we observed this shift also in

spectra not recorded on the interface but always in association with the peak at 450 cm^{-1}, characteristic of silica glass, as also seen in the spectrum in Fig. 2(b) discussed below.

The spectrum in Fig. 2(b) represents a mixture of typical phases of the crystalline and glassy phases of the silica–alumina system. The peak at 458 cm^{-1}, as already mentioned, is crystalline α-quartz superimposed on the broad band around 450 cm^{-1} typical of glassy silica. The broad peaks at 302, 415, 960 and 1104 cm^{-1} are typical of polycrystalline mullite, one of the expected phases in well-fired porcelain.[30]

The two peaks at 230 and 420 cm^{-1} observed in Fig. 2(c) (recorded on the interface between the bulk and the glaze) are typical of cristobalite, a high-temperature polymorph of SiO_2. The development of cristobalite requires heat treatment for a long duration, which typically occurred in old ceramic kilns.[20] 'Dragon kilns', of the type used for Longquan wares, were first developed by potters in south China in the Shang dynasty (16–11th centuries BC) and refined in subsequent centuries. They consist of long tunnels built on the slope of a hill, with later examples fired by both large fireboxes at the feet of the tunnels, and by side stoking along the kilns' lengths. They reached their zenith in the early 12th century AD when an example approaching 140 m was built in Fujian province. This was capable of firing 10^5 vessels in a single setting. Longquan kilns were somewhat shorter, but would still have provided suitable conditions for the formation of cristobalite.[31]

Peaks at 143 197, 399, 513 and 639 cm^{-1} originate from the anatase phase of TiO_2 [Fig. 2(d)] and were observed in many of the spectra recorded on the bulk and also the glaze of the shard. TiO_2 is present (0.2–2.0%) in most Chinese ceramic raw materials and its relative ratio with respect to iron oxides helps determine the shade of green in celadon glazes when fired in a reducing atmosphere.[28] The very large Raman cross-section of TiO_2 phases makes even these relatively small percentages easy to detect. In the same spectrum [Fig. 2(d)], peaks between 1000 and 1700 cm^{-1} are also observed and are attributed to carbonaceous and organic phases, which have previously also been observed in ceramic glazes. These residues arise from firing in a reducing atmosphere and from contamination, respectively.[18]

In some of the spectra, the characteristic anatase high-intensity peak at 143 cm^{-1} occurs at 153 cm^{-1}, as seen in Fig. 2(e). The relative intensity of the peak has also decreased in these spectra and the FHWM increased from 6 to 15 cm^{-1}. Simultaneously, the other peaks broadened and shifted slightly to 203, 403, 504 and 623 cm^{-1} with the appearance of a new small peak at 285 cm^{-1}. It is well known that three polymorphs of TiO_2 exist in nature, namely the stable rutile phase and the metastable anatase and brookite phases, which convert to rutile on heating. Brookite converts directly to rutile, whereas anatase can convert directly or via brookite to rutile. The temperature of the anatase–rutile phase transformation is furthermore influenced by the size of the particles, the presence of other minerals and the amount of brookite present, and has been extensively studied.[32–36] Although pure brookite has a strong peak at 153 cm^{-1}, the other strong peaks associated with the brookite phase at 245, 320, 364 and 449 cm^{-1} are absent in the spectra, so it is assumed that the observed spectrum is a transition phase between anatase → brookite → rutile. The firing temperature was therefore not high enough to cause a complete transformation to the rutile phase under these specific conditions. It has been recorded that this peak occurs at 153 cm^{-1} for nanosized anatase particles, which could be another explanation for the shift, but as it is known that the porcelain had been heated to at least 1200 °C, the former explanation is more likely.

The body of the spouted vessel could be analysed on the bottom rim, where the glaze had not been applied. Similarly to the body of the shard, in some spectra only crystalline α-quartz [Fig. 3(a)] with the most prominent peak at 462 cm^{-1} was observed. In most spectra both glassy alumina silicate with its broad band around 450 cm^{-1} and crystalline α-quartz are clearly observed [Fig 3(b)]. Spectra of TiO_2 in the rutile phase with bands at 144, 246, 441 and 605 cm^{-1} were also recorded and are an indication that the body of the spouted vessel was fired at a higher temperature than the shard, as the phase transformation to rutile has taken place [Fig. 3(c)]. The relative intensity of the 143 cm^{-1} band, with FWHM equal to ~10 cm^{-1}, is an indication that there is still anatase present, as in pure rutile samples the relative intensity of this band is significantly decreased, with an FWHM of ~3 cm^{-1}. The sharp peak at 1084 cm^{-1} in the rutile spectrum is the characteristic C–O stretch vibration of calcium carbonate.

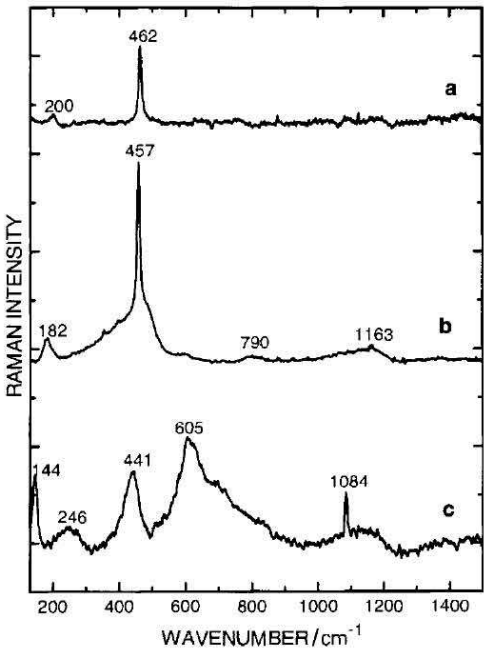

Figure 3. Spectra recorded on the bulk of the spouted vessel: (a) α-quartz; (b) glassy silica and α-quartz; (c) rutile.

$CaCO_3$ breaks down during firing at about 800 °C, liberates carbon dioxide and converts to CaO. Therefore, it is probably contamination, which occurred after firing.

Raman analysis of the body of both the shard and spouted vessel is in agreement with the silica-rich composition of Southern Song celadon bodies from the Longquan kilns. The presence of rutile in the body of the vessel indicates that the firing temperature of the bulk of the teapot was probably higher than for the shard.

Raman spectra of the glaze

Small white particles and micron-sized bubbles suspended in the glaze could be distinguished under the microscope [Plate 1(e)] and made it possible to record a spectrum of α-quartz on a specific particle with the 100× objective (not shown). The α-quartz crystallites and bubbles suspended in the glaze (also observed in Vietnamese celadon[23]) are typical of celadon glazes and, together with the formation of anorthite and wollastonite crystals in the glaze, responsible for their jade-like texture.[28,31]

A glaze is a dense alumina–silicate glassy phase doped or mixed with other metallic oxides, which act as flux to lower the temperature of the glass transition. The addition of metallic cations breaks the Si—O linkages, which decreases the degree of polymerization in the Si—O network and consequently requires a lower firing temperature.

The Raman spectra of porcelain glazes consist of two broad bands around 500 and 1000 cm^{-1}. The band around 500 cm^{-1} originates from the ν_2 bending vibration of isolated SiO_4 tetrahedra and that around 1000 cm^{-1} to coupled ν_1 and ν_3 Si–O stretching vibrations.[19] In highly connected tetrahedral structures the bending modes have a high Raman intensity and in weakly connected tetrahedral units, as caused by the addition of fluxing agents, the intensity of this band decreases and the stretching modes become more intense. The relationship between the Raman index of polymerization ($I_p = A_{500}/A_{1000}$, where A is the area under the Raman band), the glass composition and the processing temperature are well documented.[21–27]

In the Raman spectrum of the glaze of the Mapungubwe shard [Fig. 4(a)], the first peak around 500 cm^{-1} is obviously more intense than the peak around 1000 cm^{-1} and indicates a highly connected structure of SiO_4 tetrahedra. The average value of $I_p = 1.6$ for the glaze of the Mapungubwe shard places it in the same category as Vietnamese porcelain glazes, which according to the graphs in Refs 21–27 is a phase between Vietnamese calcium rich celadon glazes, with $I_p \approx 1.2$, and hard-paste porcelain glazes ($2.7 < I_p < 7$). It has been shown that the composition of Chinese Southern Song celadon glazes is very similar to that of their Vietnamese counterparts and in both cases CaO (~10%) was used as chief fluxing agent. Although exceptions are, of course, possible it would seem that the Mapungubwe shard's index of polymerization does not exactly match that of the relatively Ca-rich ancient Vietnamese (or Southern Song) glazes, but

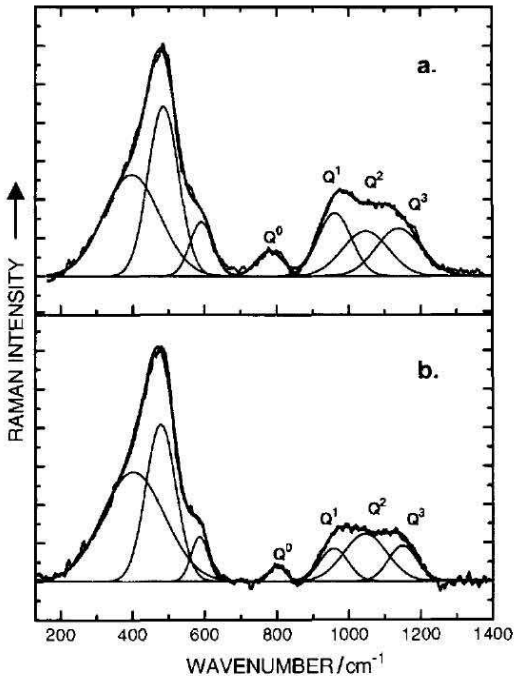

Figure 4. Spectra recorded of the glaze: (a) shard; (b) spouted vessel.

rather a transition stage between glazes with Ca as main fluxing agent and feldspathic glazes with potassium as chief fluxing agent. Parallel evolution in time to glazes relatively richer in $K_2O + Na_2O$ and lower in CaO occurred in both China and Vietnam.

Spectra recorded of the glaze of the spouted vessel [Fig. 4(b)] are very similar to that obtained for the shards and have an average $I_p = 2.6$, which is just below the I_p of modern hard-paste porcelain glazes.

The different components of the stretching envelope of porcelain glazes were assigned in the literature to silica vibrations with zero (Q^0 or isolated SiO_4, ca 800–850 cm^{-1}), one (Q^1 or Si_2O_7 groups, ca 950 cm^{-1}), two (Q^2 or silicate chains), three (Q^3 or sheet-like region, ca 1100 cm^{-1}) and four (Q^4, SiO_2 and tectosilicates, ca 1150–1250 cm^{-1}) bridging oxygens per tetrahedral group. We did not differentiate between Q^3 and Q^4 components and the positions of the deconvoluted peaks of the glaze spectra of the shard and the spouted vessel are compared in Table 3. The positions conform to the expected values for silica-based glazes. Q^1 has the highest intensity in the glaze of the shard [Fig. 4(a)] with

Table 3. Positions of the components (wavenumbers/cm^{-1}) of the stretching envelope in the Raman spectra of the glazes of the shard and spouted vessel

	Q^0	Q^1	Q^2	Q^3–Q^4
Mapungubwe shard	780	961	1047	1139
Teapot	800	957	1045	1148

Q^3–Q^4 the least intense and in this resembles that of Ca-rich celadon glazes of Vietnam. In the stretching envelope of the glaze of the spouted vessel Q^2 is the most intense component [Fig. 4(b)], which is also the case for the glazes of modern hard paste porcelains. The Q^1 and Q^3–Q^4 components are slightly more intense than for the modern high-temperature glazes and this result is supportive of the classification of the glaze as an intermediate composition between Vietnamese Ca-rich celadon glaze and K-feldspar glaze fired at higher temperatures.

The Raman spectra recorded of the glazes of the Mapungubwe shard and the spouted vessel classified it as belonging to a family of glazes between Ca-rich glazes and glazes of modern hard-paste porcelains. It indicates that both the shard and spouted vessel may have been manufactured at a later stage than their official museum classifications. This result motivated us to also analyse the shard with other analytical methods, namely XRD and XRF spectroscopy.

XRD

XRD measurements are supportive to the information obtained with Raman spectroscopy, as it also gives an indication of the relative quantity of a specific phase present within a material. Only the shard could be studied owing to size restrictions of the sample holder. Glassy (amorphous) phases cannot be identified by XRD and therefore, although the glaze was analysed, no usable results were obtained.

In Fig. 5 the diffraction pattern of the body of the shard is presented. The peaks of the main components are indicated as α-quartz (Q) and mullite (M). The mullite peaks largely overlap with those of sillimanite, a precursor to the formation of mullite. Raman data, however, confirmed the presence of mullite and therefore only mullite peaks are indicated in Fig. 5. The ratio of the highest mullite peak (d = 3.39 Å) to the most intense peak of quartz (d = 3.34 Å) is 0.26 and resembles that attributed to porcelain of the Qing dynasty produced in Jingdezhen.[37] The small percentage of mullite present is supportive of the fact that the shards originate from southern China, rather than northern China, as the raw materials used in northern China were rich in kaolin and would result in higher percentages of mullite.[38]

Traces of corundum, K-feldspar, plagioclase feldspar and iron may be present, as indicated in Fig. 5. All of these minerals are typical of Chinese raw materials and support the Chinese origin of the celadon. The elemental iron detected is in accordance with the greyish tone of the body.

XRF spectroscopy

XRF has become one of the major techniques used in the study of porcelain, as it non-destructively determines the percentage of the major oxides present in the porcelain body and glaze.[39–41]

The spouted vessel could not be analysed with our current experimental setup. In Table 4, the main oxide compositions of two of the Mapungubwe shards are compared with those of the Longquan celadon glazes originating from the Five Dynasties to the Ming period.[28] The small difference in quantitative analyses on the two Mapungubwe shards could be ascribed to different orientations of the pieces in the spectrometer and thus more of the porcelain body analysed in the one and more glaze in the other. The Uniquant 5 software includes algorithms for irregularly shaped or small

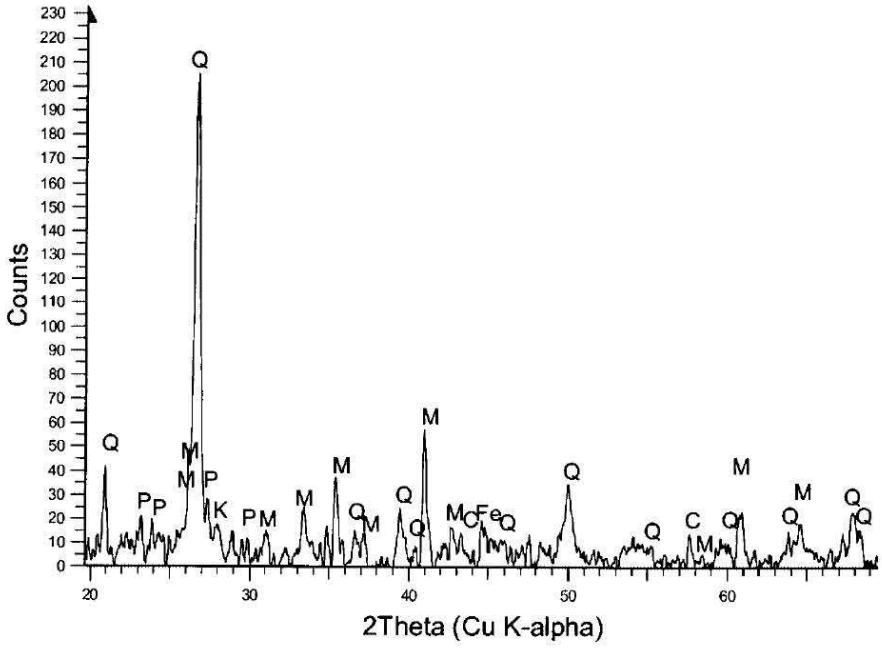

Figure 5. X-ray diffraction trace. Q = quartz, M = mullite, Fe = iron, P = plagioclase feldspar, K = K-feldspar, C = corundum.

Table 4. Comparison of the XRF glaze analysis of the Mapungubwe sample with Longquan celadon glazes (wt%)

	SiO_2	Al_2O_3	TiO_2	Fe_2O_3	CaO	MgO	K_2O	Na_2O	MnO	P_2O_5
Five Dynasties[a]	59.4	16.0	0.4	1.8	16.0	2.0	3.4	0.3	0.6	–
Northern Song[a]	63.2	16.8	0.2	1.4	13.0	1.1	3.3	0.6	0.4	–
Southern Song[a]	68.6	14.3	0.02	0.7	10.4	0.4	5.0	0.1	–	0.14
Yuan[a]	67.4	16.7	0.2	1.5	6.8	0.6	5.5	1.1	0.4	–
Ming[a]	67.6	15.0	0.3	1.4	6.3	1.7	6.5	1.1	–	–
Mapungubwe shard A	67.1	15.7	0.2	2.63	4.37	1.22	6.53	0.82	0.22	0.44
Mapungubwe shard B	68.19	15.72	0.13	2.03	4.48	0.52	6.98	0.994	0.189	0.40

[a] Ref. 28.

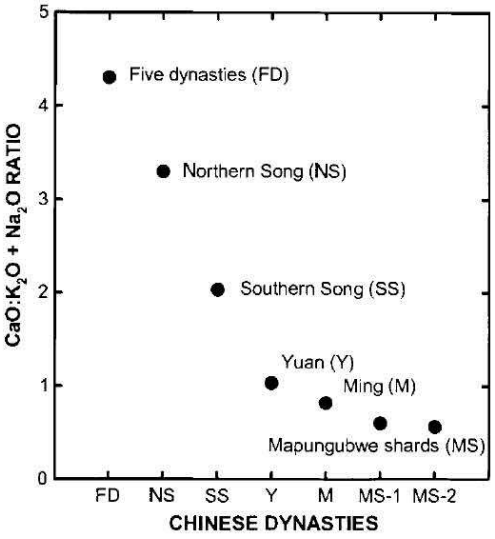

Figure 6. Comparison of the CaO:K_2O ratio of Chinese celadon glazes from Five Dynasties to Ming.

samples, but in some of these cases the samples were irregularly shaped and small and the number of unknowns tested the software's resolving power. It is obvious that the main oxide composition of the glaze of the Mapungubwe shard closely resembles that of a glaze from the Yuan or early Ming period, rather than that of the Song dynasty (Table 4). The main difference is the CaO:$K_2O + Na_2O$ ratio, which decreased with advancing centuries (Fig. 6), whereas the Al_2O_3 and SiO contents show only small variations (Table 4). A similar evolution (decrease in CaO content) was observed in Vietnamese celadon, but in a smaller time range (12–15th centuries), as illustrated in Fig. 1 of Ref. 20.

The potassium oxide concentration in the glaze is much higher than in hydromica, which was the main source of the potassium oxide in the porcelains of southern China. Chinese researchers believe that the additional potassium was derived from wood ashes fairly rich in potassium oxide and/or from the use of less weathered glaze stones that contained some primary potash feldspar.[42]

The P_2O_5 content of the glazes examined may suggest the former. The presence of relatively high levels of P_2O_5, MgO and MnO usually shows that plant ash has been part of the glaze recipe to supply CaO, as plant ash is rich in these compounds whereas limestones and calcium-bearing clays are not.[28]

Impact on the chronology of the pre-history of southern Africa

The Raman and XRF data suggest that the Mapungubwe shard was possibly manufactured at a later date than previously assumed. This result is extremely important for the chronological history of sub-Saharan Africa as the current opinion is that the last occupation date of Mapungubwe hill is 1280 AD.[43,44] According to carbon dating of Mapungubwe and Great Zimbabwe, it has been stated that the initial growth of Great Zimbabwe as a major centre can be firmly placed to the third quarter of the 13th century, after Mapungubwe's decline.[43]

Celadon shards manufactured in the Yuan or early Ming dynasty, buried in the occupation levels on the hill, suggest that the last occupation of Mapungubwe could be later than currently believed.

XRF results from shards excavated at Great Zimbabwe

The results obtained from the Mapungubwe shard motivated us to initiate a study on other shards excavated at related southern African Iron Age sites for comparative purposes. A few celadon shards excavated at Great Zimbabwe (purchased from Hall[10] and presented to the South African Museum in 1894 by the British South African Company) were analysed with XRF and the results are summarized in Table 5. It is clear that there is a difference in CaO:$K_2O + Na_2O$ ratio between these shards and the Mapungubwe shard. Assigning the shards to a specific dynasty is not straightforward. The maturing temperatures of ceramic glazes are dependent on the total of all the oxides used as fluxing agents, in particular the four oxides CaO, MgO, K_2O and Na_2O, which for Longquan celadon glazes are the main fluxing agents. In Fig. 7, the total fluxing contents in Longquan celadon glazes from the Five Dynasties to early Ming[45] are compared with those of the Mapungubwe and Great Zimbabwe glazes. On this score the Mapungubwe glazes seem higher firing than the Great Zimbabwe shards and much more in the style of the Yuan–Ming range at Longquan. From this view, the Great Zimbabwe shards seem closer to Southern Song examples.

Table 5. Comparison of the XRF glaze analysis of the Mapungubwe sample with the glazes of samples excavated at Great Zimbabwe, (wt%)

	SiO_2	Al_2O_3	TiO_2	Fe_2O_3	CaO	MgO	K_2O	Na_2O	MnO	P_2O_5
Mapungubwe shard A	67.1	15.7	0.2	2.63	4.37	1.22	6.53	0.82	0.22	0.44
Mapungubwe shard B	68.19	15.72	0.13	2.03	4.48	0.52	6.98	0.994	0.189	0.40
Great Zimbabwe 669A	62.01	15.96	0.11	1.49	10.87	0.73	5.66	0.81	0.41	1.17
Great Zimbabwe 669B	64.00	15.58	0.09	1.33	10.30	0.58	5.85	0.75	0.37	0.64
Great Zimbabwe 669C	60.25	17.89	0.15	1.83	10.23	0.78	5.65	0.80	0.63	0.99
Great Zimbabwe 669D	63.28	15.93	0.13	1.92	8.07	0.89	6.53	0.99	0.56	1.11
Great Zimbabwe 7890	64.17	14.19	0.12	2.34	9.19	0.58	5.97	1.50	0.31	0.49

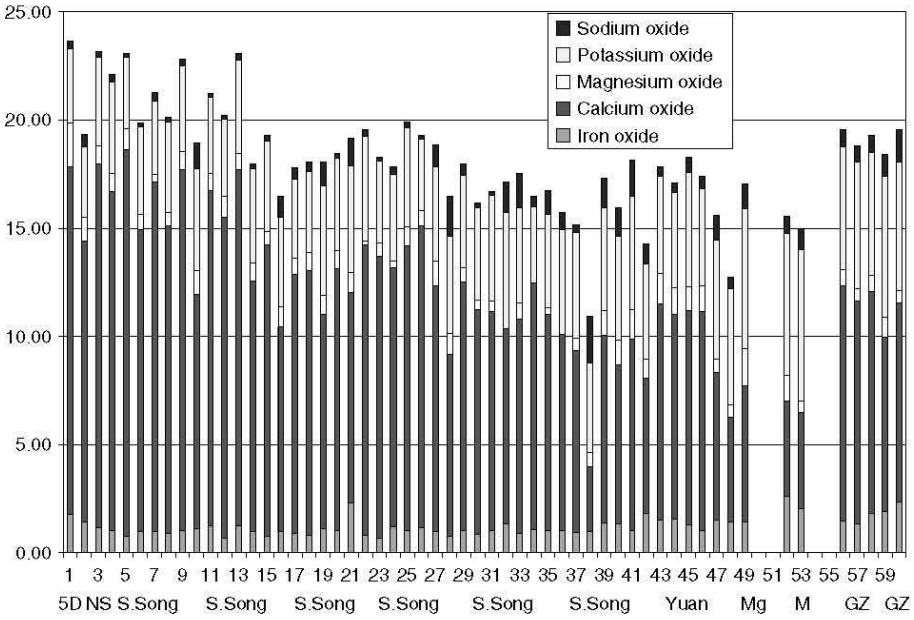

Figure 7. Totalled potassium + sodium oxide levels in Longquan celadon glazes (wt%). Five Dynasties to early Ming. Includes Mapungubwe (M) and Great Zimbabwe (GZ) shards.

However, the $K_2O + Na_2O$ levels in the Great Zimbabwe shards are very much of the Yuan–Ming trend, which is more significant (Fig. 8). The high alkali metal content in the Great Zimbabwe shards is more important than their CaO levels, and perhaps indicative of a Yuan–Early Ming production date at Longquan.[45] This is in contrast to the current literature classification of most of the shards excavated at Great Zimbabwe as entirely Ming.[8]

CONCLUSION

Comparison of the Raman spectra of the glaze of the Mapungubwe shard with literature values made it possible to link the firing temperature and composition of the glaze to a later manufacturing date than previously assumed. In this we illustrated the intrinsic value of the systematic classification of the composition of porcelain glazes according to their Raman spectra undertaken by Colomban and co-workers. The validity of the Raman analysis was confirmed by the oxide composition of the glaze as determined with XRF spectroscopy. Relating this result to manufacturing processes in ancient China was only possible with the help of recent research on Chinese ceramics, which resulted in accurate databases.[28,45]

These results suggest that the manufacturing time of the shard may have been the Yuan or early Ming dynasty rather than the Southern Song. Regina Krahl, Chinese ceramic expert, classified the shards according to their appearance as 14th-century Yuan (R. Krahl, personal communication). This too differs from the results of the seven carbon dates obtained from material from Mapungubwe hill, which dates the last occupation of the hill as 1280 AD, and coincides with the end of the Southern Song dynasty.[39,40] The small sampling size of the carbon dating, and the fact that the calibration curve used in the dating process at this period of time is rather ambiguous, have motivated a project, to be undertaken by

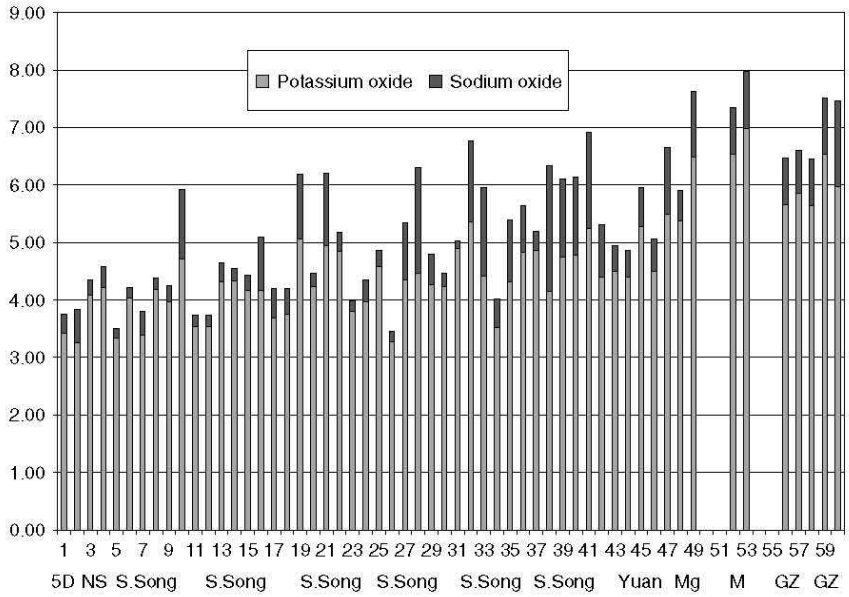

Figure 8. Totalled flux contents in Longquan celadon glazes (wt%). Five Dynasties to early Ming. Includes Mapungubwe (M) and Great Zimbabwe (GZ) shards.

the Quaternary Dating Unit of the CSIR, Pretoria, to obtain additional carbon dates from Mapungubwe hill.

The Raman spectra of the glaze of the spouted vessel suggest that the museum classification might be reconsidered. In the light of the extensive research undertaken since the 1970s at Chinese kiln sites and improvement of non-destructive techniques to analyse museum objects, a project has been initiated to classify all of the objects in the Van Tilburg Collection with more modern methods.

The celadon shards found at Mapungubwe are related to all the imported ceramics excavated at other Iron Age inland sites, and also the African east coast. Therefore, we have initiated a project to study all of these imported ceramics and glass beads with modern analytical methods. The preliminary results from this study, presented in this paper (Table 3), of a few shards excavated at Great Zimbabwe, confirmed that dating the shards with greater accuracy and objectivity would provide supplementary data to obtain a fuller picture of the chronology of trade along the East African coast.

Acknowledgements

The authors thank Iziko Museums of Cape Town (incorporating the South African Museum) for the loan of the shards from their collection. We also thank A. E. Duffey, curator of the van Tilburg, Museum, University of Pretoria (UP), for comments on the manuscript, the Laboratory for Microscopy and Microanalysis, UP, for help with the photographs and the Chemistry Department, UP, for the use of the Raman instrument.

REFERENCES

1. Paver FR. *Illustrated London News* 1933; 8 April: 494.
2. Fouche L. *Mapungubwe: Ancient Bantu Civilization on the Limpopo*. Cambridge University Press: Cambridge, 1937; 1.
3. Meyer A. *The Archeological Sites of Greefswald, Stratigraphy and Chronology of the Sites and a History of Investigations*. V& R Printing Works: Pretoria, 1998; 203.
4. Chittick HN. In *The Peopling of the East African Coast East in Africa and the Orient: Cultural Syntheses in Pre-Colonial Times*, Chittick HN, Rotberg RL (eds). Holmes and Meier Publishers: New York, 1975; 1.
5. Chittick HN. *Kilwa, an Islamic Trading City on the East African Coast. 2. The Finds*. The British Institute in Eastern Africa, Memoir 5. Kenya Litho: Nairobi, 1974; 308.
6. Chittick HN. *Manda, Excavations at an Island Port on the Kenya Coast*. The British Institute in Eastern Africa, Memoir 9. Oxford University Press: Oxford, 1984; 65.
7. Kirkman J. In *Studies in African History*, Stahl KM (ed). Mouton: The Hague, 1963; 45.
8. Garlake PS. *J. Afr. History* 1968; **9**(1): 13.
9. Caton Thompson G. *The Zimbabwe Culture: Ruins and Reactions*. Frank Cass: London, 1971; 185.
10. Hall RN. *Pre-historic Rhodesia*. T. Fisher Unwin: London, 1909; 237.
11. Horton M. *Shanga: the Archaeology of a Muslim Trading Community in the Coast of East Africa*. The British Institute in Eastern Africa, Memoir 14. London, 1996; 303.
12. Hobson RL. *Chinese Pottery and Porcelain, an Account of the Potters Art in China from Primitive Times to the Present Day. Vol. 1, Pottery and Early Wares*. Cassell: London, 1915; 76.
13. Meyer A, Esterhuizen V. *S. Afr. J. Ethnol.* 1994; **17**(3): 103.
14. Zoppi A, Lufrumento C, Castellucci EM, Migliorini MG. *Spectrosc. Eur.* 2002; **14**(5): 17.
15. Sakellariou K, Miliani C, Morresi A, Ombelli M. *J. Raman Spectrosc.* 2004; **35**: 61.
16. Colomban Ph, Milande V, Lucas H. *J. Raman Spectrosc.* 2004; **35**: 68.
17. Colomban Ph, Treppoz F. *J. Raman Spectrosc.* 2001; **32**: 93.
18. Colomban Ph, Sagon G, Faurel X. *J. Raman Spectrosc.* 2001; **32**: 351.

19. Liem NQ, Thanh NT, Colomban Ph. *J. Raman Spectrosc.* 2002; **33**: 287.
20. Liem NQ, Sagon G, Quang VX, Tan HV, Colomban Ph. *J. Raman Spectrosc.* 2000; **31**: 933.
21. Colomban Ph, March G, Mazerolles L, Karmous T, Ayed N, Ennabli A, Slim H. *J. Raman Spectrosc.* 2003; **34**: 205.
22. Colomban Ph. *J. Non-Cryst. Solids* 2003; **323**: 180.
23. Colomban Ph, Liem NQ, Sagon G, Tinh HX, Hoành TB. *J. Cult. Heritage* 2003; **4**: 187.
24. Milande V, Le Bihan L. *J. Raman Spectrosc.* 2004; **35**: 527.
25. Colomban Ph, Truong C. *J. Raman Spectrosc.* 2004; **35**: 195.
26. Colomban Ph, Sagon G, Huy LQ, Liem NQ, Mazerolles L. *Archeometry* 2004; **46**: 125.
27. Colomban Ph. In *Proceedings of CIEC 9, 9th European Interregional Conference on Ceramics, Bardonecchia, Italy*, Negro D, Montanaro L (eds), AIMAT – Polytecnicum di Torino, 2004; 6–14.
28. Wood N. *Chinese Glazes*. A&C Black: London, 1999; 27.
29. Wood N. In *Taoci No. 1. Revue Annuelle de la Société Française d'Étude de la Céramique Orientale, Actes du Colloque ''Le 'Bleu et Blanc' du Proche-Orient à la Chine.''* Monique Crick: Paris, 2000; 15.
30. McMillan P, Pitiou B. *J. Non-Cryst. Solids* 1982; **53**: 279.
31. Kerr R, Wood N. In *Joseph Needham: Science and Civilisation in China. Volume 5, Chemistry and Chemical Technology: Part 12 – Ceramic Technology*, Needham J, Cullen C (eds). Cambridge University Press: Cambridge, 2004; 347.
32. Gotić M, Ivanda M, Popović S, Musić S, Sekulić A, Turković A, Furić K. *J. Raman Spectrosc.* 1997; **28**: 555.
33. Huang PJ, Chang H, Yeh CT, Tsai CW. *Thermochim. Acta* 1997; **297**: 85.
34. Hu Y, Tsai HL, Huang CL. *J. Eur. Ceram. Soc.* 2003; **23**: 691.
35. Gouma PI, Mills MJ. *J. Am. Ceram. Soc.* 2001; **84**: 619.
36. Okada K, Yamamota N, Kameshima Y, Yasumori A, Mackenzie KJD. *J. Am. Ceram. Soc.* 2001; **84**: 1591.
37. Leung PL, Yang B. *Nucl. Instrum. Methods Phys. Res. B* 1999; **155**: 452.
38. Sundius N, Steger W. 1963. In *Sung Sherds*, Palmgren N, Sundius N, Steger W (eds). Esselte: Stockholm, 1963; 375.
39. Wu J, Leung PL, Li JZ, Stokes MJ, Li MTW. *X-Ray Spectrom.* 2000; **29**: 239.
40. Yu KN, Miao JM. *Appl. Radiat. Isot.* 1997; **48**: 959.
41. Wu J, Leung PL, Li JZ, Stokes MJ, Li MTW. *X-Ray Spectrom.* 2000; **29**: 253.
42. Zhou R, Zhang F, Cheng Y. 1973; 'Technical studies on Lung-ch'üan celadons of successive dynasties,' *Chinese Translations No. 7*, Proctor P (transl). Victoria and Albert Museum in association with the Oriental Ceramic Society: London, 1977; 16–18 (originally in K'ao-ku Hsüeh-pao. 1. 1973; 1: 131–156).
43. Huffman TN, Vogel JC. *S. Afr. Arch. Bull.* 1991; **46**: 61.
44. Vogel JC. In *The Archeological Sites of Greefswald, Stratigraphy and Chronology of the Sites and a History of Investigations*, Meyer A (ed). V& R Printing Works: Pretoria, 1998; 296.
45. Hongjie L. *Ancient Chinese Pottery and Porcelain Database*. Xi'an, 1996.

MAPUNGUBWE OBLATES CHAPTER 4

Only three celadon shards were excavated on Mapungubwe hill, but thousands of glass beads were found. Together with the gold beads and other gold artefacts excavated in the "royal" graves on the hill, it places the Mapungubwe excavations in the realm of great finds in Africa. Discovering the provenance of the beads will be a great advancement in recreating the pre-colonial history of South Africa and provide a better understanding of the origin of the African bead tradition.

Dr. Philippe Colomban and his research group have studied ancient artefacts (glasses, porcelain, enamels, etc) extensively and have accumulated databases of Raman spectra, representative of production technologies used in the Antique, European, Mediterranean, Islamic and Asian worlds. I used the procedures developed by his group to study the "Mapungubwe Oblates", which is the largest group of beads in the Mapungubwe collection. A detailed profile of the characteristics of the beads have been compiled, but so far the provenance could not be established, as the combination of all the characteristics does not exactly match any of the known bead technologies of the ancient world. We are continuing to analyse the other beads in the collection and plan to expand the study to other bead collections in Africa and hope eventually to discover the origin of the beads.

The work was presented as a poster at the *20th International Conference on Raman Spectroscopy* held in Yokohoma, Japan, 20-25 August 2006 and the full results published in the Journal of Raman Spectroscopy. It forms chapter 4.

Linda C Prinsloo and Philippe Colomban**, "**A Raman spectroscopic study of the Mapungubwe oblates; glass trade beads excavated at an Iron Age archaeological site in South Africa".

JOURNAL OF RAMAN SPECTROSCOPY
J. Raman Spectrosc. (2007)
Published online in Wiley InterScience
(www.interscience.wiley.com) DOI: 10.1002/jrs.1816

JRS

A Raman spectroscopic study of the Mapungubwe oblates: glass trade beads excavated at an Iron Age archaeological site in South Africa

Linda C. Prinsloo[1]* and Philippe Colomban[1,2]

[1] Department of Physics, University of Pretoria, Pretoria, South Africa
[2] Laboratoire Dynamique, Interactions et Réactivité (LADIR), UMR 7075 CNRS-Université Pierre et Marie Curie, 2 rue Henry Dunant, 94320 Thiais, France

Received 22 December 2006; Accepted 23 April 2007

Oblate seed beads (2–4 mm) excavated on Mapungubwe hill, an Iron Age site in South Africa, were analysed with Raman microscopy and supportive techniques to determine the glass technology and pigments used to produce the beads. The Raman spectra and XRF analysis of the beads classify the glass as a typical soda/lime/potash glass similar to Islamic glass from the 8th century (Ommayad), but with higher levels of aluminium, iron and magnesium. The turquoise, bright green, bright yellow and orange colours were obtained by utilizing a combination of cassiterite (SnO_2) and lead tin yellow type II ($PbSn_{1-x}Si_xO_3$). Doping with cobalt and manganese produced dark blue and plum-coloured beads. The Fe-S chromophore was detected through its resonance-enhanced spectrum in the black beads. Corrosion of the black beads was investigated and an organic phase detected on the beads, which might have influenced the corrosion process. This detailed profile of the glass technology used to produce the Mapungubwe oblates might eventually help to determine their provenance. Copyright © 2007 John Wiley & Sons, Ltd.

KEYWORDS: ancient glass trade beads; pigment identification; Fe-S chromophore

INTRODUCTION

In a recent study, the Raman spectra and XRF analysis of the glaze of Chinese celadon shards excavated on Mapungubwe Hill, an Iron Age site in South Africa, suggested that the shards were manufactured in a later century than the original classification.[1] In order to obtain supportive evidence for these results, which will have an impact on the chronology of the whole region, a Raman spectroscopic study of the glass trade beads, excavated at the same site was undertaken.

Mapungubwe is a small flat-topped sandstone plateau situated in the Limpopo valley close to the present-day borders of South Africa, Botswana and Zimbabwe. An ancient legend, suggesting certain death upon ascending the hill, helped to protect the last resting place of the rulers of a prehistoric African trade kingdom (~1000–1290 A.D.) for more than seven centuries until its discovery in 1933.[2]

Excavations on Mapungubwe hill during 1933–1940 exposed three 'royal' burials, in which gold funerary objects, gold beads and bangles were found together with imported glass beads. The sheer volume of beads recovered is staggering; from one burial alone 26 037 glass beads were counted, of which 24 808 were black. In comparison, the total number of beads excavated at Great Zimbabwe is 400 and at Manda, an island port on the Kenyan coast, 1150.[3,4] This makes the collection of the Mapungubwe beads, with an excavation time span from a Stone Age culture at bedrock to the time when the site was permanently abandoned (currently believed to be 1280 A.D.), invaluable. Furthermore, the central position of Mapungubwe hill, situated at the confluence of the Limpopo and Shashe rivers, made it from the earliest time accessible through old camel caravan routes to Egypt and the Mediterranean trade, and via the Limpopo river to the monsoon-based African east coast trade reaching as far as China. Furthermore, trade along the African west coast was accessible via the interior through Botswana and Angola, where Portuguese mariners traded in beads from Europe 150 years before they rounded the Cape of Storms and also dominated the African east coast trade.

Previous studies of the beads proposed that they were made in India, medieval Venice or Fustat, the Fatimid capital of Islamic Egypt (900–1250 A.D.).[5–14] Of special interest is a large number of beads, known as the Mapungubwe oblates

*Correspondence to: Linda C. Prinsloo, Department of Physics, University of Pretoria, Pretoria, South Africa.
E-mail: linda.prinsloo@up.ac.za

(Fig. 1), which have been shown to differ in appearance and chemical composition from beads excavated at other sites along the African east coast.[9,12–14]

It has been established that Raman spectroscopy is an excellent and non-destructive method to characterize glasses and porcelain glazes, as many features about the production process of the glass are encapsulated within a Raman spectrum.[15–19] Furthermore, Raman spectroscopy has been shown to greatly contribute to the understanding of the corrosion processes in historic glasses.[19–21]

In this paper we record the first results of our study of glass trade beads excavated on Mapungubwe hill and compare it with those obtained from different production technologies used in the Antique, European, Mediterranean, Islamic and Asian worlds.[17] In time we hope to extend our research to beads excavated at other inland sites such as Great Zimbabwe, sites along the African east and west coasts, as well as the heirloom beads of various African ethnic groups such as the Venda and Ndebele. In order to establish the provenance of these beads, comparison with beads excavated at possible sites of origin is of the utmost importance.

EXPERIMENTAL

Samples

Our first priority was to investigate the small seed beads (2–4 mm) excavated from the 'royal burials' on Mapungubwe hill and known as the Mapungubwe oblates. [Oblate beads have been reheated to the point at which the entire

Figure 1. (a) Mapungbwe oblates: from top to bottom: cobalt blue, orange, black, yellow, plum, turquoise and green. (b) Larger black beads. (c) Corroded black beads.

DOI: 10.1002/jrs

length of the bead has a smoothly rounded profile. Length must be less than diameter (from Ref. 13) (Fig. 1(a))]. The brilliantly coloured beads (cobalt, blue, orange, black, yellow, plum turquoise and green) were manufactured by the drawn method, usually associated with mass-produced beads. The ends were reheated and the glass is of a good quality without large bubbles.

Mixed in between the huge number of black beads were larger black beads, some cylindrical shaped and some round or oblate (Fig. 1(b)). These were also included in the study, as well as two black glass samples from glass-making sites around the Indian Ocean, (Arikamedu, India, and Giribawa, Sri Lanka) for comparative purposes.

Experimental techniques

A multichannel notch-filtered INFINITY spectrograph (Jobin-Yvon-Horiba SAS, Longjumeau, France) equipped with a Peltier-cooled CCD matrix was used to record Raman spectra using 532 nm and 633 nm as excitation wavelengths. Some spectra were recorded with an XY Raman spectrometer from Dilor (liquid-nitrogen-cooled CCD), using the 514.5 nm (Coherent Innova 90 Ar^+-laser) and 568 nm (Spectra-Physics krypton laser) lines as exciting radiation. In both cases collection of the scattered light in the backscattering geometry was made through an Olympus confocal microscope with either a long distance ×50 or ×100 microscope objective. Optimum recording conditions were obtained by varying laser power (<10 mW at sample), microscope objective and size of the confocal hole. A few spectra were also recorded in the macro configuration of a Dilor XY instrument with the 406.7 nm line of a Kr^+ laser.

Mid-infrared transmission spectra were recorded of powdered samples pressed into KBr pellets (1 mg sample/100 mg KBr) using a Bruker 113v Fourier transform infrared (FTIR) spectrometer. The resolution was 2 cm^{-1} and 32 scans were signal-averaged in each interferogram.

The chemical composition of the Mapungubwe oblates was determined with X-ray fluorescence (XRF) spectroscopy. A Sufficient number of beads (60–80) of each colour were selected to cover the bottom of a liquid sample holder and introduced into the ARL 9400XP+ wavelength dispersive XRF spectrometer. Analyses were executed using the UniQuant 5 software program, specifying the weight and area of the sample. The software analyses for all elements between F and U and only elements above the detection limits are reported.

SEM-EDS was used to determine the elemental composition of individual beads. A Jeol 5800 LV scanning electron microscope combined with a Vantage EDS analytical system with an accelerating voltage of 20 kV was used. The beads were coated with a 10 nm gold coating to create conductive surfaces.

The OriginPro 7.5 peak-fitting module was used to fit Gaussian peaks to the Raman spectra according the method previously described. A constraint of full width at half-maximum (FWHM)<100 was placed on all peaks, except for the Lorentzian peak defined at 980 cm^{-1} with a fixed FWHM at 20 cm^{-1} and previously assigned to the signature of calcium-rich 'crystalline' nanoprecipitates.

RESULTS AND DISCUSSION

Characterization of the Mapungubwe oblate glass

The Raman spectrum of the amorphous phase of a glass consists of two broad bands around 500 and 1000 cm^{-1}. The band at ~500 cm^{-1} originates from the ν_2 bending vibrations of isolated SiO_4 tetrahedra and the one at ~1000 cm^{-1} from the coupled ν_1 and ν_3 Si–O stretching vibrations. In highly connected tetrahedral structures the band representing the bending modes have a high Raman intensity, and in weakly connected tetrahedral units, as caused by the addition of fluxing (ionic) agents, the intensity of this band decreases and the band representing the stretching modes becomes more intense. The relationship between the Raman index of polymerization ($I_p = A_{500}/A_{1000}$ with A being the area under the Raman band), the glass composition and the processing temperature is well documented.[15–17]

In Fig. 2 the spectra of the glass of the Mapungubwe oblates are presented and it is clear that the spectra have more or less the same shape. In order to make a

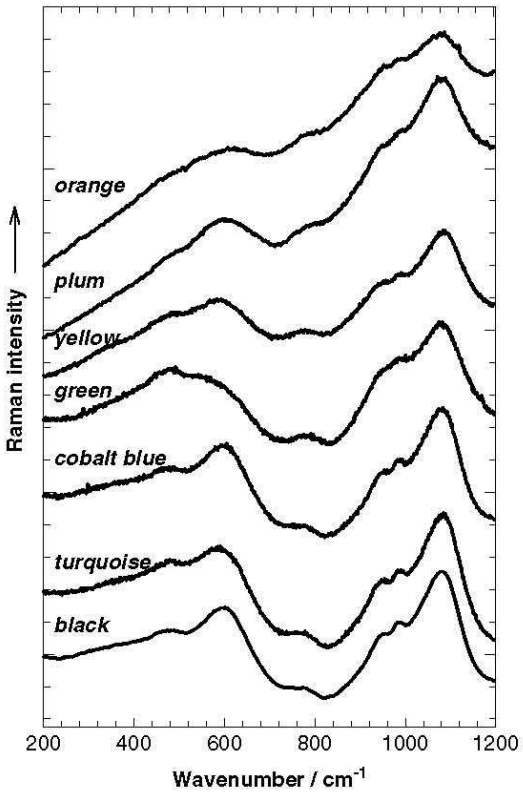

Figure 2. Raman spectra of the Mapungubwe oblates according to colour.

more detailed comparison between the spectra, a four-point baseline was subtracted from each spectrum as previously described.[15–17] The calculated polymerization index (I_p) of all the colours glass ($0.75 < I_p < 0.99$) classifies it as a typical soda/lime/potash glass, in the same category as Saljukids (11–13th century), Kutahya (17th century), Omayyads (8th century) or Phoenician/Roman glass.[17]

This is in agreement with the XRF results presented in Table 1A, which in Table 1B is reduced to the seven major oxides (normalized to 100% to remove the contribution of most pigments and other additives from the major glass composition), commonly used to facilitate the comparison between different glass types. It is very clear that the same basic glass recipe was used to produce all the beads (SiO_2 ~66%, Na_2O ~10%, Al_2O_3 ~9%, CaO ~5%, K_2O ~4% and MgO ~3%).

The different components of the stretching envelope of porcelain glazes were assigned in the literature to silica vibrations with zero (Q^0, 800–850 cm^{-1}), one (Q^1, ~950 cm^{-1}), two (Q^2, ~ 1020–1040 cm^{-1}), three (Q^3, ~1100 cm^{-1}) and four (Q^4, ~1150–1250 cm^{-1}) bridging oxygens per tetrahedral group. It has been shown that the position and relative ratio of the area under each peak can be used to differentiate further between closely related technologies and therefore a peak-fitting procedure (see 'Experimental Techniques') was applied to all the spectra to extract these parameters for each glass colour.[17] The results are summarized in Table 2 and an example of the fitting procedure (yellow glass) is shown in Fig. 3. It is evident from the table that the Mapungubwe oblates form a clearly defined group with very similar Raman parameters in accordance with their related chemical compositions.

The envelope maxima of the Si–O stretches at ~1090 cm^{-1} for all the colours refines the classification according to the polymerization index to Omayyad glass from the 8th century and the basic glass recipe is part of group 3 ('$Na_2O + K_2O + CaO$' glass), as defined in Ref. 17. However, a closer look at Table 2 lifts out other differences between the Raman parameters, such as $A\nu\,Q_2/A\nu\,Q_1 = 0.25$ for Omayyad glass, but $0.60 < A\nu Q_2/A\nu Q_1 < 0.94$ for the Mapungubwe oblate glass and is therefore not an exact fit. This is verified by the compositional analysis of the glass (Table 1) as the Mapungubwe oblate glass has higher concentrations of aluminium, iron, magnesium and potassium than Omayyad glass[17]; this supports the continuous effort that is being made to increase the scope of the database.

Pigments

The craft of colouring glass has been practiced since antiquity, although it was initially limited to essentially the blue and

Table 1A. XRF analysis of the Mapungubwe oblate beads

wt%	Black	Green	Yellow	Plum	Cobalt	Turquoise	Orange
SiO_2	61.71	58.90	56.34	60.96	65.46	61.99	53.57
Na_2O	10.36	8.54	9.44	11.44	10.14	9.84	8.17
Al_2O_3	8.97	7.52	7.57	8.43	8.22	8.58	7.9
CaO	6.24	4.30	3.78	5.11	4.72	4.38	4.03
K_2O	4.27	3.67	3.81	4.08	3.77	3.87	3.03
PbO	0.08	[a]7.82	[a]6.93	[a]0.46	0.01	[a]0.91	[a]9.52
SnO_2	0.05	[a]2.34	[a]1.66	[a]0.15	0.01	[a]2.54	[a]2.21
MgO	3.85	2.37	2.50	3.97	2.87	2.73	2.93
Fe_2O_3	1.50	1.53	1.48	1.54	[a]2.08	1.59	1.28
Cl	0.95	0.53	0.71	0.60	0.67	0.73	0.51
P_2O_5	0.89	0.55	0.57	0.53	0.83	0.72	0.7
SO_3	[a]0.31	0.18	<0.01	0.27	0.21	0.23	<0.01
Co_3O_4	<0.01	<0.01	<0.01	<0.01	[a]0.17	0.01	0.01
TiO_2	0.25	0.26	0.31	0.25	0.27	0.29	0.24
S	[a]0.10	<0.01	<0.01	<0.01	<0.01	<0.01	<0.01
CuO	0.10	[a]1.04	0.05	0.03	0.01	[a]1.23	0.08
BaO	0.10	0.08	[a]0.24	0.14	0.10	0.09	[a]0.20
MnO	0.08	0.07	[a]0.37	[a]1.80	0.06	0.06	[a]0.54
As_2O_3	<0.01	<0.01	<0.01	<0.01	[a]0.21	0.01	0.07
SrO	0.07	0.05	0.07	0.01	0.07	<0.01	0.06
ZrO_2	0.02	0.02	0.03	0.02	0.02	0.02	0.03
ZnO	0.02	[a]0.13	0.04	0.05	0.02	0.05	[a]0.72
U_3O_8	<0.01	<0.01	0.02	<0.01	<0.01	<0.01	0.03
NiO	<0.01	0.01	<0.01	<0.01	<0.01	0.01	0.02

[a] Chemicals used as pigments.

Table 1B. Normalised compositions of the seven major oxides of the Mapungubwe oblate beads

wt%	Black	Green	Yellow	Plum	Cobalt	Turquoise	Orange
SiO_2	63.7	67.8	66.3	63.8	67.3	66.7	66.2
Na_2O	10.7	9.8	11.1	12.0	10.4	10.6	10.1
Al_2O_3	9.3	8.7	8.9	8.8	8.5	9.2	9.8
CaO	6.4	5.0	4.7	5.3	4.9	4.7	5.0
K_2O	4.4	4.2	4.5	4.3	3.9	4.2	3.7
MgO	[a]4.0	2.7	2.9	[a]4.2	3.0	2.9	3.7
Fe_2O_3	1.5	1.8	1.7	1.6	[a]2.1	1.7	1.6

[a] Chemicals used as pigments.

Table 2. Main Raman parameters of the Mapungubwe oblates according to colour

Sample	I_p	νQ_0	νQ_1	νQ_2	νQ_3	νQ_4	$A\nu Q_0$	$A\nu Q_1$	$A\nu Q_2$	$A\nu Q_3$	$A\nu Q_4$	$A\nu Q_2$/ $A\nu Q_3$	$A\nu Q_2$/ $A\nu Q_1$
Black	0.83	781	949	1026	1083	1104	0.5	13.8	12.7	16.9	9.7	0.75	0.92
Green	0.75	785	953	1023	1083	1125	1.0	17.5	11.3	17.7	9.3	0.64	0.65
Yellow	0.78	783	944	1021	1089	1114	0.8	14.2	13.3	17.1	10.8	0.78	0.94
Plum	0.72	780	957	1037	1087	1129	0.5	19.6	11.7	20.0	5.5	0.60	0.60
Cobalt	0.80	785	961	1038	1089	1129	0.8	15.9	9.1	19.3	9.9	0.47	0.57
Turquoise	0.76	780	947	1026	1087	1114	0.7	14.6	12.2	18.2	10.4	0.67	0.84
Orange	0.74	784	953	1036	1091	1119	1.0	18.0	11.1	20.5	5.9	0.54	0.62

Ip, index of polymerization; Q_n, centre of gravity wavenumber (in cm^{-1}) of the Si–O stretching Q_n component; AQ_n, component area (% of the total peak area).

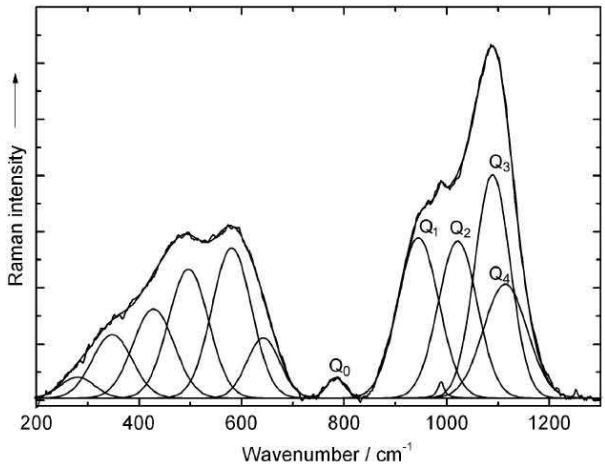

Figure 3. Example of the peak-fitting procedure applied to yellow glass.

green colours. The Mapungubwe oblates display a varied colour palette, indicating quite a high degree of chemical engineering competence, because colouring is dependent on the composition of the basic glass, as well as the nature and composition of the colouring substance.[22] The technology involved in colouring a glass and the pigments used may give an indication of where the glass was produced. Complicating the issue, though, is the fact that pigment ores (e.g. cobalt ores), as well as glass cullet, were exported all over the world to secondary glass working sites.

The Raman spectra of the pigments/opacifiers used to obtain the Mapungubwe oblate colour palette (Fig. 1(a)) are presented in Fig. 4. Spectra of the pure pigments could be obtained from some samples by focussing the laser beam on small crystallites, which were visible within the glassy matrix using the ×100 objective of the microscope.

The well-known spectrum of the anatase phase of TiO_2 (Fig. 4(a)) was recorded on many of the beads and correlates with the XRF measurements (Table 1), which determined the presence of ~0.25% TiO_2 in all the glass beads under study. The rutile phase was not detected in any of the spectra. Although TiO_2 is not a pigment as such but an opacifier, its presence together with that of iron (present in all the samples, Table 1) can be used by varying the Fe : Ti ratio, firing temperature and oxidation conditions to obtain a large variety of differently coloured glasses as richly illustrated in the celadon glazes of Chinese potters.[23]

The turquoise, bright green, bright yellow and orange colours were obtained by utilizing a combination of cassiterite (SnO_2) and lead tin yellow type II ($PbSn_{1-x}Si_xO_3$). The very strong characteristic peak of cassiterite at 630 cm^{-1} was observed in the Raman spectra of the bright green and turquoise beads (Fig. 4(b) and (c)) and the spectrum of lead tin yellow type II, with characteristic strong peak at 137 cm^{-1}

DOI: 10.1002/jrs

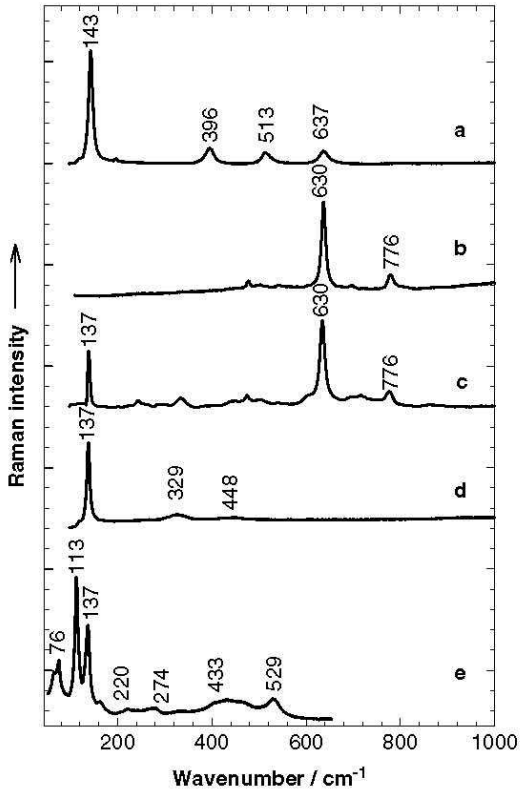

Figure 4. Raman spectra of pigments/opacifiers: (a) TiO_2 anatase, (b) cassiterite (c) cassiterite and lead tin yellow type II (d) Lead tin yellow type II (e) lead tin yellow type II and red lead.

was identified on the yellow and green beads (Fig. 4(c) and (d)).[24] Lead-tin oxides have been employed since antiquity as a yellow pigment and opacifier.[25] In Table 3 the Pb/Sn ratio for each colour bead is given. In conjunction with Table 1 the variation in the ratio of lead tin yellow type II and cassiterite to obtain a large variation in colours and opacity can be deducted. CuO (1.04 wt%) and ZnO (0.13 wt%) were added to the basic yellow glass recipe to obtain the green colour, while the turquoise colour was obtained by adding CuO (1.25 wt%), a small presentation of lead tin yellow type II and cassiterite as opacifier. Copper in its oxidized state (Cu^{2+}) is responsible for a fine turquoise-blue (for glazes/glasses with sodium and potassium as main fluxing ions[23]) or green (in transparent lead, lime and lime-alkali glazes/glasses[23]) colour in glasses and as it completely dissolves in the melt it cannot be observed with Raman spectroscopy. The combination of Cu (blue for the sodium-potassium-calcium glass) and lead tin yellow type II to obtain a green colour has also been observed in green glass beads excavated in Sri Lanka.[18]

In the spectrum of the orange bead, Raman bands originating from lead tin yellow type II can also be distinguished, but in addition a very strong signal at 113 cm^{-1} and a peak at 529 cm^{-1} are observed (Fig. 4(e)). In Table 3 it can be seen that, in comparison with the yellow glass, the lead:tin ratio for the orange glass is higher,

Table 3. Lead: tin ratio

Sample	Pb	Sn	Pb/Sn
Black	0.1	–	–
Green	7.3	1.9	3.8
Yellow	6.4	1.3	4.9
Plum	0.4	0.1	4
Cobalt blue	–	–	–
Turquoise	0.8	2.0	0.4
Orange	8.8	1.7	5.2

and as the extra peaks occur at wavenumbers very near to that of red lead oxide, it can be deducted that it was incorporated into the lead tin yellow pigment to modify the colour to orange. A similar spectrum has previously been reported in Islamic ceramics from Dougga in Ifriqiya, one sample dating from the 11–12th century (Ziridos period), the other from the 17–18th century (Ottoman period).[26] Furthermore, in Table 1 it can be seen that Zn has been added to the pigment mixture of the orange beads. In a collection of 18–19th century *anime* (semi-finished glass used as opacifier–colourant in other transparent glasses) recipe collections from the Darduin family, Murano, Italy, the addition of zinc to lead-antimonate-tin yellow pigments to obtain the required shade of yellow or orange in glass has been documented. In reconstruction experiments of some of these recipes (potter's yellow type II) it was noted that red Pb_3O_4 forms as by-product when burnt lead, antimony oxide and ZnO are used as ingredients.[27,28]

BaO and MnO are also present in the yellow and orange beads and were added intentionally, as it is not present in the basic glass of the other colour beads or related to the presence of Sn, Mn, Zn or Pb. Mn is known to act as a decolorant for iron impurities and it is most likely that it was added for this purpose. In modern glass, Ba lowers the melting temperature and decreases the tendency towards devitrification, but it is not known if this was the reason for its inclusion in this glass.

The dark blue beads are coloured with cobalt, which has been in use since antiquity to colour Roman and Egyptian glass (from cobalt containing alum/natron from the western oases of Egypt[29]). A deep blue colour is obtained with 0.2% cobalt or even less. Cobalt is a rare element in the earth's crust and up to the 12th century A.D. the export of cobalt pigments could be related to only two production regions, namely Qamsar and Anarak in Persia and the Erzgebirge Mountains in Saxony, which were geologically rich enough to support, for long periods of time, a trade route over Europe, North Africa and the East as far as China. In both these regions the cobalt is associated with arsenic.[30,31] The cobalt ore in Germany is associated with Ag-bearing minerals and Ni, Bi, Zn or Mo are usually present. Recently, it has been shown that early primary glass production (high Al, high Ca glass) took place at Ile-Ife in southwestern Nigeria

and utilized cobalt associated with high levels of manganese to manufacture dark blue beads.[32]

The cobalt ore, imported from Iran, used in the famous Jingdezhen (China) blue-and-white ware during the 14th to early 15th centuries was rich in iron (Fe : Co = 3:1) and sometimes contained arsenic, nickel and copper.[23] In the 15th century, cobalt ore rich in manganese was discovered in southern China and replaced the imported product.[23]

It has been shown that the cobalt ore used in Vietnam over a long period of time was associated with Mn, and in a large study of more than 550 glass samples from sites from Afghanistan, Pakistan, India, Sri Lanka, Thailand, Malaysia, Indonesia, Vietnam and Cambodia, it was found that all the cobalt blue beads examined contained cobalt associated with large quantities of Mn.[33–36]

The cobalt used to colour the Mapungubwe cobalt blue beads is associated with arsenic and iron (Table 1). The Fe : Co (iron concentration obtained by subtracting the mean value of Fe concentration of the basic glass batch) ratio matches the 3 : 1 ratio obtained in early Chinese ware and the As_2O_3 / CoO weight ratio of ~1.24 indicates that the Co : As ratio in the chemical formula of the ore was probably 1 : 1 (some arsenic evaporates during the glass-making process).[31] The absence of Mn makes it unlikely that the cobalt beads originated from the above-mentioned sites around the Indian Ocean or southwestern Nigeria and the absence of Bi, Ni and Mo might also be an indication that the ore originates from Iran rather than Europe. However, large variations in the concentrations of elements in natural ore do occur.

Most ancient glasses and medieval glasses that do not contain any deliberately added colourant have a 'natural' green colour owing to iron as contaminant in the raw materials from which the glass was made.[37] Manganese was added to ancient glasses to remove the green colour caused by iron impurities through reduction, and an excess of manganese results in plum-coloured glass (Mn^{3+}). In the case of the plum-coloured Mapungubwe oblate beads, Mn as well as a small amount of lead tin yellow type II (perhaps to enhance the colour or contamination) was detected (Table 1).

Iron has previously been identified as the pigment in the black beads excavated at Mapungubwe, but the iron content of the Mapungubwe oblates (1.5%) is not enough to obtain a black colour in the form of the reduced iron oxide FeO. At least 6% iron oxide is necessary to colour the glass black and the 1.5% iron oxide combined with 0.2% TiO_2 (Table 1) would result in the typical greens of Chinese celadon glazes.[23] Raman spectra recorded (532 nm excitation) on black Mapungubwe oblate beads are shown in Fig. 5. Figure 5(a) is the characteristic spectrum of carbon, with the broad D and G bands centered at ~1300 and ~1600 cm^{-1}. Prominent peaks in the low wavenumber region dominate the bands originating from the glass in the other spectra in Fig. 5. The two sharp peaks at 330 and 357 cm^{-1} have the appearance of a crystalline phase and occur very near the peaks of pyrite (FeS_2) at 351, 386 and 443 cm^{-1}, which could have been used as pigment.[38] According to the XRF results in Table 1, the iron concentration in the black beads does not differ from that of the other beads, but the sulfur concentration is higher. It is therefore more likely that sulfur was added to the basic glass recipe to form the Fe-S chromophore traditionally used to produce amber glass and which in sufficiently high concentrations appears black.

During the cooling of a soda-lime-silica glass melt containing iron oxides and sulfur species, ferrous iron (Fe^{2+}) reacts with sulfite (SO_3^{2-}) causing increases in the Fe^{3+} (ferric ion) and S^{2-} (sulfide) concentrations, which are required for the formation of a chromophore based on $Fe^{3+} - S^{2-} - 3O^{2-} - nNa^+$ complexes in the silicate glass. The amber colour intensity of the chromophore depends strongly on the melting temperature, the alkali concentration in the glass, the total iron concentration of the melt and the oxidation state of the melt, which has to be reducing to form[39,40] S^{2-}. Except for the amber chromophore containing ferric iron in tetrahedral co-ordination with three oxygens and one sulfur, other iron-sulfur species that occur in the melt are ferrous iron in octahedral co-ordination with oxygen, ferric ion in tetrahedral co-ordination with oxygen, sulfur as sulfate and sulfur as sulfide but not in association with iron.[39,40] This large variation of structures and the resultant environments of the chromophore are probably responsible for the large variation in the Raman spectra (Fig. 5(b–e)). Carbon is usually added as reducing agent to produce modern amber glass and it could have been the case here as well (Fig. 5(a)) or carbon could have been the pigment and the formation of the Fe-S chromophore fortuitous.

Furthermore, the Raman peaks occur at more or less the same wavenumbers (290, 320, 344, 370 and 400 cm^{-1}) as

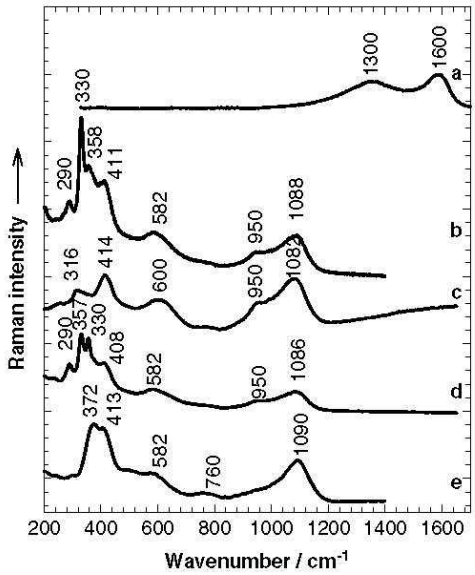

Figure 5. Raman spectra recorded on the black glass (a) amorphous carbon; (b), (c), (d) and (e) pigment in black glass recorded on different positions.

DOI: 10.1002/jrs

Fe-S stretching bands originating from [2Fe-2S] clusters in proteins, which vary in intensity and position with the wavelength of the exciting laser.[41] Resonance effects have also been observed in other pyrite structures such as IrS_2 and MgS.[42,43]

It is quite interesting to note that it was recently reported that although some black Bird Star beads (produced in South or Southeast Asia, 4–9th c.) are coloured with Mn, some are suspected to be coloured with an iron-sulfur combination.[44]

The larger black beads

The Raman spectra of the larger black beads (Fig. 1(b)) are compared to that of a black Mapungubwe oblate in Fig. 6. As it has previously been suggested that the black beads could have been made at factories around the Indian Ocean, the spectra of two samples from famous glass-making sites (Arikamedu, India and Giribawa, Sri Lanka), are also included. It is clear that the spectra of the two larger black beads are different from that of the Mapungubwe oblate but very similar to that of the Indian and Sri Lankan beads. At a first glance the spectra appear to be of a glass with very high polymerization index ($I_p = 1.7$), but comparison with the spectra in Fig. 5 of the black pigment in the Mapungubwe oblate glass indicates that the peak at ~415 cm^{-1} may also originate from the Fe-S chromophore. This was confirmed by recording spectra with different exciting wavelengths on the cylindrical black bead (Fig. 7). The shift of the strong 415 cm^{-1} peak (532 nm laser line, 200 s accumulation time) to 365 cm^{-1} with a sharp decrease in intensity in the spectrum recorded with the red laser line (1000 s accumulation time) clearly shows that the peaks are resonance-enhanced in the blue-green part of the spectrum.

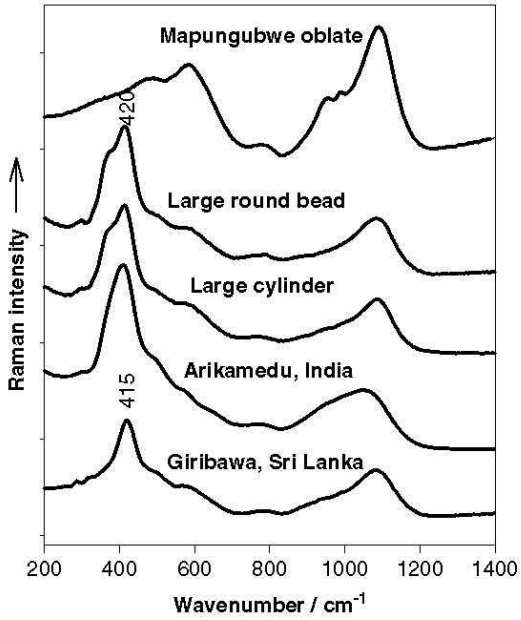

Figure 6. Raman spectra of the different black glass beads in comparison with black glass from Arikamedu (India) and Giribawa (Sri Lanka).

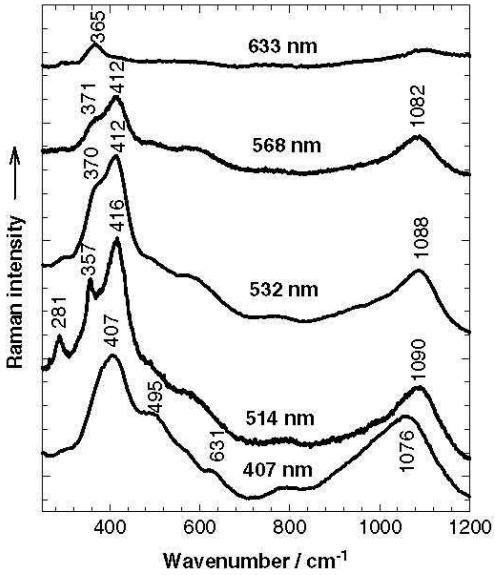

Figure 7. Raman spectra recorded on the cylindrical black bead with different exciting laser lines (633, 514, 568, 532 and 407 nm).

In contrast to the Mapungubwe oblates, in which the spectrum varied according to the position probed on the sample (Fig. 5), it was not possible to record spectra from these beads in which the strong resonance peak is absent. This can perhaps be ascribed to higher iron concentrations in the larger beads (Table 4), as well as differences in composition of the fluxing ions.

The main elements (wt%) present in the glass of the specific beads used for the Raman analyses (obtained with EDX measurements) are given in Table 4 and it is clear that three different glass recipes were used to manufacture the beads. In Fig. 8 this is graphically illustrated and the relative

Table 4. EDX analysis of main elements in the black beads, as well as corroded Mapungubwe oblate

Element (wt%)	Mapungubwe oblate	Mapungubwe oblate (corroded)	Cylindrical bead	Large round bead
Na	7.32	0.94	13.92	0.53
Mg	0.6	0.74	0.51	0.43
Al	7.26	9.57	6.99	8.0
Si	60.38	63.88	55.64	59.53
P	0.74	1.61	0	0
Cl	3.91	0.53	4.92	2.83
K	8.57	4.22	9.1	15.82
Ca	5.42	10.84	3.18	5.13
Ti	0.74	1.18	0.58	0.82
Fe	3.89	4.89	5.15	6.01
Pb	0.52	0.0	0.0	0.9
Mn	0.1	0.0	0	0

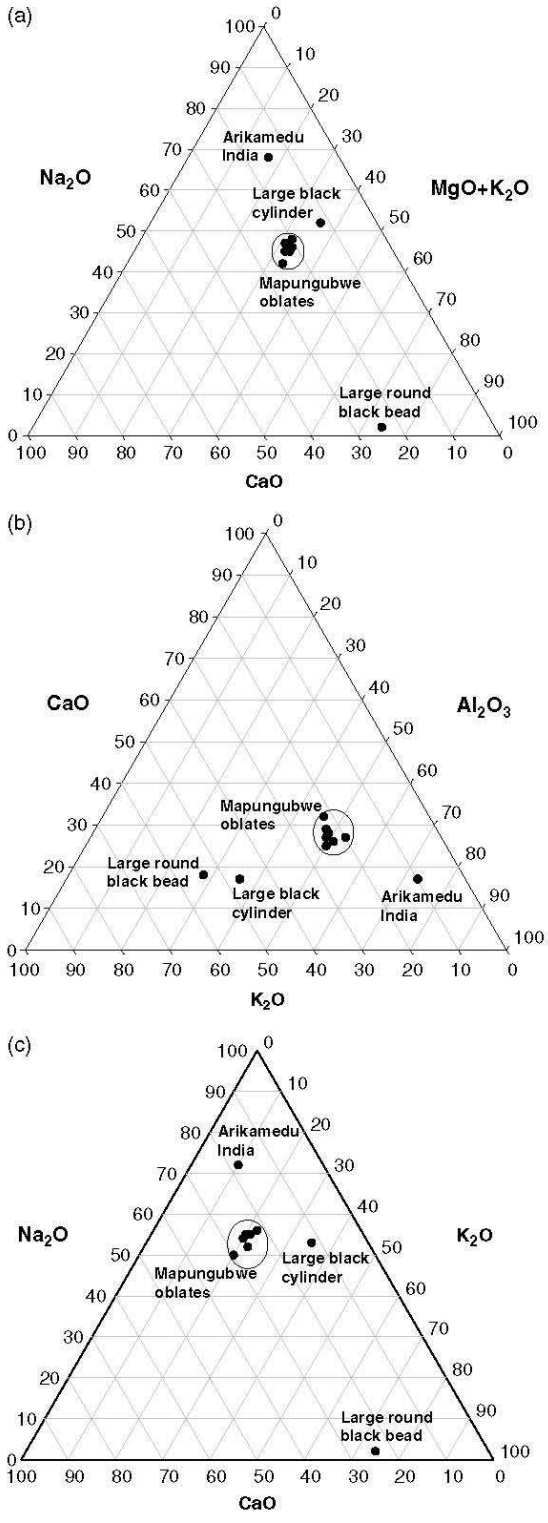

Figure 8. Comparison of relative concentrations of ions of the beads in this study: (a) CaO, ($MgO + K_2O$) and Na_2O; (b) K_2O, Al_2O_3 and CaO; (c) CaO, K_2O and Na_2O.

concentrations of the fluxing ions are also compared to those of the beads from Arikamedu (compositional analysis of the beads from Giribawa were not available). (It should be noted that three different analysis techniques have been used: XRF for Mapungubwe oblates, SEM-EDX for larger black beads and LA-ICP-MS for the Arikamedu bead. The techniques all have different detection limits and sampling sizes and interpretation of data should be seen in this light.) In all three graphs the Mapungubwe oblates form a separate group and it can be presumed that the black beads originated from three different sites. The beads selected for analysis have been chosen on the basis of physical appearance and therefore do not exclude the possibility that there may be even more chemical variations among similar looking beads. Comparing these diagrams to similar ones in Ref. 34, it becomes clear that the glass composition closely resembles that of beads excavated in Bara, Pakistan (1 B.C.), as well as some other sites around the Indian Ocean.[33–36]

EDX measurements are not sensitive enough to quantify the wt% of the light carbon and oxygen atoms, but a visual comparison between the data shows that there is relatively more carbon and oxygen present in the large cylindrical bead than in the large round or Mapungubwe oblate beads. Furthermore, the FTIR spectra (Fig. 9) of the Mapungubwe beads show that water (bands at 3370 and 1640 cm^{-1}) is present in the glass of the cylindrical beads, but absent from the round and Mapungubwe oblate beads. This information might contribute to tracing the origin of the beads.

White corrosion

All the previous studies on the glass beads from Mapungubwe commented on the large number of black glass beads that displayed signs of corrosion (Fig. 1(c)). In some instances

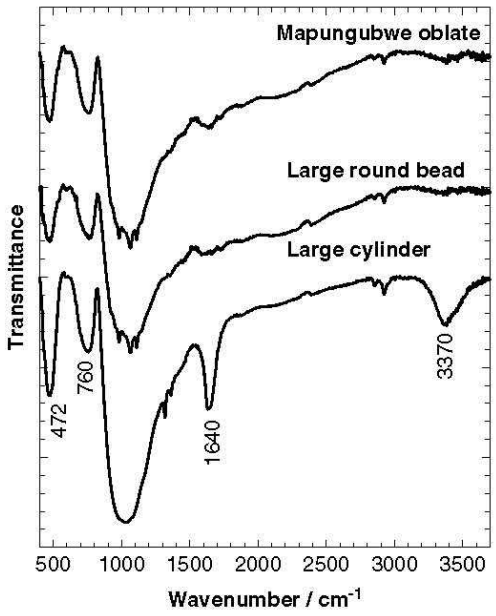

Figure 9. (a) FTIR spectra of the three different types of black glass beads excavated at Mapungubwe.

beads are uniformly white or yellow on the outside, but still black inside (Fig. 10).

Raman spectra of pristine glass (black) of the cylindrical and large round beads are compared to that of the corroded part of the bead (white) in Fig. 11(a). The difference between the spectra is obvious, and the disappearance of the peak at 950 cm^{-1} in the spectra of the white glass is in accordance with the depletion of Na and K ions. The absence of the peak attributed to the Fe-S chromophore is an indication that either sulfur or iron is absent in the corroded glass.

In Fig. 11(b) the Raman spectra of pristine and corroded black glass of a Mapungubwe oblate are compared. The I_p value has increased to 1.7, an indication of a highly polymerized network, the centre of gravity of the envelope arising from the Si–O bending modes having shifted downwards to 482 cm^{-1}, which is near that of pure silica glass and similar to that previously observed in highly corroded museum glass.[21] Table 4 shows the depletion of the sodium and potassium ion concentration as expected in corroded glass.

It has been shown that glasses high in fluxing agents (Na_2O, K_2O) and low in stabilizing ions (Ca, Mg) are more prone to corrosion than those in which this ratio is reversed, but for the Mapungubwe oblates the relative ratios of these ions are approximately the same for all the colours. The corrosion is also detected on all three types of beads with different compositions as far as the fluxing ions are concerned.

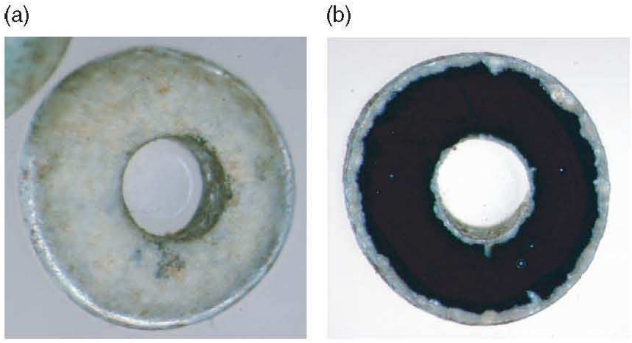

Figure 10. Black bead appearing white due to corrosion. (b) Cross-section of the same bead.

Organic phase detected on most beads

An organic phase was detected on most beads excavated in the grave area and could have originated from a lubricant of the grass roots used to string the beads or could also have been applied during funerary rites. The archives of the bead collection do not have any record of any cleaning or waxing agents that were used to clean the beads after excavation, so it is presumed that the owners of the beads applied the organic phase.

From the Raman spectrum (Fig. 12) it is clear that a C=O bond and an aromatic C=C are present. In industrial

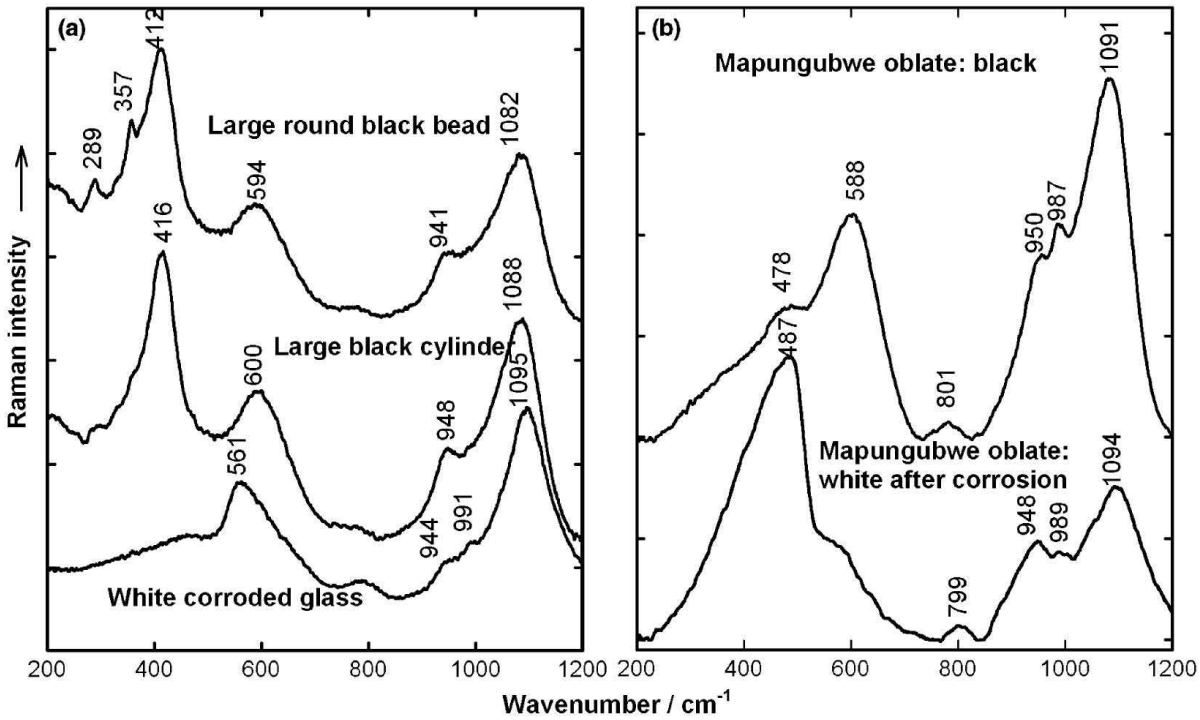

Figure 11. (a) Comparison of Raman spectra recorded on the black part of the cylindrical and large round bead with a spectrum recorded on the white glass (large cylinder) and (b) comparison of Raman spectra recorded on the black part of a Mapungubwe oblate with a spectrum recorded on white glass of the same bead.

DOI: 10.1002/jrs

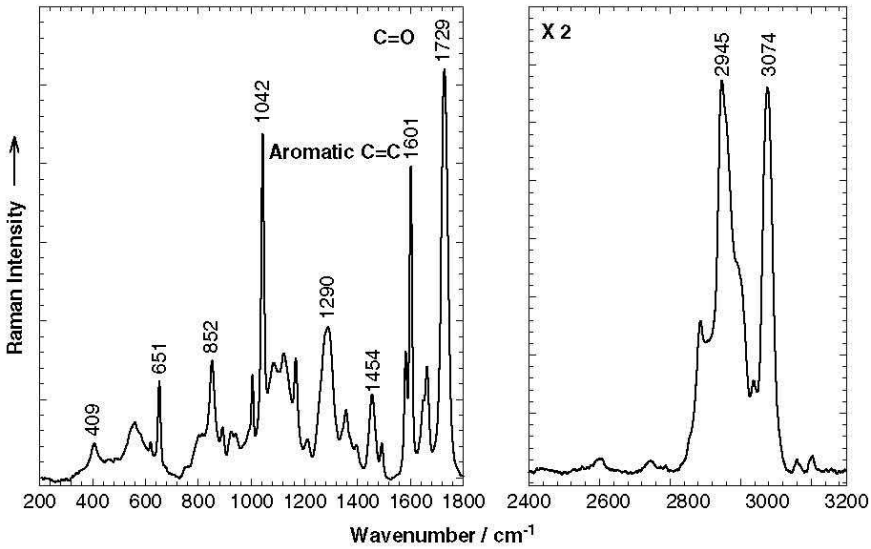

Figure 12. Raman spectrum of the organic phase detected on most beads from the 'royal burials'.

pyrite flotation processes, this is characteristic of some collectors, which through chemisorption or through electrostatic interaction influence the surface chemistry. This could have promoted the preferential depletion of sulfur ions leading to the discolouration of the black beads and the amber colour where the corrosion process has not been completed.

CONCLUSIONS

Using Raman spectroscopy and supportive techniques we have determined a profile of the glass technology used to produce the Mapungubwe oblates. We have shown that there are a number of characteristics of the beads that may eventually help to determine their provenance.

In the first place, although soda/lime/potash glass was produced throughout the ancient world, the high aluminium content eliminates many production centres such as a glass-making factory in Amsterdam, to which many of the trade beads to the North American Indians have been traced, and medieval Venice (9–13th c.).[45–46] Furthermore, the beads used in Refs. 10 and 11 to claim Fustat (old Cairo) as the origin of the Mapungubwe beads (according to a Ce-depleted rare earth element pattern (REE)) also do not have the same basic glass composition as the Mapungubwe oblates.

Second, the pigment palette is quite specific and can also contribute to establishing the provenance of the beads. The cobalt, associated with arsenic, eliminates all sources where cobalt associated with large quantities of manganese were used such as the beads studied in Refs. 32–34.

Considering both the nature of the glass (related to Omeyyad glass) and the pigments used (cobalt associated with arsenic, orange/yellow pigments), it would seem that there is some relationship to Mediterranean/Islamic production technologies, although it has not been possible to find an exact fit with the data currently available to us.

The unique Raman spectra of the pigment in the orange coloured beads, as well as the resonance Raman spectra of the Fe-S chromophore in the black beads, are exceptional tools to identify similar technologies. In combination with the composition of the basic glass recipe used, it should be possible to make a positive identification of glass from possible production sites, which exhibits all the same parameters, as the origin of the beads. This information would make an invaluable contribution towards the understanding of trade routes through and around Africa.

Acknowledgements

The authors thank B. Gratuze (CNRS-IRAMAT, Orléans) and Laure Dussubieux (The Field Museum of Natural History, Chicago) for valuable discussions and the use of their reference samples. From the University of Pretoria we thank Dr Alan Carr (Department of Physics) for the photograph, Maggi Loubser (XRF and XRD Laboratory) for XRF, Andre Botha (Electronmicroscopy Unit) for the EDX measurements and Me. Sian Tiley of the Mapungubwe Museum for the loan of the beads and for the request of an export permit (No.80/06/06/004/52) from the South African Heritage Resources Agency on our behalf. From the Laboratoire Dynamique, Interactions et Réactivité(LADIR), Paris, we thank Me. Aurelie Tournie for help in recording and analysing some spectra. The financial assistance of the NRF and CNRS towards this research is hereby acknowledged.

REFERENCES

1. Prinsloo LC, Wood N, Loubser M, Verryn SMC, Tiley S. *J. Raman Spectrosc.* 2005; **36**: 806.
2. Fouche L. *Mapungubwe: Ancient Bantu Civilization on the Limpopo.* Cambridge University Press: Cambridge, 1937; 1.
3. Chittick HN. *Manda, Excavations at an Island Port on the Kenya Coast, The British Institute in Eastern Africa, Memoir 9.* University Press Oxford: Oxford, UK, 1984; 65.
4. Beck HC. Appendix in *The Zimbabwe Culture: Ruins and Reactions*, Caton-Thompson G (ed). Frank Cass: London, 1971; 185.
5. Beck HC. The beads of the Mapungubwe district. In *Mapungubwe*, Fouché L (ed). Cambridge University Press: Cambridge, 1937; 104.

6. Gardner GA. *Mapungubwe II*. J. L. van Schaik: Pretoria, 1963; 32.
7. Van Riet Lowe C. *The Glass Beads of Mapungubwe, Archaeological Series No. 9*, Union of South Africa: Archaeological Survey, Pretoria, 1955.
8. Van der Sleen WGN. *Man* 1956; **56**: 27.
9. Davison CC, Clark JD. *Azania* 1974; **9**: 75.
10. Saitowitz SJ. Glass Beads as Indicators of Contact and Trade in Southern Africa ca. AD 900-AD 1250, Unpublished PhD Thesis, University of Cape Town, Cape Town, 1996.
11. Saitowitz SJ, Reid DL, Van der Merwe NJ. *S. Afr. J. Sci.* 1996; **92**: 101.
12. Wood M. In *The South African Archaeological Society Goodwin Series*, vol. 8, Leslie M, Maggs T (ed), The Society: Cape Town, 2000; 78.
13. Wood M. *Glass Beads and Pre-European Trade in the Shashe-Limpopo Region*, Unpublished MSc Thesis, University of the Witwatersrand, Johannesburg, 2005.
14. Robertshaw P, Glascock MD, Wood M, Popelka RS. *J. Afr. Archaeol.* 2003; **1**: 59.
15. Colomban Ph, March G, Mazerolles L, Karmous T, Ayed N, Ennabli A, Slim H. *J. Raman Spectrosc.* 2003; **34**: 205.
16. Colomban Ph, Milande V, Lucas H. *J. Raman Spectrosc.* 2004; **35**: 68.
17. Colomban Ph, Tournie A, Bellot-Gurlet L. *J. Raman Spectrosc.* 2006; **37**(8): 841.
18. Welter N, Schüssler U, Kiefer W. *J. Raman Spectrosc.* 2007; **38**(1): 113.
19. Colomban Ph, Etcheverry M, Asquier M, Bounichou M, Tournie A. *J. Raman Spectrosc.* 2006; **37**(5): 614.
20. Robinet L, Coupry C, Eremin K, Hall C. *J. Raman Spectrosc.* 2006; **37**: 789.
21. Robinet L, Coupry C, Eremin K, Hall C. *J. Raman Spectrosc.* 2006; **37**: 1278.
22. Carabatos-Nédelec C. Raman scattering of glass. In *Handbook of Raman Spectroscopy: From the Research Laboratory to the Process Line*, Lewis IR, Edwards HGM (ed). Marcel Dekker: New York, 2001; 423.
23. Wood N. *Chinese Glazes*. A & C Black: London, 1999; 63.
24. Clark RJH, Cridland L, Kariuki BM, Harris KDM, Withnall R. *J. Chem. Soc., Dalton Trans.* 1995; **16**: 2577.
25. Biek L, Bayley J. *World Archaeol.* 1979; **2**(1): 1.
26. Colomban Ph, Sagon G, Louchi A, Binous H, Ayed N. *Rev. Archeom.* 2001; **25**: 104.
27. Sandalinas C, Ruiz-Moreno S, López-Gil A, Miralles J. *J. Raman Spectrosc.* 2006; **37**: 1146.
28. Dik J, Hermes E, Peschar R, Schenk H. *Archaeometry* 2005; **47**(3): 593.
29. Shortland AJ, Tite MS, Ewart I. *Archaeometry* 2006; **48**: 153.
30. Gratuze B, Soulier I, Barrandon JN, Foy D. *Rev. Archéom.* 1992; **16**: 97.
31. Zuchchiatti A, Bouquillon A, Katona I, D'Alessandro A. *Archaeometry* 2006; **48**: 131.
32. Lankton JW, Akin Ige O, Rehren T. *J. Afr. Archaeol.* 2006; **4**(1): 111.
33. Colomban Ph, Sagon G, Huy LQ, Liem NQ, Mazerolles L. *Archaeometry* 2004; **46**(1): 125.
34. Dussubieux L. *L'apport de l'ablation laser couplee a l'ICP-MS a la caracterisation des verres: application a l'etude du verre archeologique de l'Ocean Indien*, Unpublished PhD Thesis, Universite d' Orleans, Orleans, 2001.
35. Dussubieux L, Gratuze B. *Rev. Archéom.* 2003; **27**: 67.
36. Lankton JW, Dussubieux L. *J. Glass Stud.* 2006; **48**: 121.
37. Schreurs JWH, Brill RH. *Archaeometry* 1984; **26**(2): 199.
38. Ushioda S. *Solid State Commun.* 1972; **10**: 307.
39. Beerkens RGC. *Glass Sci. Technol.* 2003; **76**(4): 166.
40. Beerkens RGC, Kahl K. *Phys. Chem. Glasses* 2002; **43**(4): 189.
41. Fu W, Drodzdzewski PM, Davies MD, Sligar SG, Johnson MK. *J. Biol. Chem.* 1992; **267**(22): 15502.
42. Sourisseau C, Cavagnat R, Fouassier M, Jobic S, Deniard P, Brec R, Rouxel J. *J. Solid State Chem.* 1991; **91**: 153.
43. Wolverson D, Bradford C, Prior KA, Cavenett BC. *Phys. Stat. Sol. (b)* 2002; **229**(1): 93.
44. Lankton JW, Dussubieux L, Rehren Th. A study of mid-first millennium CE Southeast Asian specialized glass beadmaking traditions. *Proceedings of the 10th International Conference of the European Society of Southeast Asian Archaeologists*, September, 2004, London, 2006.
45. Karklins K, Hancock RGV, Baart J, Sempowski ML, Moreau JF, Barham D, Aufreite S, Kenyan I. *Archaeometry* 2001; **43**(4): 503.
46. Verità M, Renier R, Zecchin S. *J. Cult. Herit.* 2002; **3**: 261.

DOI: 10.1002/jrs

This study was initiated on a field trip to the Mapungubwe Heritage site in December 2001 under the leadership of Prof. Andri Meyer (Archeology Department, University of Pretoria), who spent a large part of his life excavating the Mapungubwe archaeological site. The other team members were Prof. Ian Meiklejohn (Department of Geography, Geoinformatics and Meteorology of the University of Pretoria) and Isabelle Barrier (see photo's in article), at that time an Archaeology student from the University of Pretoria.

The results of this study were presented as a poster contribution at the *3rd International Conference on the Application of Raman Spectroscopy in Art and Archaeology* held in Paris, 31 Aug. –3 Sept. 2005 and the full results published in the Journal of Raman spectroscopy and follows as chapter 5.

L C Prinsloo, Rock hyraces: a cause for San rock art deterioration?

The poster won a Young Investigater's award at the conference

The unique properties of hyrax urine and its use as traditional medicine that came under my attention during this study motivated me to send a hyraceum sample to Prof. Anna Jäger, Department of Medicinal Chemistry, University of Copenhagen, Denmark. She tested the sample for affinity to the GABA-benzodiazepine receptor and obtained a positive result, which supports its use as traditional medicine for the treatment of epilepsy. In order to establish if there is a connection between the hyrax diet and the activity of the samples we asked Prof. Louis Scott if we could use samples from his large collection of hyraceum samples, collected in different biomes, for further testing. The results from this study are published in an article and were presented at an international conference.

Jäger AK, Olsen A, Prinsloo LC and Scott L. 54th Annual Congress on Medicinal Plant Research, 29 August-2 September, Helsinki, Finland. Planta Medica, 2006, 72: 993.

Andreas Olsen, Linda C. Prinsloo, Louis Scott and Anna K. Jäger, Hyraceum, The fossilised metabolic products of rock hyraces, shows affinity to the GABA-benzodiazepine receptor, *South African Journal of Science* 2007; **103:** 437.

JOURNAL OF RAMAN SPECTROSCOPY
J. Raman Spectrosc. 2007; **38**: 496–503
Published online 15 January 2007 in Wiley InterScience
(www.interscience.wiley.com) DOI: 10.1002/jrs.1671

JRS

Rock hyraces: a cause of San rock art deterioration?

Linda C. Prinsloo*

Department of Physics, University of Pretoria, Pretoria, South Africa

Received 25 July 2006; Accepted 11 October 2006

San rock art sites are found throughout southern Africa, many showing signs of deterioration. In order to conserve this invaluable heritage, a long-term multidisciplinary project has been launched to monitor the rate of their deterioration and determine the various chemical processes that are possibly contributing to the decay. This study was initiated to establish if Raman spectroscopy could contribute to this project and since rock hyrax colonies live in close proximity to many of these archaeological sites, the possible influence of their metabolic products on the deterioration process was investigated.

The precipitates from the urine of rock hyraces were analysed with Raman and Fourier-transform infrared (FTIR) spectroscopy. Where the urine was in contact with the faeces, the precipitates are a mixture of vaterite (a rare polymorph of $CaCO_3$) and the hydrated salt calcium monohydrocalcite (also rarely found in nature). On areas where this contact is at a minimum the common and stable polymorph of $CaCO_3$, calcite, is the main component. SEM micrographs and XRD analysis support the Raman and FTIR results.

XRD, FTIR and preliminary GC-MS analyses of hyraceum, the fossilised mixture of faeces and urine, identified an inorganic phase (potassium chloride, with small concentrations of other salts, e.g. vaterite and weddelite) and an organic phase, which is a cocktail of various aromatic compounds, mainly amides, alcohols and acids. These compounds could contribute to the crystallisation of these rare carbonates, as well as other uncommon salts detected on the cave walls, such as syngenite. The presence of phosphates in the urine may further act as a stabilizing agent. Copyright © 2007 John Wiley & Sons, Ltd.

KEYWORDS: vaterite; monohydrocalcite; syngenite; oxalate; rock art

INTRODUCTION

The hyrax is so unlike other animals that although evolutionarily linked to elephants and sea cows, it is placed by itself in a separate order, namely Hyracoidea.[1] They are primitive subungulates that have changed in the course of evolution from ancestral fossil forms that have been found in the early Oligocene deposits (35 millions years ago) of the Egyptian Fayum region.[1] Rock hyrax (*Procavia capensis*) is one species of the genus *Procavia* and is distributed all over Africa. They are of considerable economic importance to the African people as food, as well as for their pelts.[1]

The small stockily built mammals are about the size of a rabbit with short legs, a rudimentary tail and small rounded ears (Fig. 1(a)). They are gregarious animals and huddle together at night under rock overhangs or in caves, while most of their day is spent basking in the sun, continuously on the lookout for avian predators.[2] The soles of their feet are naked, having a thick skin padded with glandular tissue that exudes and keeps the surface permanently moist.[1] This enhances the traction of their feet and enables them to move with great agility across rock faces, covering it in time with a hard black layer.

They are mixed feeders, selecting phenological stages of all their food plants to obtain the required diet and utilising plant parts most advantageous to them during a particular season. They eat a variety of grasses, forbs and shrubs, including some that are highly aromatic and others known to be poisonous to other species.[1]

Hyrax intestinal tracks have certain features that are unusual among mammals. Posterior to the stomach, and connected to it by the small intestine, they have a large sac in which cellulose in food is broken down by fermentation. Posterior to and connected to the sac by a short length of intestine is a fermentation chamber (caecum), which produces short-chain fatty acids (acetic acid: 63.9%, propionic acid: 22.9% and butyric acid: 6%) at a rate of nearly 10 mmol/100 ml/h to serve as an energy source.[3]

They urinate and defecate in latrines, which occasionally through continued use may assume very large proportions.[1]

*Correspondence to: Linda C. Prinsloo, Department of Physics, University of Pretoria, Pretoria 0002, South Africa.
E-mail: Linda.Prinsloo@up.ac.za

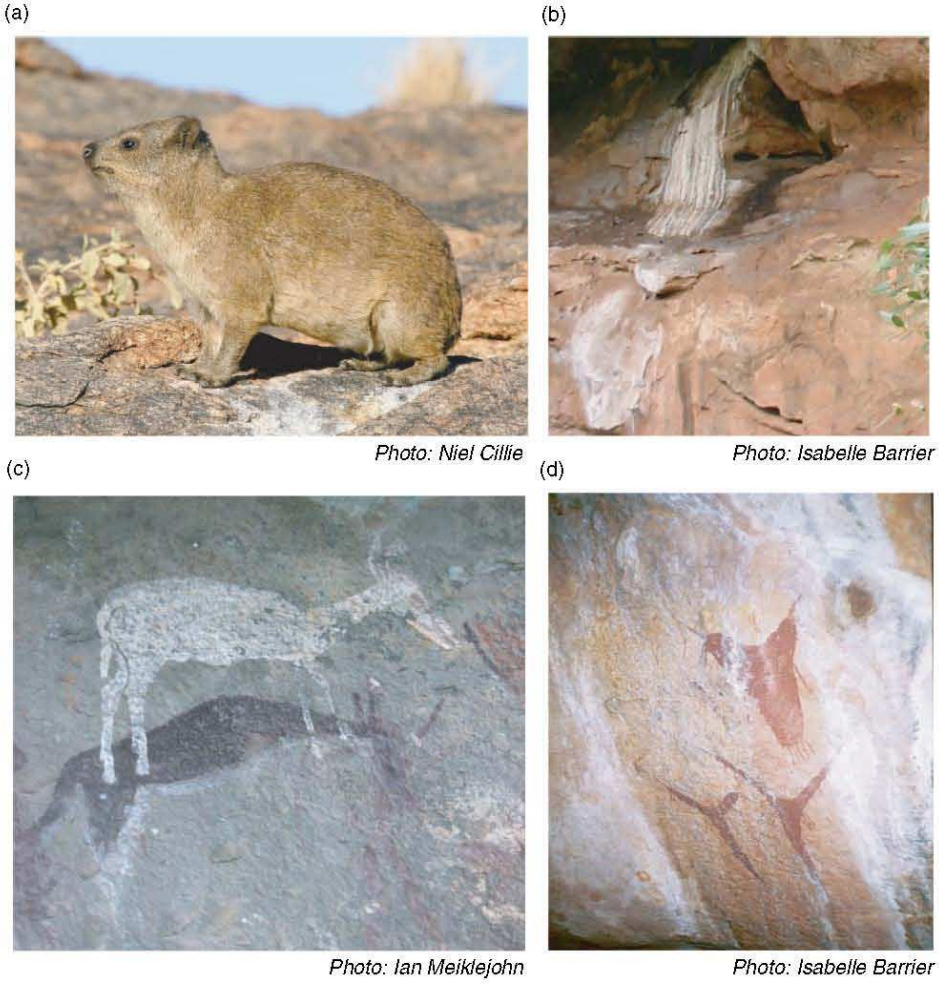

Figure 1. (a) Rock hyraces (*Procavia capensis*); (b) Rock hyrax urine in cave inhabited by rock hyraxes; (c) Rock painting (Battle cave, Injisuthi valley, Kwazulu Natal Drakensberg) of a buck transcending to the spirit world upon slaying; (d) White precipitates defacing San rock art in Venus shelter (Mapungubwe National Park), believed to have been used for initiation rites.

The urine crystallises as a white precipitate (Fig. 1(b)), and where the urine and faecal pellets mix, a thick black resinous crust is formed, which in the dry arid regions of South Africa can accumulate and become metres thick. This substance is called 'dassiepis' (Afrikaans vernacular) or hyraceum and is still being sold as traditional medicine in South Africa and exported to France for use as fixative in the perfume industry. Embedded in the fossilised hyraceum are animal hairs and plant remains, which form an invaluable DNA record and palæo-environmental history that stretches back millions of years and has been used in various studies to determine the variation in the plant population due to climatic changes.[4–6]

Rock hyraces and their genetic predecessors were part of the African landscape for millions of years, and when the earliest hominid species made their first appearance, they vied with the rock hyraces for the same caves and overhangs as shelters. The, in many instances, Clarens Formation sandstone cave walls provided a canvas for their San (previously known as Bushmen) hunter-gatherer descendents, whose paintings reflect their history and spirituality over a 25 000 year time span (Fig. 1(c) and (d)).

San rock art sites are found throughout southern Africa; unfortunately this heritage is rapidly being lost through natural weathering processes, which is a cause of concern to many researchers.[7] In order to develop techniques for its preservation, a long-term multidisciplinary project has been launched to monitor the rate of their deterioration and determine the various geological, chemical, mechanical and biological processes that are possibly contributing to the decay. Since rock hyrax colonies live and have lived in close proximity to many of these archaeological sites, the possible influence of their metabolic products on the deterioration process will be taken into account.

Raman spectroscopy has been used successfully to analyse pigments and substrata in prehistoric rock art,[8–12] and in this study its usefulness as a complementary technique in the study of San rock art deterioration is explored for the

DOI: 10.1002/jrs

first time. Specifically, rock hyrax urine and faeces were analysed with Raman and Fourier-transform infrared (FTIR) spectroscopies and XRD measurements. A few crystalline samples collected on the cave walls at rock art sites in the Mapungubwe National Park were also studied.

EXPERIMENTAL

Samples

A sample of the precipitates of rock hyrax urine was collected outside a cave in the Mapungubwe National Park situated at the confluence of the Limpopo and Shashe rivers, South Africa. It formed part of a multidisciplinary study to determine the condition of the San rock art in the area and to determine whether Raman spectroscopy could play a role in future studies in this regard. Samples of crystalline growths were collected on rock faces that showed signs of weathering, and as at all the rock art sites a strong pervading smell indicated the presence of rock hyraces, their urine precipitates (Fig. 1(b)), in appearance very similar to the crystal growths deforming the rock art (Fig. 1(d)), were also collected.

Urine samples, used for verification purposes, were collected in the Karoo and Gamkaskloof National Parks, Western Cape Province. Fresh samples were obtained from the National Zoological Garden, Tshwane, South Africa. The hyraceum sample was collected near Richmond in the Karoo.

Experimental techniques

Raman spectra were recorded on an XY Raman spectrometer from Dilor using the 514.5 nm line of a Coherent Innova 90 Ar^+-laser as exciting radiation. The sample was pressed into a KBr pellet to reduce fluorescence and the spectra were recorded in a back-scattering configuration with an Olympus microscope attached to the instrument. The spectral resolution for all the measurements was 2 cm^{-1}. Optimum recording conditions were obtained by varying the laser power, microscope objective and size of the confocal hole.

A Perkin-Elmer FTIR spectrometer was used to record the mid-infrared transmission spectra. The resolution was 2 cm^{-1} and 32 scans were signal-averaged in each interferogram.

Powder X-ray diffraction data was recorded with a Siemens D501 automated diffractometer equipped with a secondary graphite monochromator. The applied potential was 40 kV and the corresponding current 40 mA. Cu Kα radiation was used as the primary X-ray beam. A pattern was recorded from 3 to 70° (2θ) in steps of 0.05°. The measuring time was 1 s and the scanning speed 3°(2θ) per minute.

Electron micrographs were obtained using a JSM-6000F scanning electron microscope (JEOL, Tokyo, Japan).

Luminescence spectra of rock hyrax urine were recorded at room temperature (monochromator: HR 640, Jobin Yvon; photomultiplier: TE-10-RF, Products for Research Inc.) using He–Cd (325 and 442 nm), Ar^+ (514.5 and 488 nm) and He–Ne (632.8 nm) lasers as excitation sources.

RESULTS

Rock hyrax urine

Initial attempts to obtain the Raman spectra of the crystalline precipitates from the urine were unsuccessful owing to a large fluorescence background excited by the 514.5 nm laser line. Since dilution of a sample in an inert matrix helps to reduce fluorescence, the urine sample was pressed into a KBr pellet. In the visual mode of the microscope attached to the Raman instrument, small round spheres imbedded in the KBr matrix could clearly be distinguished. A combination of the 100× objective of the Olympus microscope attached to the Raman instrument and a small confocal hole made it possible to record the spectra on individual spheres. Two unmistakably different Raman spectra were obtained indicating that the spheres were chemically distinct (Fig. 2(a) and (b)).

The spectra identified the two crystalline phases as vaterite and monohydrocalcite. The Raman spectra of carbonates are dominated by the symmetric stretching vibration (ν_1) of the CO_3 group, which occurs at 1084 cm^{-1} for calcite and at 1069 cm^{-1} for monohydrocalcite, and is split into two (1090 and 1077 cm^{-1}) for vaterite owing to a lowering of symmetry and the resultant removal of the degeneracy of CO_3^{2-} in the centro-symmetric calcite structure.[13–15] This distinct difference between the Raman spectra of monohydrocalcite and vaterite makes it possible to distinguish unambiguously between them.

In the spectrum of monohydrocalcite, ν_1 (1069 cm^{-1}) can be clearly identified, but a strong fluorescence background masks the other weaker bands, and the only other features in the spectrum is a weak lattice vibration at 212 cm^{-1} and traces of ν_2 at 880 cm^{-1}.[14,15] The spherulites on which

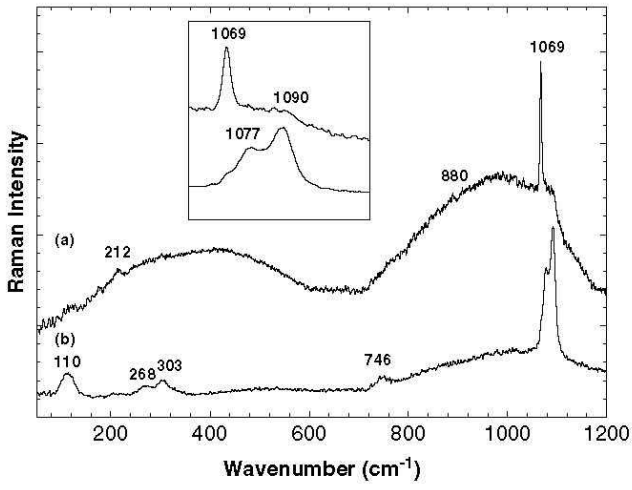

Figure 2. Raman spectra of rock hyrax urine: monohydrocalcite (a) and vaterite (b).

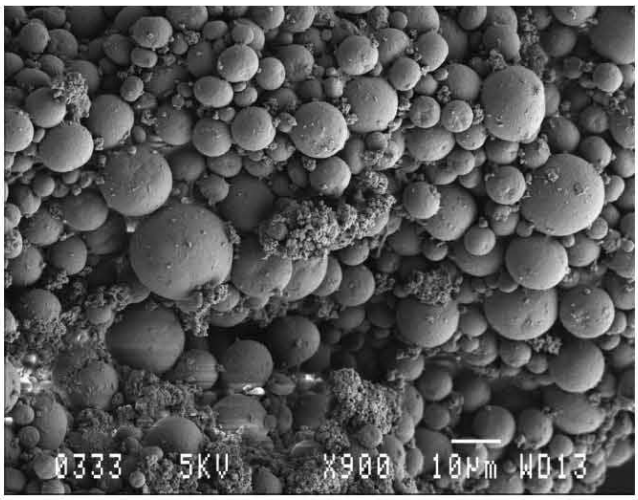

Figure 3. Electron micrograph of rock hyrax urine precipitates.

the vaterite spectra were recorded did not have this high background and ν_4 can be seen at 746 cm^{-1} as a small, broad band. The intensity is too low to observe the splitting that is characteristic for this band in vaterite spectra. Lattice modes are observed[13] at 110, 268 and 303 cm^{-1}. Vaterite and monohydrocalcite are known to crystallise with spherical morphologies. This is verified in the electron micrograph (Fig. 3) recorded of the urine precipitate. In fact it has become common practice to differentiate between vaterite and calcite using electron micrographs, as the rhombohedral calcite crystals are easily distinguishable from the vaterite spheres.[16–22] The morphology and size of the spheres, which varies between 0.1 and 30 µm, are consistent with reported literature values.[16–22]

The result was verified with XRD measurements (Fig. 4), which semi-quantitatively indicated that more or less equal amounts of vaterite and monohydrocalcite were present in this specific sample.

The transmission infrared spectrum of the crystallised hyrax urine recorded from the same KBr pellet used for the Raman measurements is shown in Fig. 5(b). The spectrum has features of both vaterite and monohydrocalcite. The ν_3 vibration is split into two for both carbonates (vaterite: 1420, 1490; monohydrocalcite: 1406, 1485).[13] As the peak positions are close to each other, the two very strong bands at 1409 and 1485 cm^{-1} (Fig. 5(b)) encompass these peaks for both carbonates and clearly distinguishes it from calcite (Fig. 5(a)), which has one ν_3 band at ~1438 cm^{-1}. A clear indication of the presence of monohydrocalcite is the totally symmetric Raman mode (ν_1), which is a forbidden mode in calcite and appears as a sharp peak (1069 cm^{-1}) superimposed on the split ν_1 peaks of vaterite (1088 and 1070 cm^{-1}). The other peaks in the FTIR spectrum of monohydrocalcite occur at 580, 699, 762 and 873 cm^{-1} and are all observed in the spectrum in Fig. 5(b).[13]

The spectrum in Fig. 5(a), identified as that of calcite with ν_3 at 1438, ν_2 at 873 and ν_4 at 712 cm^{-1}, was recorded from a sample collected in the Karoo National Park, where the urine was not in contact with the faeces (visually observed as whiter in colour). In both FTIR spectra recorded of the

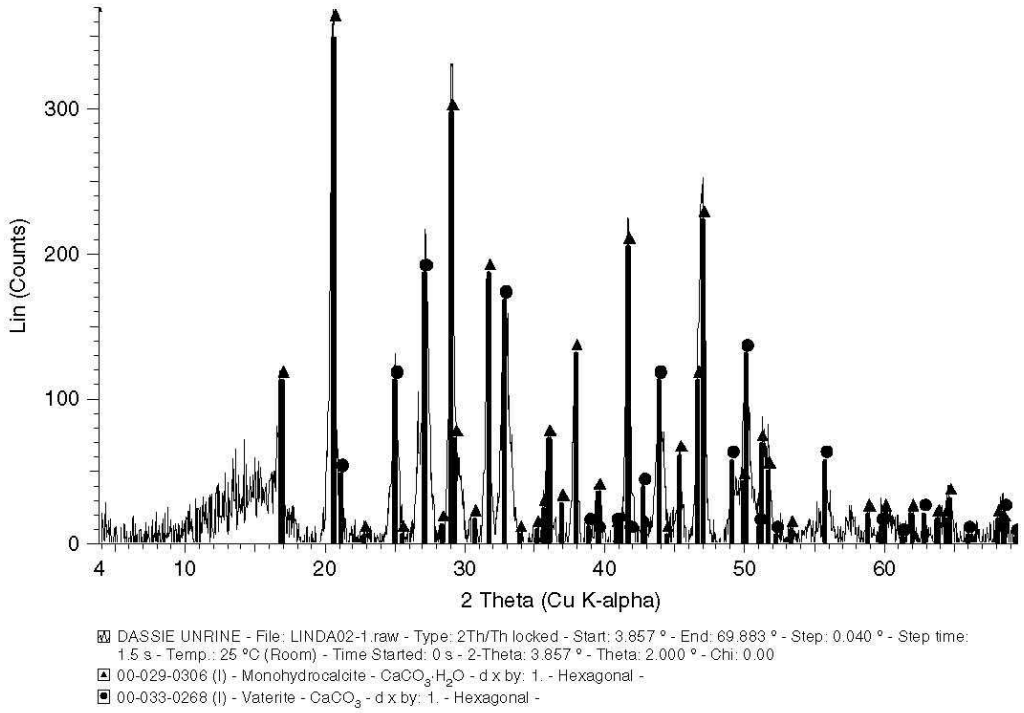

Figure 4. XRD spectrum of rock hyrax urine: ▲ = monohydrocalcite, ● = vaterite.

JRS

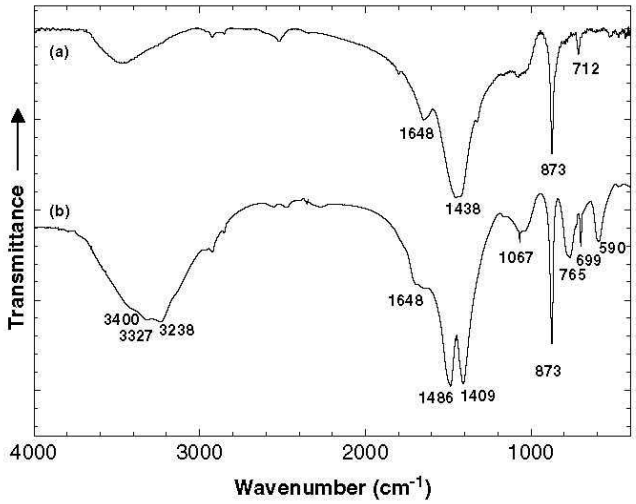

Figure 5. FTIR spectrum of rock hyrax urine (a) not in contact with faeces (calcite) (b) in contact with faeces (vaterite and monohydrocalcite).

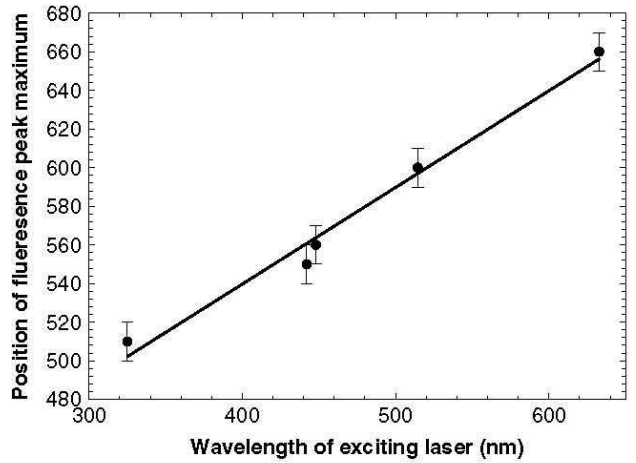

Figure 6. Wavelength of the exciting laser plotted against the position of rock hyrax urine fluorescence maximum.

urine, a band is observed around 1648 cm^{-1}, which indicates the presence of an organic phase.

In the Raman spectra recorded of monohydrocalcite, a strong fluorescence background was observed. This motivated the recording of luminescence spectra of rock hyrax urine, using UV (325 nm and 441 nm), blue (488 nm), green (514.5 nm) and red (632.6 nm) lasers as exciting lines. In Fig. 6, the peak maximum of the fluorescence is plotted against the wavelength of the exciting laser and it is clear that a linear relationship exists. Thus, rock hyrax urine absorbs light over the whole spectrum and releases this energy with a shift to longer wavelengths. At this stage it is not clear if this phenomenon has any biochemical or biophysical significance, e.g. as cue for avian predators similar as found for the UV fluorescent urine of voles and some Australian mammals.[23,24]

Monohydrocalcite ($CaCO_3 \cdot H_2O$) was first made in the laboratory in 1930, and in 1959 the first mineral deposition was identified. It is a rare mineral found in the Shiowakka cold saline spring in Japan in summer and also in Germany, Russia and the Czech Republic. It has also been detected in guinea pig bladder stones and tiger-shark otoliths.[25] The occurrence of vaterite in nature is nearly as rare as that of monohydrocalcite and has only seldom been observed, for instance, in the roots of germinating chickpea seeds, otoliths of the coho salmon and in frozen shrimp shells.[26,27]

These two unstable carbonates revert to calcite in solution and upon heating. It is therefore quite remarkable that it remains stable in hyrax urine, which for some samples could be hundreds of years old. Furthermore, the urine is found on rocky outcrops, exposed to a huge variety of weather conditions. The first sample was collected in the Limpopo valley after weeks of temperatures above 38 °C and a heavy downpour the previous night. Later samples were collected in the Karoo National Park, situated in a very dry, arid region of South Africa, with day temperatures in the summer often soaring to 40 °C and dropping to below freezing in winter. Fresh samples (similar spectrum as Fig. 5(b)) were scraped off rocks in the rock hyrax enclosure at the National Zoological Garden, which is regularly hosed down. As calcite is obtained for samples not in contact with the faeces, it is suspected that a growth controlling and stabilising agent is present in the faeces.

Hyraceum

A sample of the fossilised urine and faeces mix (hyraceum) was obtained from Richmond, Karoo, Western Cape Province, in order to attempt to identify the growth controlling and stabilising agent. XRD analysis identified potassium chloride as the main inorganic component, with traces of vaterite, calcite, weddelite (calcium oxalate dihydrate), quartz and acetamide. It was not possible to record a Raman spectrum owing to excessive fluorescence of the organic phases, and only the FTIR spectrum (Fig. 7) of hyraceum could be obtained. A strong band in the OH stretch region (3100–3500 cm^{-1}) and two strong bands centred around 1601 and 1408 cm^{-1} dominate the spectrum. The broad bands mask any characteristic bands that may be present of the large variation of aromatic amides, amines, alcohols and acids that have been identified by preliminary GC-MS analyses. Natural musk was also identified as a component. Identification of specific compounds is thus impossible, using only the FTIR spectrum.

Syngenite detected on cave walls

Most spectra of the salty deposits collected on cave walls consisted of a mixture of bands that could belong to nitrates, sulfates or phosphates, and especially the broad bands typical of FTIR spectra could not be unambiguously assigned. It was possible though, to identify the relatively rare sulfate double salt syngenite ($K_2Ca(SO_4)_2 \cdot H_2O$), as seen in Fig. 8(a),

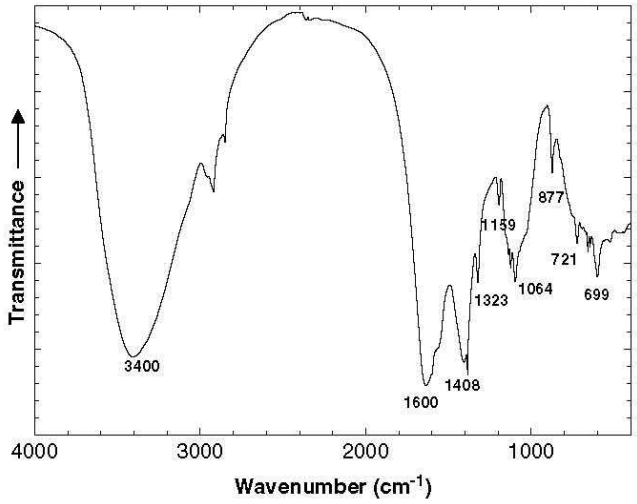

Figure 7. FTIR spectrum of hyraceum.

on one of the shards. The salt could not be separated visually from polyhalite, its co-precipitate as determined with XRD measurements and in many of the recorded spectra features of both salts were observed.

On the basis of the C_s point group symmetry for the sulfate groups in syngenite, 18 possible Raman modes have been predicted. The two strong bands at 981 and 1005 cm^{-1} are ascribed to the ν_1 modes of the two sulfate groups, which are not identical as the bond lengths and angles are different and the oxygens bonded to different cations. The weaker bands at higher wavenumbers 1081, 1120, 1140 and 1165 cm^{-1} have been assigned to the splitting of the ν_3 modes of both sulfate groups.[28] Four ν_4 modes of the two sulfate groups are observed at 607, 619, 632, 641 and 661 cm^{-1}. These results agree with the reference given in Ref. 24. The four bands at 427, 440, 471 and 491 cm^{-1} originate from the ν_2 bending modes of the sulfate anions. Thus, 16 of the predicted 18 modes are observed in our room temperature spectrum. The shoulder of the 1005 cm^{-1} band at 1013 cm^{-1} belongs to the totally symmetric stretching vibration of polyhalite (Fig. 8(c)). This is deducted from the XRD data, which indicated that polyhalite was a co-precipitate with syngenite. Both these spectra could be distinguished from $CaSO_4 \cdot H_2O$ (Fig. 8(b)), the most common sulfate salt, which was also detected.

Oxalates

The presence of rock hyraces were obvious at all the rock art sites in the Mapungubwe National Park, as large areas were covered with a smooth black coating, which becomes very slippery when wet and is attributed to rock hyrax occupation. An FTIR spectrum of this black layer is shown in Fig. 9(d), and strong characteristic bands at 1623 (anti-symmetric CO_2 stretch), 1315 (symmetric CO_2 stretch), 780 (in-plane deformation) and 518 cm^{-1} (CO_2 wagging) identified calcium oxalate monohydrate.[29] Other bands in the

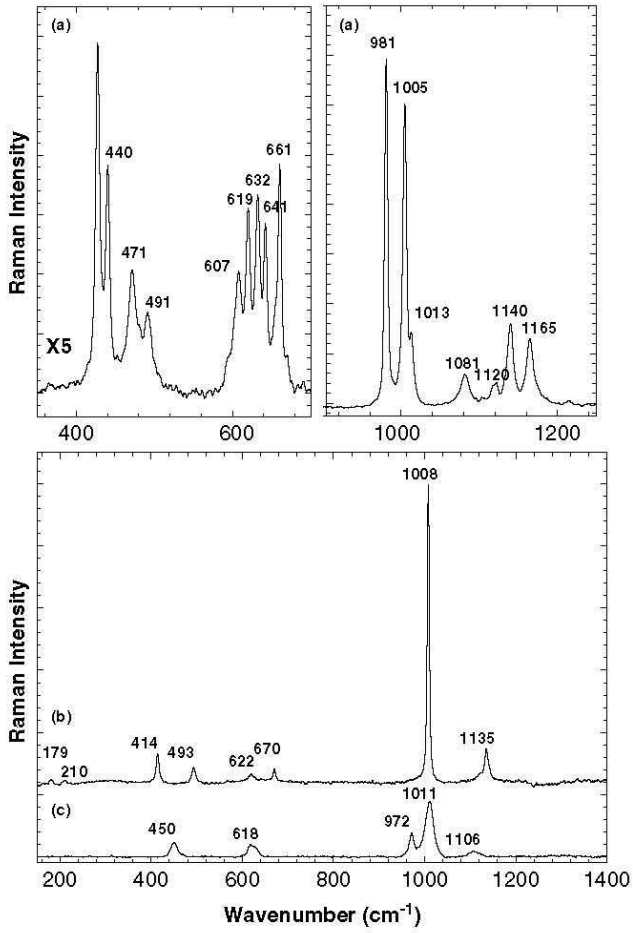

Figure 8. Raman spectrum of syngenite (a), gypsum (b) and polyhalite (c).

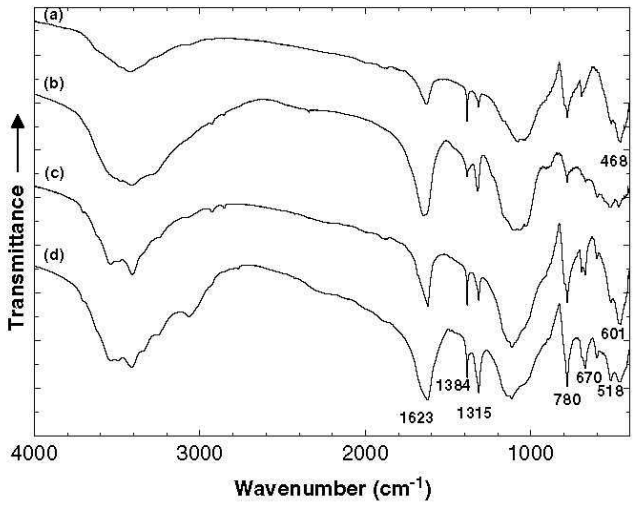

Figure 9. FTIR spectra of the salty deposits on cave walls (a–c) and (d) black layer covering cave floors, attributed to the occupation by rock hyraces.

JRS

spectra are attributed to α-quartz (broad band around 1090 and doublet at 798, 780 cm^{-1}) and possibly a nitrate (sharp peak at 1384 cm^{-1}, which varies in relative intensity and is also observed in the hyraceum spectrum). It is suspected that as the rock hyraces move around they cover the rocks with a mixture of urine, faeces and the glandular exudation of their feet.

Many of the salts collected on rock faces, where a clear sign of degradation was detected, also gave similar spectra of calcium oxalate monohydrate in varying concentrations (Fig. 9(a–c)).

Various studies have been conducted on encrustations on marble monuments and calcium oxalate mono- and dihydrate have been identified.[30,31] The presence of oxalic acid due to lichen populations are believed to be the origin of this phenomenon, but the exact mechanism is not fully understood yet.

DISCUSSION

$CaCO_3$ is one of the most abundant minerals in nature and has importance in both geological and biological systems. The formation of $CaCO_3$ occurs naturally in seawater in organisms such as coral reef and mollusc shells, where it plays an important part in the immobilisation of carbon dioxide in the global environment. Calcium carbonate is also one of the main components of scaling, which has economic importance in the chemical engineering industry. It is also used in other industrial fields as an additive to medicines, foods, papers, plastics, printing inks, etc. Besides the hydrated salts (monohydrocalcite and hexahydrocalcite), three polymorphs of $CaCO_3$, namely, calcite, aragonite and vaterite, in order of stability and solubility, exist in nature. The crystallisation process and control of the formation of the different polymorphs and hydrated salts have been extensively studied.[16–22]

It has been found that amino acids, alcohols (e.g. ethanol, isopropanol, diethylene glycol) and magnesium ions promote the formation of vaterite.[16–22] In most studies supersaturated solutions also favoured the formation of vaterite and monohydrocalcite. It has also been reported that monohydrocalcite crystals have been grown from a complex saline solution of NaCl, KCl, $CaCl_2$, $MgCl_2$ and $NaHCO_3$, complemented with cell culture mediums and various biochemical additives.[14]

It would seem that the high concentrations of KCl and abundant organic molecules present in the urine/faeces mix of rock hyraces would in fact be ideal conditions for the formation of vaterite and monohydrocalcite. Furthermore, calcium ($CaCO_3$), phosphates, magnesium and urea are also present in rock hyrax urine.[2] Mg has been shown to promote the formation of vaterite,[19] and it has been established that orthophosphate ions inhibit the degradation of carbonates.[32]

A layered stone composed of predominately calcium and magnesium oxalate with a trace of phosphate has been found in the stomach of a wild hyrax.[2] This was attributed to the presence of plants high in oxalic acid in their diet, and as the breakdown of food in the hyrax digestive system is not as effective as for ruminants, oxalic acid may still be present in their metabolic products and thus provide a source for oxalate formation on rock faces.

CONCLUSIONS

The weathering of the rock faces depicting San rock art are a complex mechanism encompassing interdependent mechanical, geological, chemical, physical and biological processes. Since 1994, ongoing studies monitor moisture and temperature changes in two caves in the KwaZulu Natal Drakensberg, and in 2003 step-scan XRD measurements were used to determine the depth of chemical changes in the Clarens Formation sandstone where weathering was observed.

The results of this first exploratory study, as to the possible use of Raman spectroscopy as a complementary technique in this project, have been extremely positive. It was possible to identify salts with microscopic resolution (between vaterite and monohydrocalcite) and also on a nanoscale (between syngenite and polyhalite). Raman spectroscopy will now be used to analyse the same samples used for the XRD measurements, and both results will be linked to temperature and moisture studies. The presence of rock hyraces, as well as bats, lichens and other plants and animals will be taken into account. Eventually, it is hoped to expand the project to include *in situ* Raman experiments, which will enable us to identify pigments (and perhaps binders) used in the paintings non-destructively.

The detection of the two rare carbonates in the urine instigated an awareness of the unique properties of hyraceum, which was used by early European settlers as well as indigenous people as traditional medicine. The Pharmaceutical University of Copenhagen is testing the validity of one of the medicinal properties ascribed to it, namely, as a cure for epilepsy, and some samples have tested positive.[32] Simultaneously, an extensive GC-MS study is under way to analyse the hyraceam fully and also to identify the volatile components of the faeces that might have the largest influence on the crystallisation processes on cave walls. As the composition of the hyraceum is dependent on the dietary intake of rock hyraces, samples from different environments will be compared (the samples used for the studies in Refs 4–6). This would provide a link to diet and composition of the urine and faeces.

Acknowledgements

The author is grateful to Sabine MC Verryn (XRF and XRD Laboratory, University of Pretoria) for making the XRD measurements, Johan Brink (Physics Department, University of Pretoria) for help with luminescence measurements and Chris van der Merwe (Laboratory for Microscopy and Microanalysis, University of Pretoria) for taking the electron micrograph.

REFERENCES

1. Smithers RHN. *The Mammals of the Southern African Subregion*. University of Pretoria: Pretoria, 1983; 553.
2. Leon B. *Aspects of the energy and water metabolism in the rock hyrax Procavia capensis and the elephant shrew Elephantulus edwardi*, PhD thesis, University of Cape Town, Cape Town, South Africa, 1981.
3. Eloff AK, van Hoven W. *Comp. Biochem. Physiol.* 1995; **80A**: 291.
4. Scott L. *Hist. Biol.* 1994; **9**: 71.
5. Scott L. *Quatern. Int.* 1996; **33**: 73.
6. Scott L, Vogel JC. *Glob. Planet. Change* 2000; **26**: 207.
7. Meiklejohn I. *S. Afr. Geogr. J* 1997; **79**: 199.
8. Edwards HGM, Newton EM, Russ J. *J. Mol. Struct.* 2000; **550–551**: 245.
9. Smith DC, Bouchard M, Lorblanchet M. *J. Raman Spectrosc.* 1999; **30**: 347.
10. Zoppi A, Signorini GF, Lucarelli F, Bachechi L. *J. Cultural Heritage* 2002; **3**: 299.
11. Edwards HGM, Drummond L, Russ J. *Spectrochim. Acta, Part A* 1998; **54**: 1849.
12. Smith DC. In *Geomaterials in Cultural Heritage, Special Publications 257*, Maggetti M, Messinga B (eds). Geological Society: London, 2006; 9.
13. White WB. In *The Infrared Spectra of Minerals*, Farmer VC (ed.). Mineralogical Society England: England, 1974; 227.
14. Smith DC, Dellinger M, Guillaume M. *Congress GEORAMAN'99 Abstracts*, Special Pub. Universidad Valladolid Press: Valladolid, 1999; 81.
15. Coleyshaw EE, Crump G, Griffith WP. *Spectrochim. Acta, Part A* 2003; **59**: 2231.
16. Manoli F, Kanakis J, Malkaj P, Dalas E. *J. Cryst. Growth* 2002; **236**(1–3): 363.
17. Manoli F, Dalas E. *J. Cryst. Growth* 2000; **218**: 359.
18. Li Q, Ding Y, Li F, Xie B, Qian Y. *J. Cryst. Growth* 2002; **236**: 357.
19. Kitamura M. *J. Colloid Interface Sci.* 2001; **236**: 318.
20. Rivadeneyra MA, Delgado G, Ramos-Cormenzana A, Delgado R. *Res. Microbiol.* 1998; **149**: 277.
21. Kitamaru M. *J. Cryst. Growth* 2002; **237–239**: 2205.
22. Kawano J, Shimobayashi N, Kitamaro M, Shinoda K, Aikawa N. *J. Cryst. Growth* 2002; **237–239**: 419.
23. Koivula M, Korpimäki E, Viitala J. *Anim. Behav.* 1997; **54**: 873.
24. Kellie A, Dain SJ, Banks PB. *J. Comp. Physiol., A* 2004; **190**: 429.
25. Gauldie RW, Sharma SK, Volk E. *Comp. Biochem. Physiol.* 1997; **118A**(3): 753.
26. Mikkelson A, Engelson SB, Hansen HCB, Larson O, Skipsted LH. *J. Cryst. Growth* 1997; **177**: 125.
27. Rautaray D, Sanyal A, Bharde A, Ahmed A, Sastry M. *Cryst. Growth Des.* 2005; **5**(2): 399.
28. Kloprogge JT, Schuiling RD, Ding Z, Hickey L, Wharton D, Frost RL. *Vib. Spectrosc.* 2002; **28**: 209.
29. Petrov I, Šoptrajanov B. *Spectrochim. Acta* 1975; **31A**: 309.
30. Rampazzi L, Andreotti A, Bonaduce I, Colombibi MP, Colombo C, Toniolo L. *Talanta* 2004; **63**: 967.
31. Maravelaki-Kalaitzaki P. *Anal. Chim. Acta* 2005; **532**: 187.
32. Jäger AK, Olsen A, Prinsloo LC, Scott L. *Planta Med.* 2006; **72**: 993.

Prof. Ian Meiklejohn of the Department of Geography, Geoinformatics and Meteorology of the University of Pretoria, did his PhD degree on rock weathering in Main Caves, Giant's Castle. Since then, in collaboration with Prof. Kevin Hall (Geography Department, University of Northern British Columbia, Canada) he has continued with studies on rock weathering and its impact on San rock art in the Ukhahlamba Drakensberg Park. The rock fragment that I analysed in this study was collected by them in the course of their research and the reference samples I used in the study I collected on one of their field trips to the Giant's Castle area.

Werner Barnard, a PhD student in the Chemistry department, did his MSc thesis on carotenoid pigments and wrote the paragraph on bacterioruberin.

The work were presented by myself as an oral contribution at the 4***th International Conference on the Application of Raman Spectroscopy in Art and Archaeology*** held in Modena, Italy, 3 – 7 Sept. 2007 and published in the Journal of Raman Spectroscopy.

Linda C Prinsloo, Werner Barnard, Ian Meiklejohn and Kevin Hall, The first Raman spectroscopic study of San rock art in the Ukhahlamba Drakensberg Park, South Africa

JOURNAL OF RAMAN SPECTROSCOPY
J. Raman Spectrosc. 2008; **39**: 646–654
Published online 19 February 2008 in Wiley InterScience
(www.interscience.wiley.com) DOI: 10.1002/jrs.1901

JRS

The first Raman spectroscopic study of San rock art in the Ukhahlamba Drakensberg Park, South Africa

Linda C. Prinsloo,[1]* Werner Barnard,[2] Ian Meiklejohn[3] and Kevin Hall[3,4]

[1] Department of Physics, University of Pretoria, Pretoria 0002, South Africa
[2] Department of Chemistry, University of Pretoria, Pretoria 0002, South Africa
[3] Department of Geography, Geoinformatics and Meteorology University of Pretoria, Pretoria 0002, South Africa
[4] Geography Department, University of Northern British Columbia, 3333 University Way, Prince George, BC., Canada, V2N 4Z9

Received 26 October 2007; Accepted 9 November 2007

San rock art sites are found throughout southern Africa; unfortunately this unique heritage is rapidly being lost through natural weathering processes, which have been the focus of various studies conducted in the uKhahlamba Drakensberg Park since 1992. It has recently been shown that the ability of Raman spectroscopy to identify salts on rock faces on a micro, as well as nano scale, can make a contribution to these projects.

In order to test the feasibility of undertaking on-site analyses, a small rock fragment with red and white pigments still attached, which had weathered off the rock face, was analysed with Raman spectroscopy under laboratory conditions, using a Dilor XY Raman instrument and a DeltaNu Inspector Raman portable instrument. A small sample of black pigment (<1 mm^2), collected from a badly deteriorated painting and a few relevant samples collected on site, were analysed as well. It was possible to identify most of the inorganic pigments and minerals detected with previous XRD and EDX measurements including whewellite and weddellite coatings, which could be a tool for carbon dating purposes. Two carotenoid pigments were detected for the first time in San rock art pigments. Animal fat was also observed for the first time on both red and white pigments, on the rock face adjacent to the paintings and in highest concentrations on the back of the rock fragment. The spectra quality makes successful on-site measurements a good prospect. Copyright © 2008 John Wiley & Sons, Ltd.

KEYWORDS: San rock art; weddellite; whewellite; haematite; red ochre; animal fat

INTRODUCTION

San rock art sites are found throughout southern Africa; unfortunately this unique heritage is rapidly being lost through natural weathering processes as the paintings are mostly found in rocky shelters and underneath overhangs, which are exposed to the elements. This has led to various projects during which factors influencing natural weathering processes such as micro-climate, rock moisture and rock temperature have been studied.[1–6]

A knowledge of the chemical composition of the pigments and binders used by the San artists is essential for the interpretation of rock weathering studies. X-ray powder diffraction (XRD), energy-dispersive X-ray spectroscopy (EDX) and paper chromatography have previously been used to analyse these pigments.[6–8] The pigments and binders mentioned in the literature were also tested in practical experiments for their mixing, colouring and weathering properties.[9,10] Although it is generally agreed that iron oxides were the pigments used to obtain the earth tones and carbon or manganese oxide the black colour, there is still much speculation about the nature of the white pigment, the type of binders used and paint application methods of the artists.

Raman spectroscopy has been used successfully to analyse pigments and substrata in pre-historic rock art and it has been shown that it could also be useful in the study of San rock art deterioration.[11–17] In this study we test the feasibility of undertaking on-site Raman measurements by first analysing a few samples under laboratory conditions.

The Ukhahlamba Drakensberg Park (a UNESCO World Heritage site)

The Drakensberg (Dragon Mountains) is the highest part of a 1000-km long escarpment that forms the chief watershed of the southern African subcontinent and the border between South Africa and the mountain kingdom of Lesotho (see

*Correspondence to: Linda C. Prinsloo, Department of Physics, University of Pretoria, Pretoria 0002, South Africa.
E-mail: linda.prinsloo@up.ac.za

map in Fig. 1). The Zulu name Ukhahlamba (a barrier of spears) is descriptive of the formidable character of this mountain range, which has its highest elevation in the Giant's Castle area.[18] The approximately 30 000 painted images (between 100–4000 years old) in nearly 600 rock-shelters in the area is one of the primary reasons why the Ukhahlamba Drakensberg Park has qualified as a World Heritage Site.[19]

San rock art

The origin and arrival of the nomadic San hunter-gatherers (also known as 'Bushman') in southern Africa is lost in the mist of time, but they were the only inhabitants of a large part of the interior of southern Africa for at least 8000 years and left behind a valuable heritage through their paintings and engravings. The animated figures depicted in San rock art participate in such activities as dancing, hunting, running and fighting – a first-hand record of the every day life of the hunters of the Stone Age (Fig. 2(a)). Further the verve, variety and engaging animation of the figures, with an overall impression of exuberant energy, are unique amongst prehistoric art. In the Drakensberg their artistry reached its pinnacle with delicate polychrome paintings, where every minute detail is painstakingly depicted.[20,21]

Findings based on 19th century ethnographical records and current research concerning the northern San still living in the Kalahari shows that a part of San art was associated with the trance experience of 'medicine men' or shamans, hence the trance dances and hallucinatory experiences of the shamans depicted in some of their paintings (Fig. 2(b)).[20,21]

In this Shamanistic interpretation not only the pictures, but also the rock face were important, the latter being perceived as a veil between the known and the mystical world. Painting, therefore became a ritual act and the paint was prepared under ceremonial circumstances. For instance, a woman had to heat *qhang qhang* (red ochre) at night during a full moon, then grind it to a fine powder and mix it with fresh eland blood to make red pigments. In this way the painting itself had the power of the eland, a large antelope revered by the San as a key symbol of life and potency.[20,21]

Samples

In this preliminary study the pigment colours most frequently used by the San, namely white, red and black were analysed under laboratory conditions. A small rock fragment (Fig. 3(a)), which had fortuitously weathered off the rock face (Barnes' shelter, Giants Castle), was used to analyse the red and white pigments. A minute piece of black pigment was collected (under licence) from a painting that has nearly disappeared from the rock face (Wilcox shelter, Giants Castle). A few control samples, such as red ochre, were also collected on site.

EXPERIMENTAL

Raman spectra were recorded with a XY Raman spectrometer from Dilor (liquid nitrogen-cooled CCD), using the 514.5 nm (Coherent Innova 90 Ar^+ laser) and yellow 568 nm (Spectra–Physics Krypton Stabilite 2017 laser) lines as exciting radiation. In both cases the scattered light was collected through an Olympus confocal microscope with a long distance ×50 microscope objective. The laser power was kept below 10 mW at the sample to prevent sample degradation.

A hand-held DeltaNu Inspector Raman instrument (weight <3 kg), equipped with a 785 nm diode laser for excitation with a maximum output power of 120 mW, was used to record spectra of the same samples. The spectral resolution of the instrument is 8 cm^{-1} and the spectral range 200–2000 cm^{-1}.

A Bruker 113v Fourier transform infrared (FTIR) spectrometer was used to record mid-infrared transmission spectra of powdered samples (1 mg) pressed into KBr (100 mg) pellets. The resolution was 2 cm^{-1} and 32 scans were signal-averaged in each interferogram.

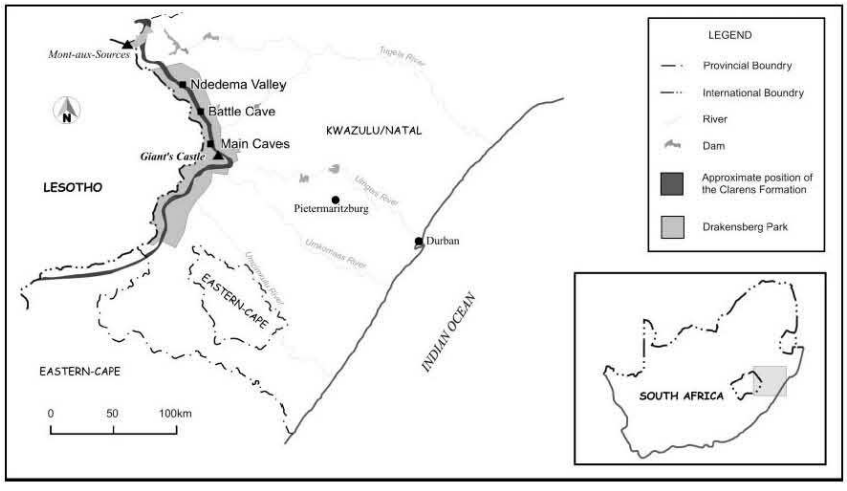

Figure 1. Map showing the Ukhahlamba Drakensberg Park in relation to the rest of South Africa.

DOI: 10.1002/jrs

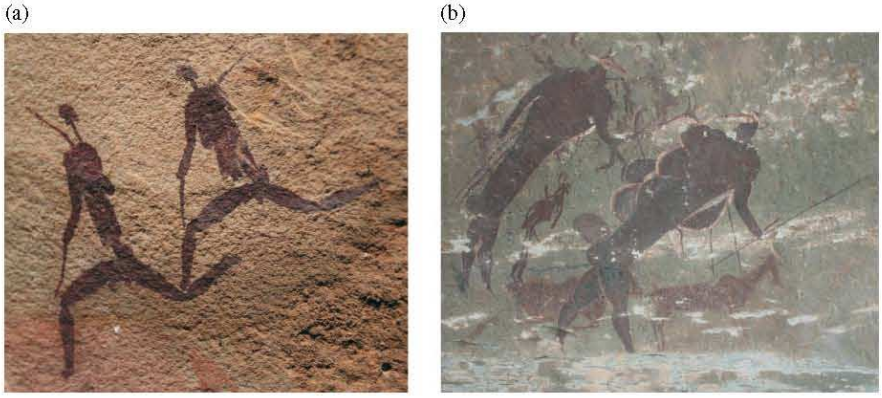

Figure 2. San paintings: (a) two San hunters running; (b) two San shamans with eland heads and hooves (therianthropes: mythological part-man and part-beast figures) depicting the blending of man with the power of the eland. The bubbles around the one figure represent the experiences of shamans during trance dances when they feel the power exploding within them.

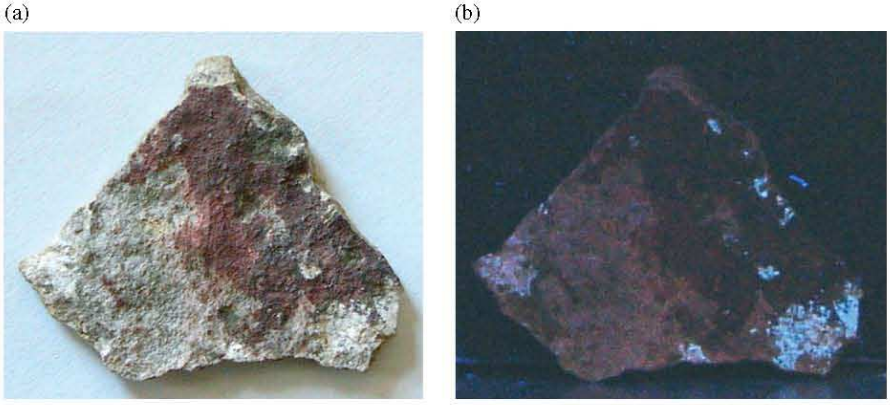

Figure 3. Photo of the shard with red and white pigment in (a) sunlight and (b) under 254 nm UV light.

X-ray diffraction data were collected using a PANalytical X'Pert Pro powder diffractometer with X'Celerator detector and variable divergence and receiving slits, with Fe filtered Co K_α-radiation (35 kV 50 mA). Different phases were identified using X'Pert Highscore plus software. Quantification (Rietveld method) of the data was done by the Autoquan/BGMN software, (GE Inspection Technologies) employing the Fundamental Parameter Approach.

RESULTS

White pigment on shard

Fluorescence of the white pigment, as seen in the photo taken under 254 nm UV light (Fig. 3(b)), made Raman spectra difficult to obtain with the 514.5 nm laser line. Only by searching for a few specific spots without fluorescence, was it possible to record the well-known spectra of α-quartz (126, 203 and 462 cm^{-1}) and two polymorphs of TiO_2, namely anatase (143 (vs), 395, 513 and 636 cm^{-1}) and rutile (230, 445 and 606 cm^{-1}).

Red pigment on shard

Red particles in the pigment could be clearly distinguished from white and grey crystallites with the 50× long distance objective of the Olympus microscope. Focusing on the grey and white crystallites, spectra of gypsum (strongest band 1007 cm^{-1}), as well as the anhydrous form anhydrite (1022 cm^{-1}), α-quartz and the anatase phase of TiO_2 were recorded.

The most prominent bands in almost all of the spectra recorded on the red particles of the pigment (Fig. 4) originate from calcium oxalate mono- (whewellite) or dihydrate (weddellite) or mixtures thereof. The two hydrates could easily be distinguished through the symmetric C=O stretch bands at 1462 and 1490 cm^{-1} for whewellite (wh) and 1476 cm^{-1} for weddellite (wd), as well as the C–C stretching vibration at 903 (wd) and 894 cm^{-1} (wh). The well-defined lattice vibrations also clearly differentiate between the two hydrates as weddellite has two bands (164 and 196 cm^{-1}) and whewellite four bands (193, 203, 222 and 249 cm^{-1}) in this region.[22] The bands around 500 and 524 cm^{-1} are due to Ca–O stretch vibrations, CaO ring deformation and O–C=O bending modes. Calcium oxalates are commonly found on

JRS

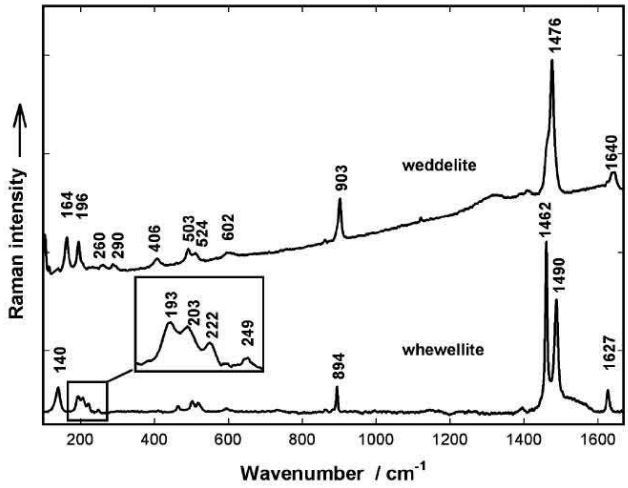

Figure 4. Examples of spectra recorded on the red pigment with the 514.5 nm laser line showing the hydrate phases of calcium oxalate.

calcite rock faces and has previously also been reported on sandstone.[23,24] In most of the spectra recorded on red parts of the sample, bands at 290, 406, 602 and ~1300 cm^{-1} are also present, which are characteristic of haematite. Although it could be expected that iron oxalates would form in the presence of oxalic acid, it was not detected.[25]

In Fig. 5 spectra recorded on the pigment are compared to spectra recorded for a red ochre found on the terrain and the ochre after it had been fired for 1 h at 650 °C (temperature of most wood-burning fires) in order to test the validity of the historical record of how the paint was produced ('San rock art'). The bands ascribed to haematite occur at the same positions in all the spectra and no shift is observed that can be attributed to heating or mixing of the pigment. The bandwidth of most of the peaks decreased with firing and six of the seven predicted Raman active first order modes of α-Fe_2O_3 (225, 245, 292, 409, 497 and 608 cm^{-1}),[26] as well as bands at 658 and 1314 cm^{-1} are observed in all the spectra. In many papers the 658 cm^{-1} band is assigned to magnetite, which normally occurs together with haematite in natural ochres and has its strongest band at this position. It has also been assigned to kaolinite in natural ochres.[27] In this case, however, the band still appears in the spectrum of the fired ochre (even stronger and narrower) where all the magnetite has been converted to haematite[26] and kaolinite has not been detected as seen from XRD analyses of the samples given in Table 1. In Refs 28–31 this band is assigned to an IR active mode which is symmetry forbidden in the Raman spectrum and its appearance in natural haematites ascribed to a lowering of symmetry in disordered structures. The two spectra recorded on the red paint differ first in the intensity of the bands originating from whewellite (1462 and 1490 cm^{-1} most intense bands) relative to the intensity of the 406 cm^{-1} band of haematite. As the spectrum with the weakest oxalate bands was recorded on a part of the paint where the outside layer has been scraped off, it appears that the oxalate was not part of the original pigment, but formed later over the paint layer. Second, the 1314 cm^{-1} band in the spectrum recorded on the inside pigment layer is much stronger than in the spectrum recorded on the outermost layer. This probably is owing to a strong resonance enhancement of this band with 568 nm excitation, which have been observed for certain forms of haematite crystallites (platelets).[30]

Two types of spectra (Fig. 6) were recorded for the fired ochre on red crystallites (note that the spectra do not resemble the Raman spectra of any of the other compounds present in the ochre–Table 1). In one spectrum the intense bands are narrow and reminiscent of a highly crystalline material, while in the other most bands have broadened and shifted to

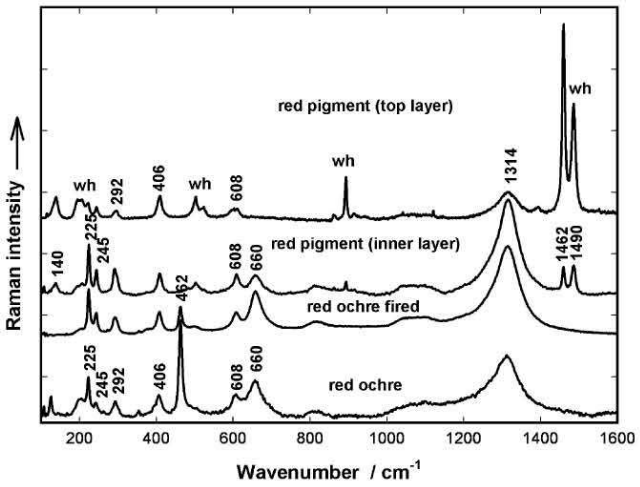

Figure 5. Spectra recorded on the red pigment on shard, red ochre and red ochre fired for 1h at 650 °C. The spectrum of the top layer of pigment was obtained with a 514.5 nm laser line and the other spectra with a 568 nm laser line.

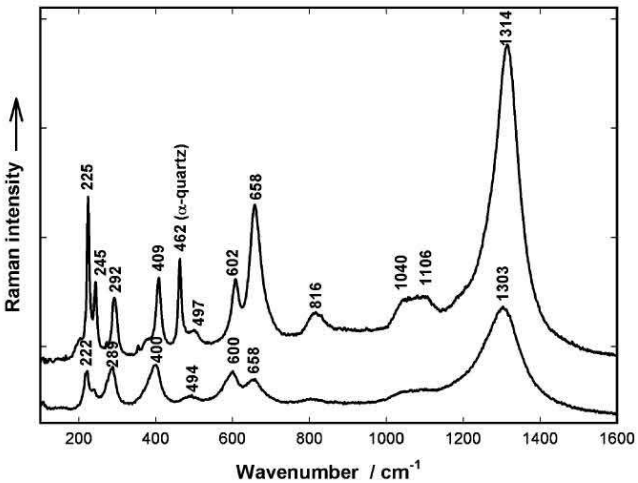

Figure 6. Comparison of two types of spectra recorded on the red particles of the ochre fired at 650 °C (both obtained with 568 nm excitation).

Table 1. XRD analysis of the red ochre and after firing at 650 °C (wt%)

	Red ochre rock	Red ochre fired
Calcite ($CaCO_3$)	0.21	0.35
Haematite (Fe_2O_3)	0.84	1.28
Magnetite (Fe_3O_4)	0.68	0.06
Microcline, intermediate1 ($KAlSi_3O_8$)	2	2.65
Muscovite $\{KAl_2(AlSi_3O_{10})(OH)_2\}$	12.43	8.11
Plagioclase $(Na,Ca)(Al, Si)_4O_8$	10.5	9.9
Quartz (SiO_2)	73.35	77.64

lower wavenumbers. This could be due to differences in size, morphology or orientation of the pigment crystallites.[29–31] It has recently also been illustrated that doping with aluminium broadens and shifts most bands in the haematite Raman spectrum to lower wavenumbers, which might be another explanation for the existence of this second spectrum.[32,33] The origin of the band at 1314 cm^{-1} has previously been attributed to a two magnon scattering process, but later work support a resonance-enhanced two-phonon process with the IR active band at 658 cm^{-1} as fundamental.[28,34] Interestingly, although this band has shifted downwards to 1303 cm^{-1}, the band at 658 cm^{-1} is still in the same position. The rather broad bands at 816 and between 1040 and 1106 cm^{-1} have previously also been noted in the spectra of a haematite single crystal and occur only in *xx* polarisation.[29]

Spectra similar to the second kind of haematite spectrum recorded on the fired sample were also obtained on the ochre and pigment on the shard (Fig. 7). A change in relative intensity and wavenumber to lower wavenumber values is observed from the natural ochre to the pigment on the shard (the spectrum of the fired ochre was recorded with the 568 nm laser and therefore not directly comparable). It has been shown that the Raman spectrum of haematite is very dependent on particle size and morphology, production process, as well as the energy of the exciting radiation. In the formation process of clay many different processes can play a role to form heterogeneous mixtures and it is quite possible that more than one type of haematite may exist in a natural ochre sample.

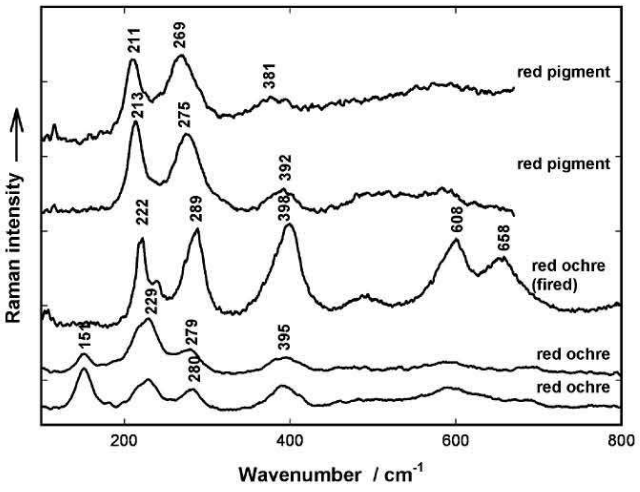

Figure 7. Comparison of the second kind of haematite spectrum as recorded on the red ochre, the ochre fired at 650 °C and on the pigment itself. All spectra recorded with 514.5 nm excitation, except for the spectrum of the fired sample, which was obtained with 568 nm excitation.

Back of shard

Gypsum was detected in most spectra recorded on the back of the shard and anhydrite in a few. Spectra of feldspar (252, 291, 330, 416, 480 and 508 cm^{-1}),[34] α-quartz, anatase and oxalates (wd and wh) were also recorded. It is suspected that sulphates, dissolved in surface water, accumulated at the back of the shard resulting in its detachment from the rock face.

FTIR measurements of shard

The small size of the area analysed with Raman microscopy and the subjective choice of its location by the operator do not give a representative analysis of a sample and therefore transmission mid-infrared spectra were recorded for the samples. In Fig. 8 the spectra of the white pigment, red pigment, back side of the rock fragment and pristine Clarens formation sandstone are compared. The pigment samples were scraped off the top of the shard and therefore reflect the composition of the top layer. The strongest bands in spectra of both the red and white pigment, originate from whewellite (782, 1316 and 1624 cm^{-1}),[35] but a band at 1655 cm^{-1} (as yet unidentified) indicates that another organic phase is present in the white pigment. The spectrum recorded on the back of the shard has bands characteristic of α-quartz (strongest peak ~1000 cm^{-1} and characteristic doublet at 779 and 798 cm^{-1}). All the other peaks are attributed to gypsum (ν_3 at 1150 cm^{-1},

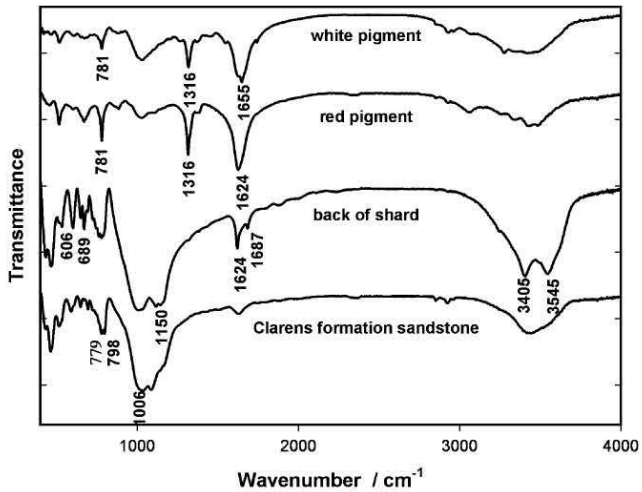

Figure 8. FTIR spectra recorded of white pigment, red pigment, back of the shard and Clarens formation sandstone.

ν_4 at 606 and 689 cm^{-1}, lattice water-stretching vibrations at 3405, 3545 cm^{-1} and bending vibrations at 1624, 1687 cm^{-1}). Notice the absence of a peak at 1316 cm^{-1} in the spectrum of pristine sandstone (only slightly visible in spectrum of the back of the shard), which indicates the absence of whewellite.

Black pigment

The spectra presented in Fig. 9 were recorded on a very small sample of black pigment collected from a severely deteriorated painting and the two characteristic broad bands of amorphous carbon (1350 and 1600 cm^{-1}) can clearly be observed. In all the spectra, except one, whewellite and weddellite in varying concentrations were observed. It is notable that the peaks assigned to Fe–O vibrations in similar spectra recorded on the red pigment are absent. Calcite (1082 cm^{-1}), gypsum (1007 cm^{-1}) and anhydrite (1022 cm^{-1}) were also detected.

Organic phases detected with 514.5 nm laser excitation

An organic phase was detected on the white pigment that can be attributed to a pigment of carotenoidal nature. In Fig. 10 the spectrum is compared to that of egg white, the yolk and a mixture. (Note that poultry eggs were used to record the spectra; the San would probably have used ostrich eggs). Egg white has been suggested as a binder for San rock art, but experimental studies have shown that egg white on its own has very poor binding properties. In contrast egg yolk is an excellent binder and has been used in the 'egg tempera' paintings of medieval frescoes.[36] The spectrum recorded on the red pigment closely resembles the spectrum of the egg yolk, with strongest bands due to lutein[37] (the carotenoid responsible for the yellow colour of the yolk) and could indicate that egg yolk (or a mixture) was used as a binder by the San artists. It is only circumstantial evidence though, as many other natural carotenoids have spectra similar to that of lutein

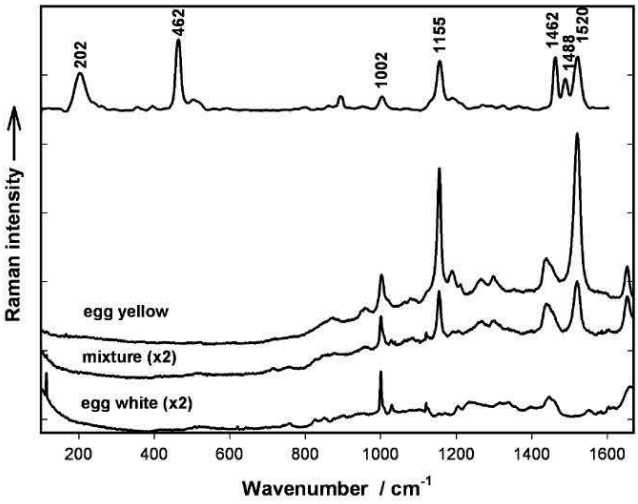

Figure 10. Organic phase detected in white pigment in comparison with spectra recorded from egg white, the yolk and a mixture.

and the presence of carotenoid pigments could also originate from lichens or other plant material. The other bands in the spectrum can be ascribed to whewellite and α-quartz.

On the black pigment another compound of carotenoidal nature was observed with the two most intense bands at 1503 and 1148 cm^{-1} assigned to the C=C and C–C stretching modes respectively (Fig. 11).[39] Also, many overtone and combination bands were observed at higher wavenumbers, which is characteristic of carotenoids due to the "carry over" of the resonance effect. The C=C stretching value of 1503 cm^{-1} is significantly lower than that of many natural carotenoids that contain nine conjugated double bonds and compares well with the reported values of certain natural marine carotenoids that have unmethylated polyacetylenic backbones.[40,41] The C–C stretching vibration

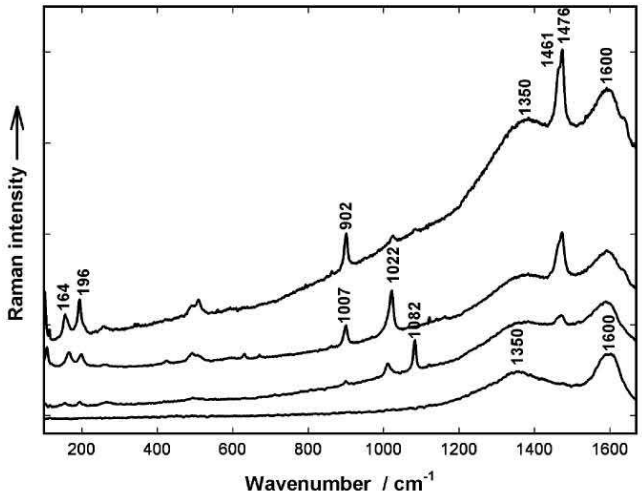

Figure 9. Various Raman spectra recorded on a small sample of black pigment.

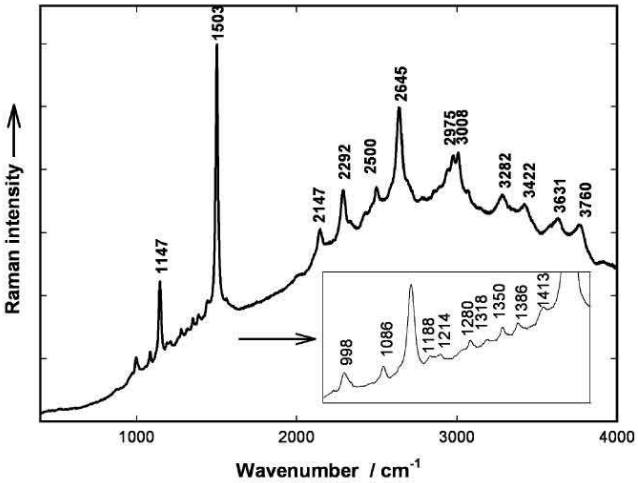

Figure 11. Resonance-enhanced spectrum of a carotenoid recorded with 514.5 nm laser line on the black pigment.

at 1147 cm^{-1} is indicative of methyl substitution (average value of ~1155 cm^{-1} of other substituted carotenoids) rather than that of the unsubstituted carotenoids that have a value of ~1130 cm^{-1}.[40] It is therefore deduced that it is a methyl substituted carotenoid with a longer than normal conjugated backbone. The reported C–C and C=C stretching modes of two long chain carotenoids, decapreno-β-carotene (at 1504 cm^{-1} and 1152 cm^{-1}) and bacterioruberin (at 1505 cm^{-1} and 1152 cm^{-1}) compare well with our data (Fig. 13).[42,43] The weaker bands reported for decapreno-β-carotene at 1002 (CH_3 deformation), 1193 (CH–CH deformation) and 1283 cm^{-1} (HC=CH in-plane rocking) as well as the only other reported band for bacterioruberin at 1000 cm^{-1} coincide with the corresponding bands in our spectrum. The C=C stretching band value is indicative of the effective conjugation length of polyacetylenic systems and applying the mathematical relationship reported in reference 39 to this carotenoid, predicts an effective conjugation length of approximately 12 conjugated double bonds. Decapreno-β-carotene and bacterioruberin each have 13 formal conjugated double bonds in their polyacetylenic backbones and the lower value predicted is rationalised by the fact that the CH_3 groups distort the backbone, lowering the effective conjugation length. Our carotenoid is probably not decapreno-β-carotene, but rather similar in structure to bacterioruberin as it has been extensively reported to be produced in nature by many different halobacteria,[43] whereas the authors could to their knowledge find no reference to any natural occurrence of decapreno-β-carotene. Supportive of this is the recent report that bacterioruberins have been detected on frescoe paintings.[44]

Results obtained with the portable instrument

On the red pigment, in agreement with the measurements with the XY instrument, bands originating from the two calcium oxalates were present in most spectra. The bands due to other inorganic phases (e.g. haematite) are very weak and not very useful.

Spectra recorded on the back of the shard (Fig. 12, bottom), had very strong bands clearly originating from an organic phase with the characteristic band of gypsum (1007 cm^{-1}) also prominent. Animal fat has quite frequently been mentioned in the literature as a possible binder for San pigments and a spectrum of fat (beef) smeared on sandstone was also recorded (Fig. 12, middle). The five bands in the spectrum is very typical of a fat and can be assigned to a carbonyl stretch ν(C=O) at 1738 cm^{-1}, a ν(C=C) stretch at 1628 cm^{-1}, the δ(C–H) conformation vibration at 1419 cm^{-1}, an in-phase methylene twisting deformation (1300 cm^{-1}) and at 1237 cm^{-1} the in-plane =CH deformation vibration.[45] The two spectra match perfectly (Fig. 12).

Animal fat was also detected on the red and white pigments, as well as on a rock fragment from the adjacent rockface. On the white pigment mixtures of anatase, whewellite as well as an unidentified organic phase (broad bands ~1243 and 1300 cm^{-1}), were also detected (Fig. 12, top). The black pigment sample was too small to record spectra on the portable instrument.

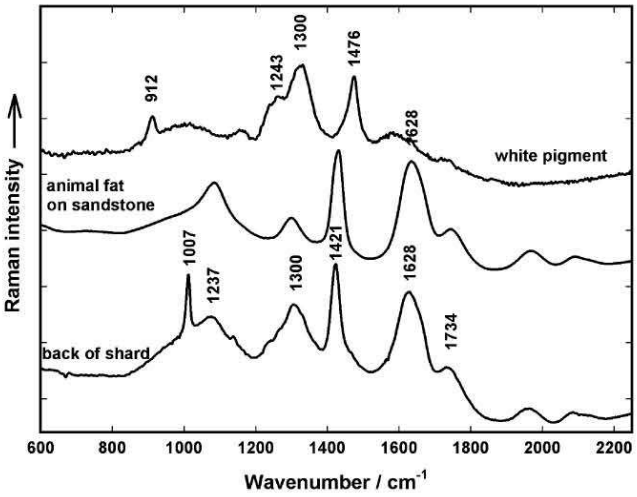

Figure 12. Spectra recorded on the back of the rock garment (bottom), animal fat on sandstone (middle) and the white pigment (top) with the 785 nm laser line of the DeltaNu portable instrument.

DISCUSSION

The combination of the three laser lines and FTIR measurements gave complementary results, which are summarised in Table 2. It can be deducted that haematite (red ochre) was the pigment used for the red colour, carbon for the black and possibly a white clay or shale for the white colour. The white

Table 2. Summary of compounds detected on the various pigments and backside of rock fragment

Compound	Red pigment	White pigment	Backside	Black pigment
Carbon	*			***
Haematite	***			
Weddellite	***	***		***
Whewellite	***	***	*	***
Gypsum	**	*	***	*
Anhydrite	*		*	
Feldspar	*		**	
α-quartz	**	**	**	**
Calcite	*	*	*	**
Rutile		*		
Anatase	*	**	*	*
Animal fat	*	**	***	not recorded

*** Present in most spectra recorded.
** in some spectra.
* in one spectrum.

pigment contains a still unknown organic phase, which is fluorescent.

Weddellite and whewellite were detected everywhere on the shard, but in highest concentrations on the pigments. The much lower intensity of bands originating from the oxalates in spectra recorded on the red pigment, where the top layer has been scraped off, suggests that it was not part of the original pigment. The detection of oxalates on the pigments may open a window to date the paintings more accurately, especially if the pigment is encapsulated between two oxalate layers as found for pigments in Spain and Texas, which protect the paint, prevent weathering and have been used for AMS ^{14}C dating of Post-Paleolithic rock art.[23,24] The origin of the oxalic acid necessary to form the oxalates has been ascribed to previous colonisation of the rock face by lichens, but it has been shown that the presence of rock hyraces in shelters may also be a source of oxalic acid.[17] Furthermore, it is suspected that San artists used plant sap as binder and as many plants have oxalic acid as a constituent of the sap it may have been introduced into the paint in this way as suggested in Ref. 5.

The ability to detect very low concentrations of carotenoid pigments with the green laser line due to the resonance effect is very useful. A careful study of the microenvironment of a painting would be necessary to determine if the presence of the carotenoids is due to deliberate addition by the artists or the previous/later presence of lichens, fungi or algae on the rock face.

Many authors have speculated that San artists used animal fat as binder and it is still used for the preparation of cosmetic and ritual body paint in San communities in the Kalahari.[10] Practical experiments have also shown that ochre mixed with animal fat has good weathering properties, but it is very difficult to draw the delicate lines that San rock art is famous for with such a mixture.[9,10] The concentration of fat on the back of the rock fragment, suggests that the surface of the rock face was first prepared for painting by covering it with fat (probably hot), which would penetrate into the sandstone and prevent the paint from soaking into it. It can however not be overlooked that the fatty layer might have another origin. Humans (other than the San) have for long periods of time occupied shelters like Barnes' shelter, where the shards were collected. (The first game ranger of the Giant's Castle Nature Reserve, Mr Barnes used the shelter as his head quarters). The fatty layer might therefore originate from cooking activities in the shelter. Rock hyraces have also inhabited the shelters and as they produce volatile short-chain fatty acids as part of their metabolic products they could also have contributed to an organic coating on the rock face.[17]

Unfortunately the fatty layer would also hinder the natural flow of groundwater through the sandstone and bring about an accumulation of soluble salts, such as sulphates behind the fatty layer (Fig. 10 supports this), which would cause the layer with the applied pigment to detach from the rock face with time.

Attempts to verify the account of how the paint was produced (firing and mixing with eland blood) has so far been unsuccessful. An in-depth study of the temperature behaviour of the natural ochres found on the terrain might provide an answer to the question if the ochres were fired before mixing the paints.

CONCLUSION

The weathering of the rock faces depicting San rock art is a complex mechanism encompassing interdependent mechanical, geological, chemical, physical and biological processes. We have shown that Raman spectroscopy could play a very useful role in unravelling the key factors that contribute to this process. As each individual rock art site has a unique microclimate, which influences the stability of the paints, an on-site study of each site will be necessary to make an input in the decision-making process for its preservation. In the same way the interpretation of the data collected on rock paintings has to be done in relation to the micro-environment of each painting, as well as the historical record of the site. The discovery of animal fat on the rock fragment collected from Barnes' shelter is exciting, but the exact origin of the fat has to be verified by similar experiments at other sites.

Acknowledgements

The authors wish to thank Heritage KwaZulu–Natal (permits 04/26 and 04/27) for permission to collect samples, Sabine MC Verryn (XRF and XRD Laboratory, University of Pretoria) for taking the XRD measurements and Stéphane Hoerlé (Rock Art Research Centre, University of the Witwatersrand) for his comments on the manuscript.

REFERENCES

1. Meiklejohn I. *S. Afr. Geogr. J.* 1997; **79**: 199, Special issue.
2. Hœrlé S, Salomon A. *S. Afr. J. Sci.* 2004; **100**: 340.
3. Hœrlé S. *S. Afr. J. Geol.* 2005; **108**: 297.
4. Hœrlé S. *Earth Surf. Processes Land.* 2006; **31**: 383.
5. Hall K, Meiklejohn I, Arocena JM. *Geomorph.* 2007; **91**: 132.
6. Arocena JM, Hall K, Meiklejohn I. *J. Geoarchaeol.* in press.
7. van Rijssen WJ. *S. Afr. Archaeol. Bull.* 1990; **45**: 58.
8. Denninger E. *S. Afr. J. Sci. Spec. Publ.* 1971; **2**: 80.
9. Johnson T. *S. Afr. Archaeol. Bull.* 1957; **12**: 98.
10. Rudner I. *S. Afr. Archaeol. Soc. Goodwin Ser.* 1983; **4**: 14.
11. Zoppi A, Signorini GF, Lucarelli F, Bachechi L. *J. Cult. Herit.* 2002; **3**: 299.
12. Smith DC, Bouchard M, Lorblanchet M. *J. Raman Spectrosc.* 1999; **30**: 347.
13. Edwards HGM, Drummond L, Russ J. *Spectrochim. Acta, Part A* 1998; **54**: 1849.
14. Edwards HGM, Drummond L, Russ J. *J. Raman Spectrosc.* 1999; **30**: 421.
15. Hernanz A, Mas M, Gavilán B, Hernández B. *J. Raman Spectrosc.* 2006; **37**: 492.
16. Ospitali F, Smith DC, Lorblanchet M. *J. Raman Spectrosc.* 2006; **37**: 1063.

17. Prinsloo LC. *J. Raman Spectrosc.* 2007; **66**: 1123.
18. Liebenberg DP. *The Drakensberg of Natal*. Cape & Transvaal Printers Ltd: Cape Town, 1972.
19. Mazel AD, Watchman AL. *Antiquity* 1997; **71**(272): 445.
20. Lewis-Williams JD. *Afr. Arts* 1985; **18**(3): 54.
21. Lewis-Williams JD, Dowson TA. *S. Afr. Archaeol. Bull.* 1990; **45**: 16.
22. Frost RL, Weier ML. *J. Raman Spectrosc.* 2003; **34**: 775.
23. Russ J, Kaluarachchi WD, Drummond L, Edwards HGM. *Stud. Conserv.* 1999; **44**: 91.
24. Hernanz A, Gavira-Vallejo JM, Ruiz-López JF. *J. Optoelectron. Adv. Mater.* 2007; **9**: 512.
25. Edwards HGM, Russell NC. *J. Mol. Struct.* 1998; **443**: 223.
26. De Faria DLA, Silva SV, de Oliviera MT. *J. Raman Spectrosc.* 1997; **28**: 873.
27. Bikiaris D, Daniilia Sister, Sotiropoulou S, Katsimbiri O, Pavlidou E, Moutsatsou AP, Chryssoulakis Y. *Spectrochim. Acta, Part A* 1999; **56**: 3.
28. McCarty KF. *Solid State Commun.* 1988; **68**: 799.
29. Bersani D, Lottici PP, Montenero A. *J. Raman Spectrosc.* 1999; **30**: 355.
30. Wang J, White WB, Adair JH. *J. Am. Ceram. Soc.* 2005; **88**(12): 3449.
31. Chernyshova IV, Hochella MF Jr, Madden AS. *Phys. Chem. Chem. Phys* 2007; **9**: 1736.
32. Zoppi A, Lofrumento C, Castellucci EM, Sciau Ph. *J. Raman Spectrosc.* 2008; **39**: 40.
33. Froment F, Tournié A, Colomban Ph. *J. Raman Spectrosc.* in press.
34. Gillet P. *Applications of Vibrational Spectroscopy to Geology* in *Handbook of Vibrational Spectroscopy* (eds). Chalmers EM, Griffiths PR, John Wiley & Sons Ltd: London 2002; 3169–3191.
35. Petrov I, Šoptrajanov B. *Spectrochim. Acta* 1975; **31A**: 309.
36. Lepot L, Denoël S, Gilbert B. *J. Raman Spectrosc.* 2006; **37**: 1098.
37. Hoskins LC. *Spectrochim. Acta* 1986; **42A**(2/3): 169.
38. Barnard W, de Waal D. *J. Raman Spectrosc.* 2006; **37**: 342.
39. Saito S, Tasumi M, *J. Raman Spectr.* 1983; **14**: 310.
40. Barnard W, de Waal D, *J. Raman Spectr.* 2006; **37**: 342.
41. Karampelas S, Fritch E, Mevellec J-Y, Gauthier J-P, Sklavounos S, Soldatos T, *J. Raman Spectr.* 2007; **38**: 217.
42. Veronelli M, Zerbi G, Stradi R, *J. Raman Spectr.* 1995; **26**: 683.
43. Marshall CP, Leuko S, Coyle CM, Walter MR, Burns BP, Neilan BA, *Astrobiology* 2007; **7**: 631.
44. Imperi F, Caneva G, Cancellieri L, Ricci MA, Sodo A, Visca P, *Environ. Microbiol.* 2007; **9**: 2894.
45. Vandenabeele P, Wehling B, Moens L, Egwards H, De Reu M, Van Hooydonk G, *Anal. Chim. Acta* 2000; **407**: 261.

CONCLUSIONS AND FUTURE RESEARCH SUGGESTIONS

CHAPTER 7

Conclusion

In conclusion it can be said that the application of Raman spectroscopy to archaeological problems in South Africa has been extremely successful and had quite a few positive outcomes.

- The results of the research projects have contributed to a better insight into the pre-colonial history of sub-Saharan Africa, a better understanding of the technology used by San artists and highlighted the unique attributes of one of our animal species.

- Since the first poster about the work was presented at an international conference held in South Africa in 2001, it has motivated other South African scientists to also apply Raman spectroscopy to studies on our cultural and natural heritage.[1-7] \

- The collaborative and multidisciplinary nature of the projects has created an awareness of the versatility of Raman spectroscopy as analytical technique.

- My work on the celadon shards led to collaboration with Dr. Philippe Colomban.

- On the international scene the work has been presented at four international conferences, I have visited the research laboratory of Dr. Colomban in France three times, where most of the experimental work for chapter 4 was done. It has placed me in personal contact with scientists doing similar rock art studies in France, Spain, Australia and America, which in the future might lead to further collaborative work. Dr. Colomban visited South Africa twice and gave a public lecture, hosted by the Spectroscopy Society of South Africa at the Sci-Enza Centre, which was well attended by people from Chemistry, Physics and Geology departments of various universities as well as from industry and the CSIR. He visited the Raman and Infrared facility in the Chemistry department and had a meeting with Prof. Ignacy Cukrowski (then Head of the Chemistry department) and gave advice about Raman instrumentation. Discussions with other staff members and their students led to the opportunity for a PhD student in the Chemistry department (Werner Barnard) to visit Dr Colomban's lab in Paris in August 2008.

- My work and visits to France has motivated a young French student (Aurèlie Tournie) to apply for a Postdoc position in the Physics department in 2009.

Future research suggestions

All four of the studies have opened new directions of research to be explored in the future, some of which are already underway.

- Chinese porcelain and Persian pottery shards have been excavated at inland archaeological sites in southern Africa, such as Great Zimbabwe, as well as sites all along the eastern coast along the ancient trade routes. Early in the 20th century, when the shards were originally classified it served as a rough dating method. In recent years, since China has opened its doors to the west, scholars such as Nigel Wood, had the opportunity to study the Chinese pottery and porcelain first hand in China, which has made it possible to detect provenance and production date more accurately. Similar in-depth research studies as performed on the Mapungubwe celadon shards would serve well to refine the interesting history of the African east coast.

- The study of the glass trade beads known as the Mapungubwe Oblates has shown that the production technology was very specific, but that the provenance of the beads is still a mystery. Clarification of their origin will help to lift the obscurity still surrounding Mapungubwe and its history. In order to do this I have started by analysing the other glass beads found at Mapungubwe and plan to expand the study to the large amount of beads that represent the African bead tradition in southern Africa.

- The research on rock hyraces and the follow-up work on hyraceam, which supports its use as treatment for epilepsy, should be continued to endeavour to find the active ingredient.

- The application of Raman spectroscopy to San rock art has been very successful and has resulted in a larger study, which entails analysing San rock art non-destructively with the use of a portable Raman instrument (from the lab of Dr Colomban) on exhibits in the Rock Art Research Institute (RARI), University of the Witwatersrand, as well as *on-site* in the Ukhahlamba Drakensberg Park and other sites around the country. The project is

undertaken in collaboration with the director of RARI, Dr Ben W Smith, who under the GDRI/STAR (CNRS) project facilitates collaboration on rock art projects in South Africa, Prof. Ian Meiklejohn (Geoinformatics and Meteorology of the University of Pretoria) and Dr. Sven Ouzman (Department of Archaeology, University of Pretoria). The results of our work will complement research studies on rock weathering and conservation.

References:

1. Kock L D, De Waal D, Raman studies of the underglaze blue pigment on ceramic artefacts of the Ming dynasty and of unknown origins. *J. Raman Spectrosc*, 2007; 38(11): 1480.
2. de Waal D, Raman analysis of underglaze pigments on porcelain art. *J. Raman Spectrosc.* 2007; 38(7): 956.
3. Legodi M , De Waal D Raman spectroscopic study of ancient South African domestic clay pottery *Spectrochim. Acta*, Part A: 2007; 66A(1): 135.
4. Barnard W, de Waal D, Raman investigation of pigmentary molecules in the molluscan biogenic matrix. *J. of Raman Spectrosc*. 2006; 37(1-3): 342.
5. Legodi MA, de Waal D, Raman analysis of red-brown and gray shards from 16th and 17th century Portuguese shipwrecks *Cryst. Eng*. 2004; Volume Date 2003, 6(4), 287.
6. de Waal Danita, Raman investigation of ceramics from 16th and 17th century Portuguese shipwrecks. *J. Raman Spectrosc.* 2004; 35 (8/9), 646.
7. de Waal Danita, Raman identification of the pigment in blue and white Ming porcelain shards. *Asian Chem. Lett.* (2004), 8(1), 57.

RESEARCH RECORD: Linda C. Prinsloo

ISI Web of Knowledge entry

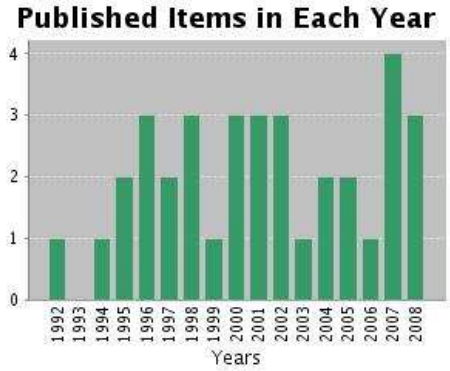

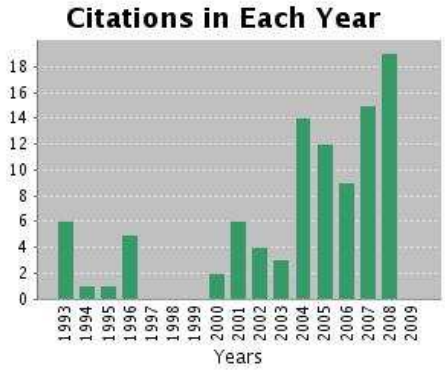

Results found:	**35**
Sum of the Times Cited	**97**
Average Citations per article	**2.77**
h-index:	**5**

PUBLICATIONS IN REFEREED JOURNALS (33)

2008: Linda C Prinsloo, Werner Barnard, Ian Meiklejohn and Kevin Hall. The first Raman spectroscopic study of San rock art in the Ukhahlamba Drakensberg Park, South Africa. ***Journal of Raman Spectroscopy,*** 39 (5): 646-654.

2008: Linda C Prinsloo and Philippe Colomban, A Raman spectroscopic study of the Mapungubwe oblates; glass trade beads excavated at an Iron Age archaeological site in South Africa, ***Journal of Raman Spectroscopy*** 39 (1): 79-90.

2008: Brink DJ, van der Berg NG and Prinsloo LC, The role of interface effects on the reflection of circularly polarised light from the thin-film structure of scarabus beetles, ***Surface and Interface Analysis***, 40, 769-771.

2007: Andreas Olsen, Linda C. Prinsloo, Louis Scott and Anna K. Jäger, Hyraceum, the fossilised metabolic products of rock hyraces, shows affinity to the GABA-benzodiazepine receptor, ***South African Journal of Science*** 103, 437-438.

2007: Brink DJ, van der Berg NG, Prinsloo L and Hodgkingson I, Unusual coloration in scarabaeid beetles, ***Journal of Physics D: Applied Physics***, **40** (7), 7, 2189-2196**.**

2007: Linda C Prinsloo, Rock Hyraces: a cause for San rock art deterioration? ***Journal of Raman Spectroscopy***, **38**: (5), 496-503.

2006: Andreas Olsen, Linda C. Prinsloo, Louis Scott and Anna K. Jäger, Hyraceum, the fossilised metabolic products of rock hyraces, shows affinity to the GABA-benzodiazepine receptor. ***Planta medica*** 72 (11): 993-993.

2005: H.W. Kunert, T. Maurice, J. Barnas, J. Malherbe, D.J. Brink, L. Prinsloo, Raman and photoluminescence study from n- and p-type 6H-SiC alpha-particle irradiated. ***Vacuum***, 78, 503-508.

2005: Linda C Prinsloo, Nigel Wood, Maggi Loubser, Sabine M C Verryn and Sian Tiley. Re-dating of Chinese celadon shards excavated on Mapungubwe Hill, a 13th century Iron Age site in South Africa, using Raman spectroscopy, XRF and XRD, ***Journal of Raman Spectroscopy***, 36,(8) 806-816.

2004: H.W. Kunert, D. Diale, L.C. Prinsloo, M. Hayes, J. Barnas, J. Malherbe, DJ. Brink, AGI Machatine and KM Hale. Optical characterization of bulk GaN silicon and magnesium doped: as grown, Hydrogen implanted, and annealed, ***The European Journal of Applied Physics,*** 27, 267-270.

2004: L.C. Prinsloo, W. du Plooy and C. van der Merwe, A Raman spectroscopic study of the epicuticular wax layer of mature mango (*Mangifera indica* L) fruit, ***Journal of Raman Spectroscopy***, 35, 561-567.

2004: H.W. Kunert, D.J. Brink, M. Hayes, J. Malherbe, L. Prinsloo, J. Barnas, A.G.I. Machatine, M.W. Diale Optical characterization of GaN doping superlattices: as grown, hydrogen implanted, and annealed (p NA), ***Physica Status Solidi (C)***, V1, Issue 2, 223-228 (2004)

2003: H. W. Kunert, D. J. Brink, F. D. Auret, M. Maremane, L. C. Prinsloo, J. Barnas, B. Beaumont and P. Gibart, Photoluminescence and Raman spectroscopy of Mg-doped GaN; as grown, hydrogen implanted and annealed, ***Materials Science and Engineering B102***, 293-297 (2003).

2002: M. V. Mzenda, S. A. Goodman, E. D. Auret and L. C. Prinsloo, Characterization of electrical charge transfer in conducting polyaniline over the temperature range 300<T (K)< 450, ***Synthetic Materials***, **127**, 279-283 (2002).

2002: I. I. Eyenga, W. W. Focke, L. C. Prinsloo and A. T. Tolmay, Photodegradation: Solution for the shopping bag "visual pollution" problem? ***Macromolecular Symposia,*** **178**, Issue 1, 139-152 (2002*). Special Issue: Polymer Characterization and Materials Science. Issue Edited by Ronald D. Sanderson, Harald Pasch.*

2002: E. Friedland and L. C. Prinsloo, Dependence of critical damage energies in diamond on electronic stopping, ***Surface and Coatings Technology,*** **158-159**, 64-68 (2002).

2001: L. C. Prinsloo, in Diamond for high-density optical recording, ***Applied Physics A***, **72,** 658-663, (2001).

2001: H-J. de Jager and L. C. Prinsloo, The dehydration of phosphates monitored by DSC/TGA and in situ Raman spectroscopy, ***Thermochimica Acta,*** **376(2)**, 187-196 (2001).

2001: H. W. Kunert, T.P. Maurice, T. Hauser, J. B. Malherbe, L. C. Prinsloo, D. J. Brink, L.A. Falkovsky, J. Camassel, Effects of hydrogen implantation and annealing on the vibrational properties of 6H-SiC, ***Materials Science Forum,*** **353-356**, 275-278 (2001).

2001: I. I. Eyenga, W. W. Focke, L. C. Prinsloo and A. T. Tolmay, Photodegradation: Solution for the shopping bag "visual pollution" problem? ***The South African Journal of Science,*** **97**, 359-362 (2001).

2001: H. W. Kunert, T. Maurice, L. C. Prinsloo, D. J. Brink, J. B. Malherbe and J. Camassel, Photoluminescence and first-order Raman spectroscopy of α-particle irradiated, ion implanted and annealed GaN/Sapphire, ***Nuclear Instruments and Methods in Physics Research B***, **181**, 286-292 (2001).

2000: A. M. Heyns, P. M. Harden and L. C. Prinsloo, A resonance Raman study of the high-pressure phase transition in chromium-doped titanite, $CaTiOSiO_4$, ***Journal of Raman Spectroscopy***, **41**, 837-841 (2000).

2000: L. C. Prinsloo and P. van der Vyver, The degree of cure of modern adhesive resin cements, ***Journal of the Dental Association of South Africa,*** **55 (10),** 544-546 (2000).

1999: H. W. Kunert, S. Juillaquet, J. Camassel, J. B. Malherbe, R. Q. Odendaal, D. J. Brink and L. C. Prinsloo, Optical properties of as-grown, α-particle and N_2^+-ion implanted GaN, ***Physica Status Solidi (b),*** **216**, 619-623 (1999).

1998: N. M. Vegter, R. F. Sandenbergh, L. C. Prinsloo and A. M. Heyns, Infrared spectroscopic analysis of the sorption products of gold di-cyanide onto activated carbon, ***Minerals Engineering,*** **11,** no. 6, 545-550 (1998).

1998: AM. Heyns, L. C. Prinsloo, K-J. Range and M. Stassen, The vibrational spectra and decomposition of α-calcium nitride (α-Ca_3N_2) and magnesium nitride (Mg_3N_2), ***Journal of Solid State Chemistry,*** **137**, 33-41 (1998).

1997: L. C Prinsloo, A. M Heyns, R. Ehrl and K-J. Range, The vibrational spectra of potassium hexafluorosilicate, K_2SiF_6, ***European Journal of Solid State and Inorganic Chemistry,*** **t.34,** 881-893 (1997).

1997: L. C. Prinsloo, P. J. van der Vyver, M. R. Ferreira and A. M. Heyns, Percentage of cement cured through various thicknesses of Cerec porcelain, ***Journal of the Dental Association of South Africa,*** **52,** 283-286 (1997).

1997: S. Bauermeister, T. A. Modro and L. C. Prinsloo, Phosphorus spectroscopic studies of mixed phosphoric-carboxylic imides, ***Sulfur and Silicon,*** **111,** 149 (1997).

1996: A. M. Heyns, L. C. Prinsloo and K-J. Range, $KSbF_6$ revisited. Part II. An infrared study of the I-II phase transition, ***Vibrational Spectroscopy***, **11,** 151-157 (1996).

1995: J. R. de Wet, G. Hodgkinson, P. C. Pistorius, L. C. Prinsloo and R. F. Sandenbergh, The influence of cyanide on the flotation of pyrite from Witwatersrand gold leach residues, ***Minerals Engineering*****, 8(11)**, 1333-1345 (1995).

1994: C. A. Strydom and L. C. Prinsloo, The thermal behaviour of caesium periodate and the kinetics of the decomposition reaction, ***Thermochimica Acta***, **241**, 43-49 (1994).

1992: K-J. Range, P. Rögner, A. M. Heyns and L. C. Prinsloo, An X-ray, Raman and IR study of α-$CsReO_4$, the high-temperature modification of cesium perrhenate, ***Zeitschrift für Naturforschung Section B, Anorganische Chemie Organische Chemie***, **47b,** 1513-1520 (1992).

ORAL CONTRIBUTIONS

INTERNATIONAL CONFERENCES (6

2007: Linda C Prinsloo*, Werner Barnard, Ian Meiklejohn and Kevin Hall The first Raman spectroscopic study of San rock art in the uKhahlamba Drakensberg Park, South Africa. ***4th International Conference on the Application of Raman Spectroscopy in Art and Archaeology,*** Modena, 3 – 7 Sept. 2007.

2003: Maggi Loubser*, Johan PR de Villiers, Sabine Verryn, Linda Prinsloo and Danita de Waal. Characterisation of XRF Fluxes using X-ray Diffraction and Raman Spectroscopy ***CSI XXXIII***, 7-12 September 2003, Granada Spain.

2002: L. C. Prinsloo*, A. Bumby, I. Meiklejohn and A. Meyer, A holistic Raman spectroscopic investigation of an archaeological site in Africa, ***XVIIth International Conference on Raman Spectroscopy***, Budapest, Hungary, 20-25 August 2002.

2001: E. Friedland* and L. C. Prinsloo, Dependence of critical damage energies in diamond on electronic stopping, ***12th International Conference on Surface Modification by Ion Beams,*** Marburg, Germany, 9-14 September, 2001.

2001: W. W. Focke, F. J. W. J. Labuschagne*, L. C. Prinsloo and S. M. C. Verryn, The use of X- ray diffraction, infrared spectroscopy and scanning electron microscopy to identify the thermal decomposition mechanism of polyhydroxycarboxylic acid salts, ***CSI XXXII (Colloquium Spectroscopicum Internationale)***, Pretoria , South Africa, 9-13 July 2001

1997: L. C Prinsloo*, Practical applications of Raman spectroscopy, ***4th International Symposium on Applied Bioinorganic Chemistry including The Carman National Physical Chemistry Conference***, Cape Town, South Africa.

*Presenting author

NATIONAL CONFERENCES (6)

2003: W. du Plooy*, L. Prinsloo, C. van der Merwe and L. Korsten, Spatial identification (using SEM) and charaterisation (using Raman & FTIR) of mango epicuticular wax. ***43rd Annual Conference of the Microscopy Society of Southern Africa***, Cape Town, South Africa, 3-5 Desember 2003.

2001: L. C. Prinsloo*, Surface Raman Spectroscopy, ***Mini-Symposium on analytical methods presented by the UP/CSIR Capital Equipment Coordination group***, 27th February 2001, Pretoria (UP).

1997: L. C. Prinsloo* and P. J. van der Vyver, Spectroscopic evidence of resin-reinforced dentine by a Raman microprobe technique, ***First Joint Congress of the South African Division and the East and Southern Africa Section (IADR XXXI),*** Cape Town, South Africa.

1996: L. C. Prinsloo* and P. J. van der Vyver, The degree of cure through various thicknesses of a composite resin, ***XXX IADR Congress (SA Division),*** Johannesburg, South Africa.

1995: L. C. Prinsloo* and P. J. van der Vyver. Degree of polymerisation of modern adhesive resin cements. ***XXIX IADR Congress (S.A. Division),*** Cape Town, South Africa.

1994: L. C. Prinsloo*, M. R. Ferreira and P. J. van der Vyver, Percentage cure of cement cured through various thicknesses of porcelain. ***XXVIII IADR Congress, SA Division,*** Pretoria, South Africa.

I was the winner of the Hugo Retief award for best presentation.

*Presenting author

POSTER CONTRIBUTIONS
INTERNATIONAL CONFERENCES (25)

2007: Linda C Prinsloo, Philippe Colomban and Aurelie Tournie, The unique "Garden Roller" beads excavated in the Limpopo valley, South Africa. ***4th International Conference on the Application of Raman Spectroscopy in Art and Archaeology,*** Modena, 3 – 7 Sept. 2007.

2006: Linda C Prinsloo and Philippe Colomban**,** A Raman spectroscopic study of the Mapungubwe oblates; glass trade beads excavated at an Iron Age archaeological site in South Africa. *20th* ***International Conference on Raman Spectroscopy***, Yokohoma, Japan, 20-25 August 2006.

2006: Andreas Olsen, Linda C. Prinsloo, Louis Scott and Anna K. Jäger, Hyraceum, the fossilised metabolic products of rock hyraces, shows affinity to the GABA-benzodiazepine receptor ***Society of Medicinal Plant Research Conference,*** Helsinki, August***.***

2005: L C Prinsloo, Rock hyraces: a cause for San rock art deterioration? ***3rd International Conference on the Application of Raman Spectroscopy in Art and Archaeology,*** Paris, 31 Aug. –3 Sept. 2005*.*

2001: W. W. Focke, F. J. W. J. Labuschagne and L. C. Prinsloo, The use of infrared spectroscopy to identify the thermal decomposition products of polyhydroxycarboxylic acid salts, ***CSI XXXII (Colloquium Spectroscopicum Internationale)***, Pretoria, South Africa, 9-13 July 2001.

2001: A. Kruger**,** A. Arlow and L. C. Prinsloo, Wet-process sulphuric production: A Raman study of the complex formation between soluble ionic impurities and orthophosphoric acid, ***CSI XXXII (Colloquium Spectroscopicum Internationale)***, Pretoria, South Africa, 9-13 July 2001.

2001: H-J. de Jager and L. C. Prinsloo, The dehydration of phosphates monitored by in situ Raman spectroscopy, ***CSI XXXII (Colloquium Spectroscopicum Internationale)***, Pretoria , South Africa, 9-13 July 2001.

2001: L. C. Prinsloo and S. Tiley, A Raman spectroscopic study of some artefacts from the Mapungubwe collection, ***CSI XXXII (Colloquium Spectroscopicum Internationale)***, Pretoria, South Africa, 9-13 July 2001.

This poster won the award for the best poster in the Raman division of the conference, as well as the award for the best overall poster at the conference, awarded by Nobel Laureate Roald Hoffmann.

2000: H. W. Kunert, T. Maurice, D. J. Brink, L. C. Prinsloo, T. Hauser, J. B. Malherbe, J. Camassel, Effect of hydrogen implantation and annealing on the Vibrationalroperties of 6H-Si, ***3rd European Conference on SiC and Related Materials (ECSCRM 2000)***, 03-09 September 2000, Erlangen, Germany.

2000: H. W. Kunert, T. Maurice*, L. C. Prinsloo, D. J. Brink, J. B. Malherbe and J. Camassel, Photoluminescence and first-order Raman spectroscopy of a-particle irradiated, ion implanted and annealed GaN / Sapphire, ***7thInternational Conference on Nuclear Microprobe Technology and Applications (ICNMTA2000)***, 10-15 September 2000, Bordeaux, France.

2000: H. W. Kunert , T. P. Maurice and L. C. Prinsloo, Raman spectra from as-grown and alpha particle irradiated n-GaAs:Si, ***XVIth International Conference on Raman Spectroscopy***, Beijing, China, 20-25 August 2000.

2000: L. C. Prinsloo, E. Friedland and S. Kalbitzer, Ion beam modification of diamond for high density optical recordings as studied with Raman spectroscopy, ***XVIth International Conference on Raman Spectroscopy***, Beijing, China, 20-25 August 2000.

2000: H. W. Kunert, T. P. Maurice, L. C. Prinsloo, J. B. Malherbe, D. J. Brink and J. Camassel, Raman spectroscopy from As-grown, Implanted and Irradiated GaN/Sapphire, ***International Symposium on Progress in Surface Raman Spectroscopy 2000,*** Xiamen, China, 14-17 August 2000.

2000: L. C. Prinsloo and M. E. Lee, Laser induced formation of a Te layer on CdTe, ***International Symposium on Progress in Surface Raman Spectroscopy 2000***, Xiamen, China, 14-17 August 2000.

2000: M. E. Lee and L. C Prinsloo, Laser induced compositional changes during Raman analysis of Cadmium Telluride***, The 16th Australian Conference on Electron Microscopy***, Canberra, 6-11 February, 2000.

1999: H.W. Kunert, J. B. Malherbe, D. J. Brink, L. C. Prinsloo, J. Camassel, J. Allegre, K. Zeaiter and C. Llinares, Optical properties of as-grown and ion implanted (N_2^+, Ar^+, alpha) GaAs nipi doping superlattices, ***7th International Conference on the formation of Semiconductor Interfaces,*** Göteborg, Sweden, 21-25 June 1999

1999: H. W. Kunert, J. Camassel, S. Juillaquet, J. B. Malherbe, D. J. Brink and L. C. Prinsloo, Optical properties of as-grown and ion implanted (N_2^+, and alpha particle) irradiated GaN, ***3rd International conference on Nitride Semiconductors,*** Montpellier, France, 6-9 July, 1999.

1998: J. D. Saunderson, L. C. Prinsloo and D. F. Langa, Low-temperature metal-induced crystallisation of amorphous silicon grown on metallised flexible substrates, ***XVIth International Conference on Raman Spectroscopy***, Cape Town, South Africa, 6-11 September, 1998.

1998: S**.** Pschorr, L. C. Prinsloo, A. M. Heyns and K-J. Range, The high pressure phase transition in TeO_2, ***XVIth International Conference on Raman Spectroscopy***, Cape Town, South Africa, 6-11 September, 1998.

1998: A. M. Heyns and L. C. Prinsloo, K-J. Range and M. Stassen, The decomposition of α-calcium nitride (α-Ca_3N_2) and magnesium nitride (Mg_3N_2) studied with infrared and Raman methods, ***XVIth International Conference on Raman Spectroscopy***, Cape Town, South Africa, 6-11 September, 1998.

1998: L. C. Prinsloo and P. van der Vyver, Percentage cure of light –activated dental composite resins through various thicknesses of porcelain, ***XVIth International Conference on Raman Spectroscopy***, Cape Town, South Africa, 6-11 September, 1998.

1996: L. C. Prinsloo and A. M. Heyns, A Raman study of magnesium nitride (Mg_3N_2), α-calcium nitride (α-Ca_3N_2) and related compounds, ***15th International Conference on Raman Spectroscopy***, 11-16 August 1996, Pittsburgh, USA.

1996: L. C. Prinsloo and C. Pistorius, A Raman study of the influence of cyanide on the flotation of pyrite from Witwatersrand gold leach residues, ***15th International Conference on Raman Spectroscopy***, 11-16 August 1996, Pittsburgh, USA.

1995: S. Bauermeister, T. A. Modro and L. C. Prinsloo, Spectroscopic studies of mixed phosphoric-carboxylic-imides. ***XIIIth International Conference on Phosphorus Chemistry*** - ICPC, Jerusalem, Israel.

1994: C. A. Strydom and L. C. Prinsloo, The thermal decomposition of caesium periodate. ***E5AC6 - 6th European Symposium on Thermal Analysis and Calorimetry***, Grado Italy.

NATIONAL CONFERENCES (13)

2000: H. W. Kunert , T. P. Maurice and L. C. Prinsloo, Raman spectra from as-grown and alpha particle irradiated n-GaAs:Si, ***45th Annual Conference. Including: 35th Annual Theoretical Seminar Solid State Physics and Materials Science Specialist Group Winter School,*** Johannesburg, South Africa, 4-7 July 2000.

2000: D. J. Brink, T. P. Maurice, L. C. Prinsloo, J. B. Malherbe, J. Camassel and H. W. Kunert Raman spectroscopy from as-grown, implanted and irradiated GaN/Sapphire, ***45th Annual Conference. Including: 35th Annual Theoretical Seminar Solid State Physics and Materials Science Specialist Group Winter School,*** Johannesburg, South Africa, 4-7 July 2000.

2000: J. B. Malherbe, T. P. Maurice**,** T. Hauser, L. C. Prinsloo, D. J. Brink, J. Camassel and H. W. Kunert**,** The H^+ implantation and annealing effect on the vibrational modes of 6H-SiC, ***45th Annual Conference. Including: 35th Annual Theoretical Seminar Solid State Physics and Materials Science Specialist Group Winter School,*** Johannesburg, South Africa, 4-7 July 2000

2000: V. M. Mzenda, S. A. Goodman, F. D. Auret and L. C. Prinsloo, The effect of annealing on the structural and electrical properties of emeraldine salt: a conducting polymer, ***45th Annual Conference. Including: 35th Annual Theoretical Seminar Solid State Physics and Materials Science Specialist Group Winter School,*** Johannesburg, South Africa, 4-7 July 2000.

2000: I. I. Eyenga, W. W. Focke, L. C. Prinsloo and A. T. Tolmay, Photodegradation: A solution for the shopping bag polution problem? ***Plastex 2000***, Expo Centre NASREC, South Africa, 24-27 May 2000.

1999: M. E. Lee and L. C. Prinsloo, Laser threshold density for non-destructive Raman analysis of CdTe, M E Lee and L C Prinsloo, ***38th Annual Conference of the Microscopy Society of Southern Africa, Bloemfontein*** , South Africa, 1-3 Desember 1999.

1999: M. E. Lee and L. C. Prinsloo, Laser irradiation damage of Cadmium Telluride, South African Institute of Physics. ***44th Annual Conference. Including: 34th Annual Theoretical Seminar Solid State Physics and Materials Science Specialist Group Winter School,*** Port Elizabeth, South Africa, 6-9 July 1999.

1999: M. E. Lee and L. C. Prinsloo, Laser threshold intensity for non-destructive Raman analysis of (001) CdTe, South African Institute of Physics. ***44th Annual Conference. Including: 34th Annual Theoretical Seminar Solid State Physics and Materials Science Specialist Group Winter School***, Port Elizabeth, South Africa, 6-9 July 1999.

1999: M. E. Lee and L. C. Prinsloo, Factors influencing Raman analysis of compound semiconductors., South African Institute of Physics. ***44th Annual Conference. Including: 34th Annual Theoretical Seminar Solid State Physics and Materials Science Specialist Group Winter School***, Port Elizabeth, South Africa, 6-9 July 1999.

1999: H. W. Kunert, J. B. Malherbe, D. J. Brink, L. C. Prinsloo, R Q Odendaal, J. Camasel, J. Allegre, K. Zeaiter and C. Llinares, Optical properties of as-grown and N_2^+, Ar^+ and alpha particle implanted GaAs superlattices., South African Institute of Physics. ***44th Annual Conference. Including: 34th Annual Theoretical Seminar Solid State Physics and Materials Science Specialist Group Winter School,*** Port Elizabeth, South Africa, 6-9 July 1999.

1999: H. W. Kunert, J. Camassel, S. Juillaquet, J. B. Malherbe, R. Q. Odendaal, D. J. Brink and L. C. Prinsloo, Optical properties of as-grown and ion implanted N_2^+, and alpha particle implanted GaN., South African Institute of Physics. ***44th Annual Conference. Including: 34th***

Annual Theoretical Seminar Solid State Physics and Materials Science Specialist Group Winter School, Port Elizabeth, South Africa, 6-9 July 1999.

1996: L. C. Prinsloo and A. M. Heyns, An infrared study of the I-II phase transition in $KSbF_6$, ***33rd Convention of the South African Chemical Institute,*** Cape Town, South Africa.

1993: L. C. Prinsloo and C. A. Strydom, Kinetics of the thermal decomposition of $CsIO_4$. ***National Electron Microscopy Conference***, Berg-en-Dal, RSA, December 1993.